Near optimal solution to the inverse problem for gravitational-wave bursts

Yekta Gürsel and Massimo Tinto

Gravitational Physics, 130-33, California Institute of Technology, Pasadena, California 91125
(Received 24 July 1989)

We develop a method for determining the source direction (θ, ϕ) and the two waveforms $h_+(t)$, $h_\times(t)$ of a gravitational-wave burst using noisy data from three wideband gravitational-wave detectors running in coincidence. The scheme does not rely on any assumptions about the waveforms and in fact it works for gravitational-wave bursts of any kind. To improve the accuracy of the solution for (θ, ϕ), $h_+(t)$, $h_\times(t)$, we construct a near optimal filter for the noisy data which is deduced from the data themselves. We implement the method numerically using simulated data for detectors that operate, with white Gaussian noise, in the frequency band of 500–2500 Hz. We show that for broadband signals centered around 1 kHz with a conventional signal-to-noise ratio of at least 10 in each detector we are able to locate the source within a solid angle of 1×10^{-5} sr. If the signals and the detectors' band were scaled downwards in frequency by a factor ι, at fixed signal-to-noise ratio, then the solid angle of the source's error box would increase by a factor ι^2. The simulated data are assumed to be produced by three detectors: one on the east coast of the United States of America, one on the west coast of the United States of America, and the third in Germany or Western Australia. For conventional signal-to-noise ratios significantly lower than 10 the method still converges to the correct combination of the relative time delays but it is unable to distinguish between the two mirror-image directions defined by the relative time delays. The angular spread around these points increases as the signal-to-noise ratio decreases. For conventional signal-to-noise ratios near 1 the method loses its resolution completely.

I. INTRODUCTION

One of the early predictions of Einstein's general theory of relativity was the existence of gravitational waves. These are transverse, quadrupole waves which travel at the speed of light. They interact with matter by changing the proper distance between test masses.

Gravitational waves are generated whenever the motion of matter results in a time-changing mass quadrupole moment. The total energy radiated in the form of gravitational waves depends on the source's mass, on the velocity of its motion and on the shape and size of its flow of matter. The estimated total energy radiated in the form of gravitational waves from a typical supernova explosion is $\lesssim 10^{52}$ ergs.[1]

The detection of gravitational waves relies on sensing the change in the proper distance induced by the wave on test masses which may be coupled together mechanically or may be free. The dimensionless wave amplitude h is related to the response of the detector by $h \sim \delta l / l_0$ where l_0 is the reference length between the test masses and δl is the change in length caused by the wave.

For a typical supernova explosion in our Galaxy the energy flux on the surface of the Earth is $\lesssim 10^6$ ergs/cm^2, depending on the asymmetry in the stellar collapse.[1] If one assumes that the mean frequency of the gravitational waves is about 1 kHz, then the corresponding dimensionless wave amplitude will be $\lesssim 10^{-18}$. Using the formula above we see that for Earth-based detectors with arm lengths of the order of 1 km the change in the distance

between the test masses is $\lesssim 10^{-13}$ cm. Since the event rate for supernovae in our Galaxy is approximately one in every 30 years, the detectors have to be capable of observing events located at larger distances in order to get a reasonable event rate. For example, for sources located in the Virgo cluster of galaxies the event rate is about 30 explosions per year. The corresponding dimensionless wave amplitude is $\lesssim 10^{-21}$ which causes a length change of $\lesssim 10^{-16}$ cm between the test masses. Although typical supernovae might turn out to be highly symmetric and thus poor gravitational-wave emitters, other sources are likely to produce wave bursts at Earth with $h \sim 10^{-21}$ to 10^{-22} (Ref 2).

The astrophysical sources of gravitational radiation are expected to emit in a wide frequency range from less than one per year for early Universe sources and cosmic strings to 10^{-4} Hz for normal binary systems or large black-hole interactions through 10^{-3}–10^{-1} Hz for compact binary stars to 10^3 Hz or so for stellar collapses and neutron-star binary coalescences.[2] The optimal choice of the detection method depends on the anticipated frequency of the radiation. This is because of the differing noise characteristics of the detector designs in different frequency ranges.

The experimental efforts for the detection of gravitational radiation with Earth-based detectors have led to two basic antenna designs: resonant bar antennas and laser interferometric antennas.

A bar detector is a solid bar whose longitudinal mechanical vibrations are monitored by very sensitive transducers.[3] It is isolated from external disturbances so

that the major cause of the oscillations of the bar is gravitational waves. Presently, only the lowest frequency normal mode of the bar is monitored. The weakness of the coupling of the bar to present transducers requires that the transducers operate only over very narrow bandwidths $\Delta f/f \ll 1$. However, in the future the development of lower-noise sensors and tighter coupling to the bars may expand the bandwidth of these detectors.[4]

A laser interferometric gravitational-wave detector consists of four test masses placed in pairs along two orthogonal directions. The relative distance between the test masses along an arm is compared to that along the other arm by forming either two delay lines or two Fabry-Pérot cavities in these arms. The outputs of the optical systems in each arm are then combined to give an interference fringe. When a gravitational wave hits the detector it changes the relative length of the arms and this can be observed by monitoring the interference fringe.[5,6] Such a detector is sensitive to a wide range of frequencies (between 500 and 2000 Hz in present prototypes; between 10 and 10^4 Hz in planned detectors). Seismic noise, thermal noise in the masses' suspensions, and gravity gradient noise produce the low-frequency cutoff; photon counting statistics, noise in the servo systems, and thermal noise in the test masses produce the high-frequency cutoff.[5-7]

Despite efforts by several experimental research groups in the world since 1960 an unambiguous detection of gravitational waves has not yet been accomplished. At present there are several groups around the world proposing to build a network of several laser interferometric gravitational-wave detectors with arm lengths longer than 1 km which could reach the required sensitivity by the turn of the century.[8-12]

The detector response is a function of four variables:[13] the angles (θ,ϕ) associated with the direction of the incoming wave and the wave's two amplitudes $h_+(t)$ and $h_\times(t)$ corresponding to the two independent polarization states referred to a given coordinate system. In order to solve for these four unknowns data from a sufficiently large network of detectors widely located on the Earth and running in coincidence are necessary. From a simple counting argument we deduce that the minimum size of the network is three if the instruments are broadband; a three detector network in principle can determine (θ,ϕ), $h_+(t)$, and $h_\times(t)$. By contrast, the minimum size is four if they are narrow band; and such a four-detector network can determine only (θ,ϕ) and the Fourier transforms of $h_+(t)$ and $h_\times(t)$ at the detectors' frequencies. To see this notice that each detector provides only its response amplitude at any given time. In addition laser interferometers have sufficient time resolution to determine the time delay between two events in two detectors. Therefore, a network of N broadband detectors can provide $2N-1$ parameters for the wave (N response amplitudes which are functions of time and $N-1$ time-independent time delays), which means that $N=3$ is the minimum to determine (θ,ϕ), $h_+(t)$, and $h_\times(t)$, while a network of N narrow-band resonant bar antennas can only provide N time-independent parameters [convolutions of $h_+(t)$ and $h_\times(t)$ with the detector transfer func-

tions], which means that $N=4$ is the minimum.

Since the waveform contains information about the nature of the emitter and information about cosmological parameters, it is very important to be able to solve the so-called "inverse problem":[14,15] the calculation of the four unknowns $[\theta,\phi,h_+(t),h_\times(t)]$ associated with a gravitational wave from the time-evolving responses of the detectors and their associated relative time delays.

In this paper we develop a data-analysis algorithm which solves the inverse problem in the case of a network of three wideband detectors (either resonant bars or laser interferometers) observing a broadband gravitational-wave burst in coincidence.[16] We will investigate in forthcoming papers the inverse problem for other types of signals: the narrow-band but frequency-sweeping signals from coalescing compact binaries, the periodic signals from spinning neutron stars, and a stochastic background of gravitational waves.

This paper's presentation of the algorithm for broadband bursts is organized as follows: in Sec. II we write the analytical expression for the response function $R(t)$ of a detector when the wavelength of the signal is much larger than the detector's size. This function depends on the direction of the source (θ,ϕ), on the wave's two amplitudes $h_+(t)$ and $h_\times(t)$, and on angles (α,β,γ) representing the geographic orientation, latitude, and longitude of the detector.

In Sec. III we develop a method of computing the time delays and solving for the wave's parameters with a network of three wideband detectors in the idealized case where the detectors are noise free. Our scheme does not rely on any assumptions about the two waveforms $h_+(t),h_\times(t)$; and in fact it works for gravitational-wave bursts of any kind. In Sec. IV we extend the method to cover noisy detector responses. In Sec. V we develop a near optimal filter for the noisy data, which is to be applied to the data before they are fed into the algorithm of Sec. IV. In Sec. VI we deduce expressions for the expected errors in our algorithm's estimates of the source locations and waveforms. The numerical implementation of our algorithm is discussed in detail in Sec. VII and the results of simulations are given in Sec. VIII. Our simulations entail detectors that operate in the band 500–2500 Hz, and broadband signals centered at 1 kHz. These simulations show, with white Gaussian noise, that the scheme is usable whenever the root-mean-squared response amplitude in each detector is greater than 10 times the root-mean-squared noise level. For lower amplitudes the resolution of the method degrades rapidly. The simulated data are assumed to be produced by three detectors: one on the east coast of the United States of America (USA), one on the west coast of the USA and one in Germany or Western Australia. If the signal-to-noise ratio is at least 10 in each detector we are able to locate the source within a solid angle of $\Delta\Omega \simeq 1\times 10^{-5}$ sr. This figure gets smaller as the signal-to-noise ratio increases; and for detectors and signals at lower frequencies and at fixed signal-to-noise ratio, it gets worse as the inverse square of the signal frequency. In Sec. IX we discuss our conclusions about the inverse problem for gravitational-wave bursts.

II. THE DETECTOR RESPONSE FUNCTION

The response of a gravitational-wave detector to a plane wave, the wavelength of which is much larger than the size of the detector, is given in the literature.[1,13,14,17,18] Here we briefly summarize the derivation of that response using the notation and the language of Dhurandhar and Tinto,[14] and we refer the reader to them for a more complete discussion. In what follows we will use geometrical units in which the speed of light c and the gravitational constant G are set to 1: $c = G = 1$.

Consider a plane gravitational wave with amplitudes $h_+(t)$ and $h_\times(t)$ associated with the two independent polarizations and with a direction of propagation $\mathbf{n}$ incident on a detector. Let the wave coordinate system be (X, Y, Z) with the wave traveling in the Z direction and let the axes with respect to which $h_+(t)$ and $h_\times(t)$ are referred be the (X, Y) axes. The detector coordinate system (x', y', z') is obtained from them by a rotation described by the Euler angles (θ', ϕ', ψ') (Fig. 1). In what follows we will choose as (X, Y) axes those for which the angle ψ' is equal to zero. Since ψ' merely determines the orientation of the waves' (X, Y) axes in the X-Y plane, this choice is just a solution of convention for identifying $h_+(t)$ and $h_\times(t)$; for any other choice,
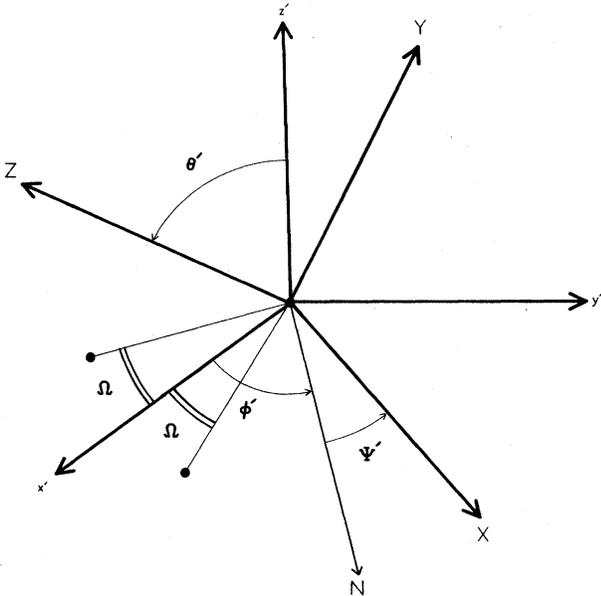

FIG. 1. The detector and the wave coordinates. The x', y', and z' axes are the detector's coordinate axes with the origin chosen to coincide with the corner mass of the interferometer. The detector lies in the x', y' plane with the x' axis bisecting the angle $2\,\Omega$ between the arms of the detector. The X, Y, Z axes are the coordinate axes for the incoming gravitational wave. The Z axis is parallel to the direction of propagation of the wave. The X, Y axes are the ones with respect to which $h_+(t)$ and $h_\times(t)$ are defined. The angles θ' and ϕ' are the usual Euler angles. The angle ψ' represents a rotation of the X, Y axes. It is measured from the line of nodes N to the X axis. In our analysis the angle ψ' is chosen to be zero.

$$[h_+(t) + ih_\times(t)]_{\text{new}} = [h_+(t) + ih_\times(t)]_{\text{old}}\, e^{2i\psi'}.$$ In the transverse-traceless (TT) gauge and in the wave coordinate system, the tensor h_{ij} has the nonvanishing components

$$h_{XX} = -h_{YY} = h_+(t), \quad h_{XY} = h_{YX} = h_\times(t). \tag{2.1}$$

In the detector coordinate system h_{ij} are complicated functions of the Euler angles.

Let us now consider the null vector $\mathbf{m}$ defined by

$$\mathbf{m} = \frac{1}{\sqrt{2}}(\mathbf{e}_X + i\,\mathbf{e}_Y), \tag{2.2}$$

where $\mathbf{e}_X$ and $\mathbf{e}_Y$ are the unit vectors in the X, Y directions, respectively. The tensor h_{ij} is then just $2h_+(t)\,\text{Re}(m_i m_j) + 2h_\times(t)\,\text{Im}(m_i m_j)$. We define the symmetric-trace-free (STF) wave tensor $W_{ij}(t)$ to be half of the tensor h_{ij}:

$$W_{ij}(t) = h_+(t)\,\text{Re}(m_i m_j) + h_\times(t)\,\text{Im}(m_i m_j). \tag{2.3}$$

The factor one-half is inherited from the geodesic deviation equation. In the detector coordinate system the components of $\overset{\leftrightarrow}{W}(t)$ can be obtained by finding the components of $\mathbf{m}$ in this system. The vector $\mathbf{m}$ can be written as

$$\mathbf{m} = \frac{1}{\sqrt{2}}[(\cos\phi' - i\,\cos\theta'\,\sin\phi')\mathbf{e}_{x'}$$
$$+ (\sin\phi' + i\,\cos\theta'\,\cos\phi')\mathbf{e}_{y'} + (i\,\sin\theta')\mathbf{e}_{z'}], \tag{2.4}$$

and we note that the vector $\mathbf{m}$ is the same as the one that appears in the Newman-Penrose formalism.[19] The vector $\mathbf{n}$ in the detector coordinate system assumes the following form:

$$\mathbf{n} = (\sin\theta'\,\sin\phi')\mathbf{e}_{x'} + (-\sin\theta'\,\cos\phi')\mathbf{e}_{y'} + (\cos\theta')\mathbf{e}_{z'}. \tag{2.5}$$

The detector can also be represented by an STF tensor D_{ij}. The form of this tensor depends on the kind of detector—whether it is an interferometer or a resonant bar.[14] For an interferometer with its arms in the direction of the unit vectors l_1 and l_2, the detector tensor D_{ij}^{int} is equal to

$$D_{ij}^{\text{int}} = l_{1i}l_{1j} - l_{2i}l_{2j}, \tag{2.6}$$

while for a cylindrical bar detector whose longitudinal axis is in the direction l, the detector tensor is

$$D_{ij}^{\text{bar}} = l_i l_j - \tfrac{1}{3}\delta_{ij}. \tag{2.7}$$

The response amplitude $R(t)$ of a detector is then simply determined by the scalar product between the STF tensor of the wave and the STF tensor of the detector:

$$R(t) = D_{ij}W^{ij}(t). \tag{2.8}$$

If there is more than one detector then it is convenient to introduce a common orthonormal coordinate system (x, y, z) and refer to it the detectors and the wave tensors. In what follows we will focus our attention on networks of three detectors. We will choose the (x, y) plane of the coordinate system to coincide with the plane defined by

the positions of the detectors and we will choose the x axis to lie in the direction of the line which connects a particular pair of detectors. The reason behind these choices is the following: a network of three wideband detectors provides two independent relative time delays which in turn yield two source directions. In this coordinate system these directions are mirror images of each other with respect to the (x,y) plane (Fig. 2). This fact makes the implementation of our method particularly

efficient and elegant if we use the (x,y,z) coordinates. In this coordinate system Eq. (2.7) becomes

$$R(t)=F_+(\theta,\phi,\alpha,\beta,\gamma)h_+(t)+F_\times(\theta,\phi,\alpha,\beta,\gamma)h_\times(t) \; ,$$

$$(2.9)$$

where β, γ are the latitude and longitude of the detector; α is measured in the plane tangent to the Earth at the location (β,γ) and it is the angle between the bisector of
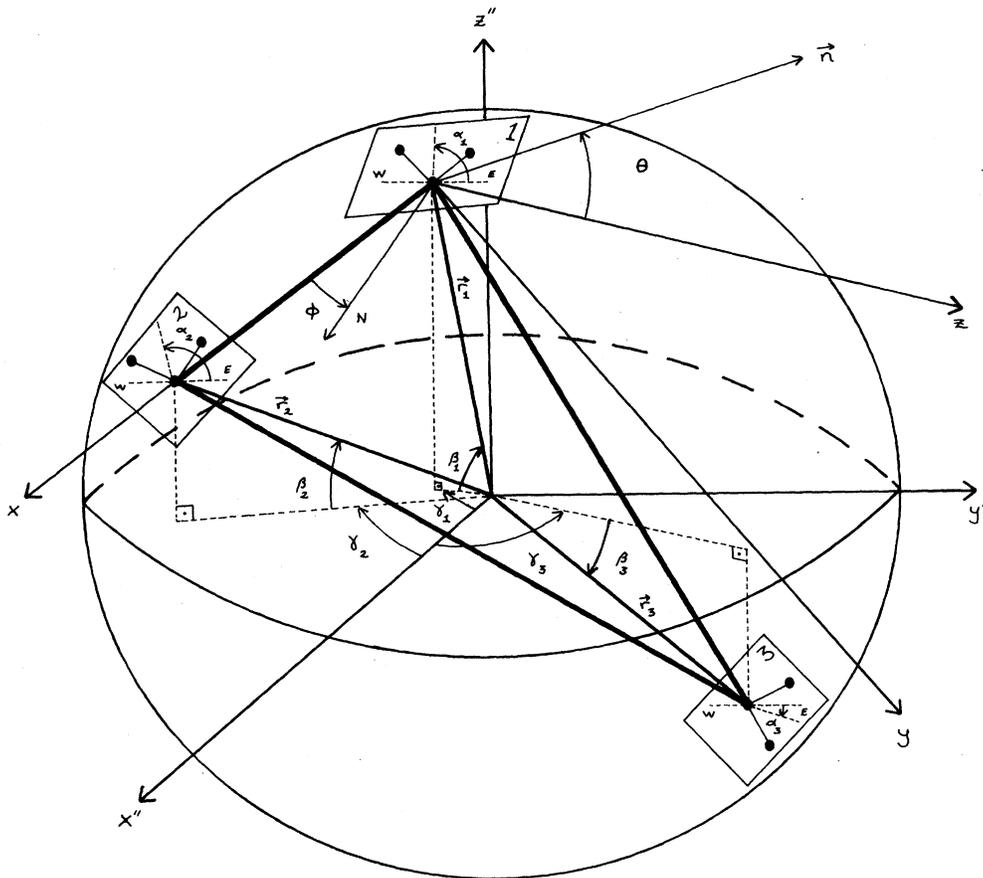

FIG. 2. The coordinate system with respect to which the source location is computed. The Earth coordinate system is defined by choosing the x'' axis to lie in the direction of the line passing through the center of the Earth and the intersection of the meridian passing through Greenwich, England and the equator. The z'' axis is chosen to lie in the direction of the line passing through the center of the Earth and the North Pole. The y'' axis is chosen to form a right-handed Cartesian coordinate system with the x'' and z'' axis. The vector r_i defines the position of detector i with respect to the origin of the Earth coordinate system. β_i, γ_i are the latitude and longitude of the detector i; α_i is the angle between the bisector of the arms of the detector i and the local east-west direction. It is measured in the plane tangent to the Earth at the location (β_i,γ_i). The x axis is chosen to coincide with the line passing through the positions of the detectors 1 and 2. The y axis is in the plane defined by the three detector locations and it is orthogonal to the x axis. The z axis is orthogonal to the (x,y) plane forming a right-handed coordinate system (x,y,z). n is the direction of propagation of the incoming gravitational wave; the Euler angles defining the source direction n in this coordinate system are denoted by θ and ϕ. θ is measured from the z axis to the source direction; ϕ is measured from the x axis to the line of nodes N in the (x,y,z) coordinate system.

the arms of the detectors and the local East-West direction; (θ,ϕ) are the Euler angles of the source in the (x,y,z) coordinate system and $h_+(t)$, $h_\times(t)$ are the two independent wave amplitudes. The "beam-pattern functions" F_+ and $F_\times$ depend only on the location and orientation of the detectors (α,β,γ) and the source direction (θ,ϕ); they are less than 1 in absolute value, except when the source direction and the polarization are precisely optimal and (for interferometers) the angle between the two arms is precisely 90°, in which case one of F_+ or $F_\times$ is ± 1 and the other is zero. A method for computing them explicitly is given in Appendix A.

We note that the response function is a linear combination of the wave's two amplitudes. Since the detectors will be widely separated on the Earth, they will register different combinations of $h_+(t)$ and $h_\times(t)$ which may be out of phase with each other. These facts may seriously affect the determination of the relative time delays between events detected at different sites.

In order to understand this point quantitatively, let us consider a realistic example: The case of a signal coming from a coalescing binary system containing compact objects (such as neutron stars or black holes). At present, among all sources of gravitational waves, these are the ones whose strengths and event rates are most confidently

understood.[20]

In the Newtonian regime, if we orient the wave's polarization axes along the axes of the elliptical projection of the orbital plane on the sky, then the wave's amplitudes assume the following form:

$$h_+(t) = 2(1+\cos^2 i)\left[\frac{\mu}{r}\right](\pi M f)^{2/3}\cos(2\pi f t) , \qquad (2.10a)$$

$$h_\times(t) = 4\cos i\left[\frac{\mu}{r}\right](\pi M f)^{2/3}\sin(2\pi f t) , \qquad (2.10b)$$

where i is the inclination of the orbit to the line of sight of the detector; M and μ are the total and reduced masses; r is the absolute distance to the binary; and f is the frequency of the waves which gradually sweeps upward as the two stars spiral together. We assume for simplicity that the orbit is circular and the frequency f does not change appreciably during the travel time of the wave from one detector to the other. From Eq. (2.9) we deduce the following expression for the response functions of two detectors located at the points $\mathbf{r}_1$ and $\mathbf{r}_2$ which are referred to the origin of the coordinate system (x,y,z):

$$R_1(t_1) = \frac{\mu}{r}(\pi M f)^{2/3}\left[\left[F_{1+}\frac{1+\cos^2 i}{2}\right]^2 + (F_{1\times}\cos i)^2\right]^{1/2}\cos(2\pi f t_1 - \mathbf{k}\cdot\mathbf{r}_1 + \xi_1) , \qquad (2.11a)$$

$$R_2(t_2) = \frac{\mu}{r}(\pi M f)^{2/3}\left[\left[F_{2+}\frac{1+\cos^2 i}{2}\right]^2 + (F_{2\times}\cos i)^2\right]^{1/2}\cos(2\pi f t_2 - \mathbf{k}\cdot\mathbf{r}_2 + \xi_2) . \qquad (2.11b)$$

We have denoted by t_1 and t_2 the (proper) time as measured at the two sites, and the phases $\xi_{1,2}$ have the following form:

$$\xi_{1,2} = \arctan\left[\frac{2F_{1,2\times}\cos i}{F_{1,2+}(1+\cos^2 i)}\right] . \qquad (2.12)$$

Notice that the time delay between the two sinusoidal detector outputs $R_1(t)$ and $R_2(t)$ is

$$\tau = t_2 - t_1 = \frac{\mathbf{n}\cdot(\mathbf{r}_1-\mathbf{r}_2)}{c} + \frac{\xi_1-\xi_2}{2\pi f} , \qquad (2.13)$$

where $\mathbf{n} = \mathbf{k}/|\mathbf{k}|$. In other words, the time shift between

the data that the experimenters compute for this signal is the sum of the real time delay $\mathbf{n}\cdot(\mathbf{r}_1-\mathbf{r}_2)/c$ and an extra delay $(\xi_1-\xi_2)/2\pi f$ depending on the relative orientations of the detectors, the inclination of the binary's orbital plane, and the frequency of the signal.

We have computed the difference $|\xi_1-\xi_2|$ in the case of circularly polarized waves ($i=0$) (Ref. 21) and for various pairs of laser interferometric detectors located in North America and Europe where they are planned to be constructed. We find that $|\xi_1-\xi_2|$ varies in the interval $[0.5,2.0]$ as the angles (θ,ϕ) vary in the ranges $[0,\pi]$ and $[0,2\pi]$, respectively. For frequencies in the interval $[100,1000]$ Hz in which the laser interferometric detec-

TABLE I. Orientations and locations of the detectors used in the simulations. β, γ are the latitude and longitude of the detector; α is the angle between the bisector of the arms of the detectors and the local east-west direction. It is measured in the plane tangent to the Earth at the location (β,γ).

	Orientation α (deg)	Latitude β (deg)	Longitude γ (deg)
Eastern site (on the east coast of USA)	72.0	45.0	−67.5
Western site (on the west coast of USA)	12.0	36.0	−115.0
Western site (as above, rotated)	57.0	36.0	−115.0
Europe (Germany)	0.0	48.0	11.5
Australia (near Perth)	76.0	−32.0	117.0

EASTERN SITE SKYMAP (h$_\times$= 1.0 h$_+$, α = 72°)

WESTERN SITE SKYMAP (h$_\times$= 1.0 h$_+$, α = 12°)

(a)

(b)

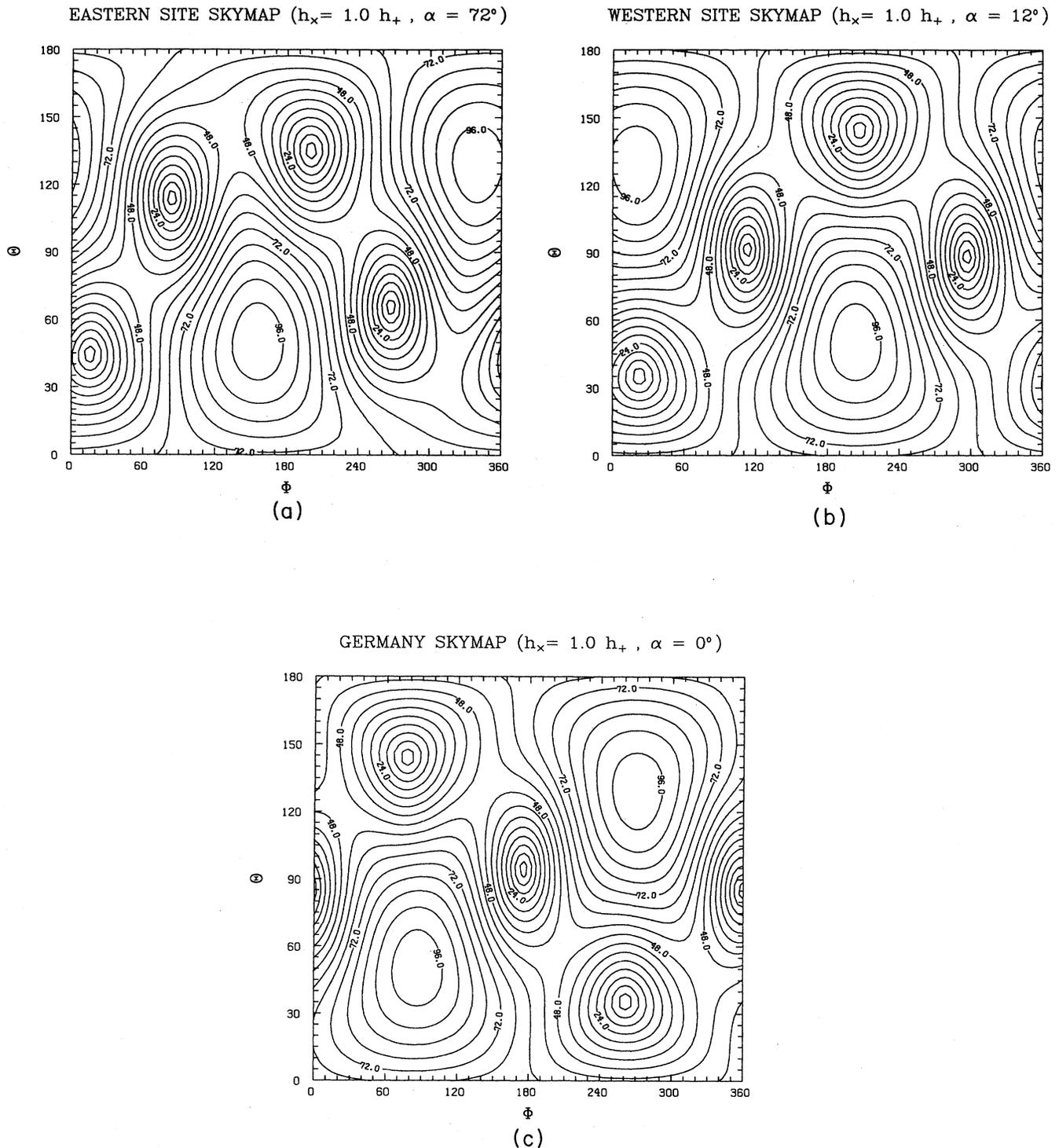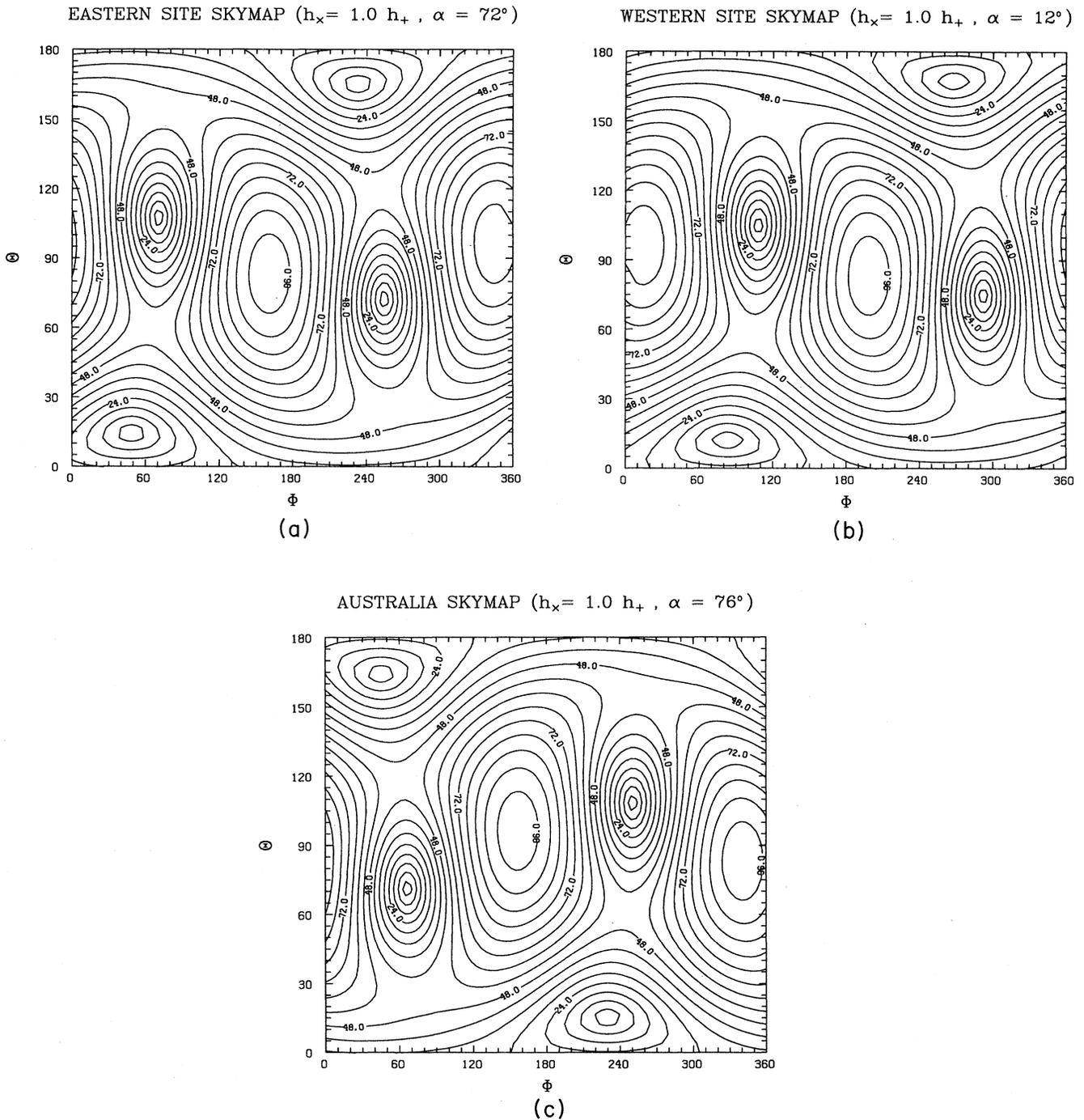GERMANY SKYMAP (h$_\times$= 1.0 h$_+$, α = 0°)

(c)

FIG. 3. (a) The contour plot of the maximum amplitude of the absolute value of the response $R_1(t) = F_{1+} h_+(t) + F_{1\times} h_\times(t)$ as a function of the source location (θ, ϕ), for a laser interferometric gravitational-wave detector located on the east coast of the United States of America as shown in Table I. The plotted values are normalized as a percentage of the absolute maximum of the function $R_1(t)$ with respect to θ, ϕ, and t. The angles θ and ϕ are the Euler angles in the coordinate system defined by two American detectors and the European detector. The detectors are optimally aligned. The sources are uniformly distributed across the sky. In (a)–(c) the waveforms are $h_+(t) = h_+ \cos(\omega t)$, $h_\times(t) = h_\times \sin(\omega t)$. The relationship between the amplitudes h_+ and $h_\times$ (which are independent of the angles θ and ϕ) is given in the title of each figure. (b) and (c) are similar patterns for the west-coast detector and the European detector. These contour plots can be thought of as "antenna beam patterns."

EASTERN SITE SKYMAP ($h_\times = 1.0\ h_+$, $\alpha = 72°$)

WESTERN SITE SKYMAP ($h_\times = 1.0\ h_+$, $\alpha = 12°$)

(a)

(b)

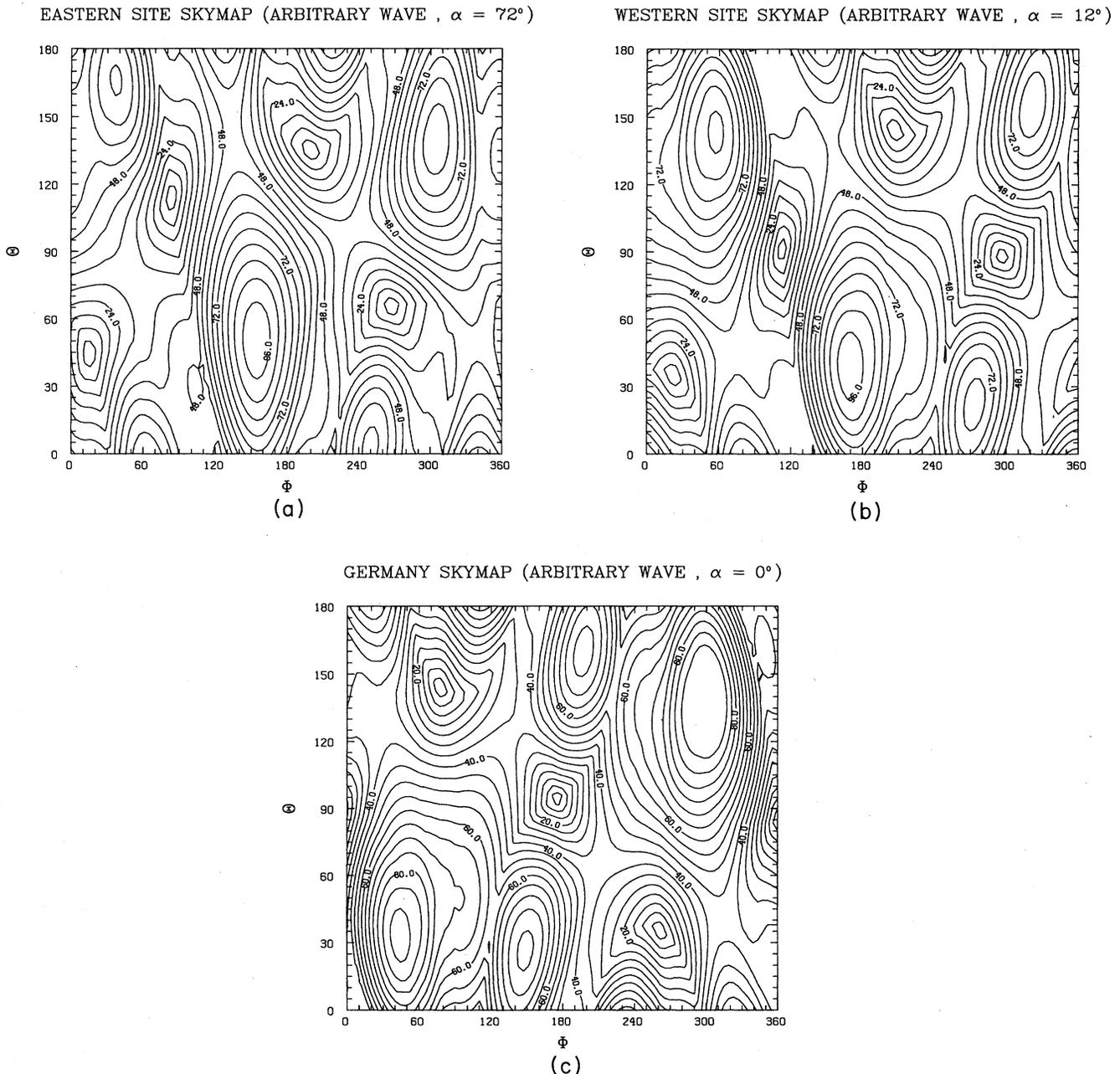AUSTRALIA SKYMAP ($h_\times = 1.0\ h_+$, $\alpha = 76°$)

(c)

FIG. 4. (a) The contour plot of the maximum amplitude of the absolute value of the response $R_1(t) = F_{1+}\ h_+(t) + F_{1\times}\ h_\times(t)$ as a function of the source location (θ, ϕ), for a laser interferometric gravitational-wave detector located on the east coast of the United States of America as shown in Table I. The plotted values are normalized as a percentage of the absolute maximum of the function $R_1(t)$ with respect to θ, ϕ, and t. The angles θ and ϕ are the Euler angles in the coordinate system defined by two American detectors and the Australian detector. Note that the coordinate system is not the same as the one in Fig. 3, although the angles are denoted in the same way. The detectors are optimally aligned. The sources are uniformly distributed across the sky. In (a)–(c) the waveforms are $h_+(t) = h_+\cos(\omega t)$, $h_\times(t) = h_\times \sin(\omega t)$. The relationship between the amplitudes h_+ and $h_\times$ (which are independent of the angles θ and ϕ) is given in the title of each figure. (b) and (c) are similar patterns for the west-coast detector and the Australian detector. These contour plots can be thought of as "antenna beam patterns."

tors are most likely to see such sources,[10] the contribution of the term $(\xi_1-\xi_2)/2\pi f$ in Eq. (2.13) will be of order 3 msec. Since the typical real time delay $\mathbf{n}\cdot(\mathbf{r}_1-\mathbf{r}_2)/c$ between the detectors will be about ±20 msec, we see that $(\xi_1-\xi_2)/2\pi f$ is about 15% of a typical real time delay implying a significant inaccuracy in the determination of the location of the source in the sky.

For other types of sources, the signal typically will

EASTERN SITE SKYMAP (ARBITRARY WAVE , α = 72°)

Θ Φ

(a)

WESTERN SITE SKYMAP (ARBITRARY WAVE , α = 12°)

Θ Φ

(b)

GERMANY SKYMAP (ARBITRARY WAVE , α = 0°)

Θ Φ

(c)

FIG. 5. (a) The contour plot of the maximum amplitude of the absolute value of the response $R_1(t) = F_{1+} h_+(t) + F_{1\times} h_\times(t)$ as a function of the source location (θ,ϕ), for a laser interferometric gravitational-wave detector located on the east coast of the United States of America as shown in Table I. The plotted values are normalized as a percentage of the absolute maximum of the function $R_1(t)$ with respect to θ, ϕ, and t. The angles θ and ϕ are the Euler angles in the coordinate system defined by two American detectors and the European detector. The detectors are optimally aligned. The sources are uniformly distributed across the sky. The two amplitudes $h_+(t)$ and $h_\times(t)$ are nonsinusoidal waveforms, shown in Figs. 6(a) and 6(b). (b) As in (a) but for the detector on the west coast of the United States of America. (c) As in (a) but for the detector in Europe.

contain many different frequencies, each of which will be phase shifted by a different amount at different locations. This implies that the shape of the signal will be different at those sites. A simple correlation scheme to deduce the location of the source will not work unless the signals are corrected for those phase shifts.

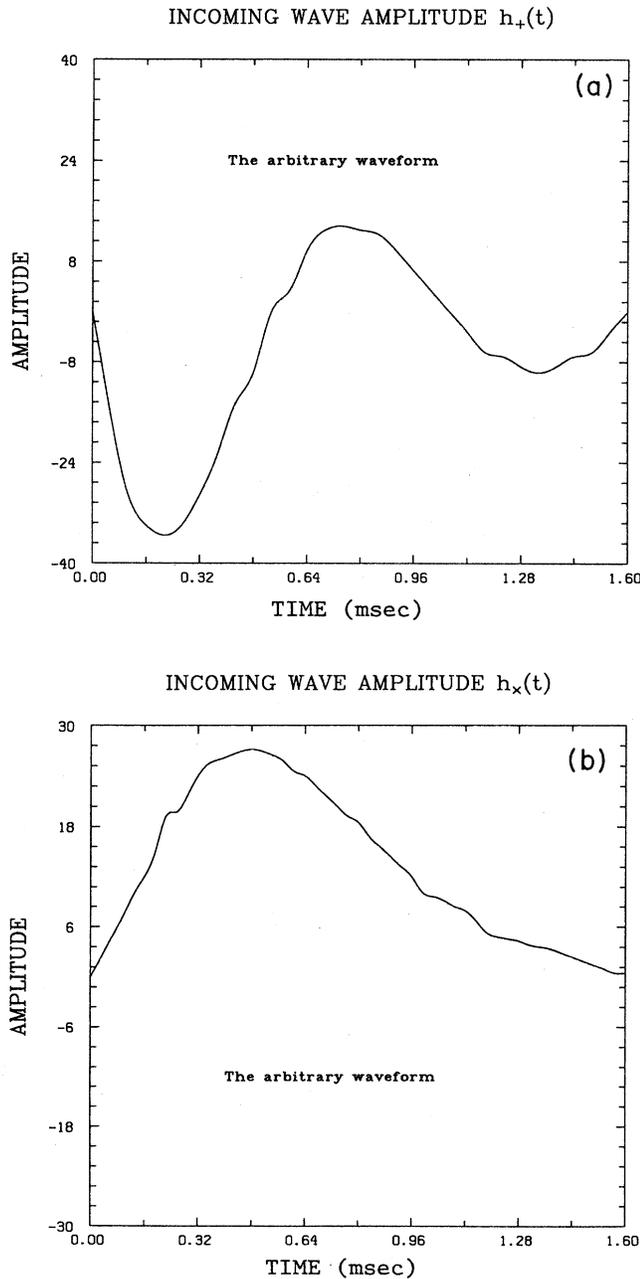As shown above, at any moment of time the response

INCOMING WAVE AMPLITUDE h+(t)

INCOMING WAVE AMPLITUDE hx(t)

FIG. 6. The two amplitudes (a) $h_+(t)$ and (b) $h_\times(t)$ of the nonsinusoidal waveform.

$$R(t) = F_+(\theta,\phi,\alpha,\beta,\gamma)h_+(t) + F_\times(\theta,\phi,\alpha,\beta,\gamma)h_\times(t)$$

of a given detector depends on the instantaneous values $h_+(t)$ and $h_\times(t)$ of the two incoming waveforms, on the direction (θ,ϕ) of the source, and on the location (β,γ) of the detector on Earth and its orientation α. For a given source location (θ,ϕ), a fixed detector location (β,γ), orientation α, and waveforms $h_+(t)$, $h_\times(t)$, the response $R(t)$ is a function of time. We plot the maximum amplitude of the absolute value of this function of time, normalized as a percentage of the absolute maximum of the function $R(t)$ with respect to θ,ϕ, and t, as a function of the source location (θ,ϕ). Figures 3–5 show the resulting contour plots for detector locations and orientations summarized in Table I. In Figs. 3 and 4, the waveforms are

$$h_+(t) = h_+ \cos(\omega t), \quad h_\times(t) = h_\times \sin(\omega t) .$$

The relationship between the amplitudes h_+ and $h_\times$ is given in the title of each figure. In Fig. 5 an arbitrary waveform with unrelated $h_+(t)$ and $h_\times(t)$ is used. The forms of these functions are shown in Fig. 6. These contour plots can be thought of as "antenna beam patterns."

III. SOLUTION TO THE INVERSE PROBLEM FOR NOISE-FREE DETECTORS

Let us assume that the clocks at the three sites have been synchronized and let us denote by $R_1(t)$, $R_2(t)$, and $R_3(t)$ the three response functions at time t of three wideband detectors located at sites 1, 2, and 3. The accuracy of the synchronization needed is well within the current technology.

If we restrict ourselves to the case of ideal, noise-free detectors, we can write their responses to a gravitational-wave burst as follows:

$$R_1(t) = F_{1+}(\theta,\phi)h_+(t) + F_{1\times}(\theta,\phi)h_\times(t) , \quad (3.1a)$$

$$R_2(t+\tau_{12}) = F_{2+}(\theta,\phi)h_+(t) + F_{2\times}(\theta,\phi)h_\times(t) , \quad (3.1b)$$

$$R_3(t+\tau_{13}) = F_{3+}(\theta,\phi)h_+(t) + F_{3\times}(\theta,\phi)h_\times(t) , \quad (3.1c)$$

where we denote the relative real time delays between detectors 1 and 2 and detectors 1 and 3 by

$$\tau_{12} \equiv \mathbf{n} \cdot (\mathbf{r}_2 - \mathbf{r}_1), \quad \tau_{13} \equiv \mathbf{n} \cdot (\mathbf{r}_3 - \mathbf{r}_1) , \quad (3.2)$$

respectively, and the functions $F_{i+}(\theta,\phi)$, $F_{i\times}(\theta,\phi)$ refer to the beam-pattern functions $F_+(\theta,\phi,\alpha_i,\beta_i,\gamma_i)$ and $F_\times(\theta,\phi,\alpha_i,\beta_i,\gamma_i)$ for the detector i. We note that the time delays τ_{12}, τ_{13} are functions of the source location (θ,ϕ). We choose the detector 1 as the reference detector without loss of generality. The functions $R_1(t)$, $R_2(t)$, and $R_3(t)$ are assumed to last only for a finite interval of time.

Let us assume that we know the exact time delays τ_{12}, τ_{13}. We will drop this assumption later when we derive our method for solving the inverse problem. From Eqs. (3.1) we see that the waveforms $h_+(t)$ and $h_\times(t)$ are the same functions in the three detectors at times related by the relative time delays τ_{12}, τ_{13}, but the responses are different because they are different linear combinations of

$h_+(t)$ and $h_\times(t)$ with different coefficients F_+ and $F_\times$. The two independent relative time delays τ_{12}, τ_{13} provide two source directions which are mirror images of each other with respect to the (x,y) plane. We denote these directions (θ_A,ϕ_A) and (θ_B,ϕ_B). For each source direction J where $J = A$ or $J = B$, we can solve for $h_{J_+}(t)$, $h_{J_\times}(t)$ as linear combinations of two of the three response functions. By inverting for instance Eqs. (3.1b), (3.1c) we deduce the following expressions for $h_{J_+}(t)$ and $h_{J_\times}(t)$:

$$h_{J_+}(t) = \frac{F_{J\,3\times}R_2(t+\tau_{12})}{F_{J\,2+}F_{J\,3\times} - F_{J\,2\times}F_{J\,3+}}$$
$$- \frac{F_{J\,2\times}R_3(t+\tau_{13})}{F_{J\,2+}F_{J\,3\times} - F_{J\,2\times}F_{J\,3+}} , \qquad (3.3a)$$

$$h_{J_\times}(t) = \frac{F_{J\,2+}R_3(t+\tau_{13})}{F_{J\,2+}F_{J\,3\times} - F_{J\,2\times}F_{J\,3+}}$$
$$- \frac{F_{J\,3+}R_2(t+\tau_{12})}{F_{J\,2+}F_{J\,3\times} - F_{J\,2\times}F_{J\,3+}} . \qquad (3.3b)$$

Since we know the explicit form for the output from detector 1 as given in Eq. (3.1a), by substituting Eqs. (3.3a), (3.3b) into Eq. (3.1a) we obtain two expressions for the output from detector 1 in terms of two outputs from detectors 2 and 3 respectively. The result is

$$T_J(t,\tau_{12},\tau_{13}) = \eta(\theta_J,\phi_J)R_2(t+\tau_{12}) + \zeta(\theta_J,\phi_J)R_3(t+\tau_{13}) , \qquad (3.4)$$

where the functions $\eta(\theta,\phi)$ and $\zeta(\theta,\phi)$ have the following form:

$$\eta(\theta,\phi) = \frac{F_{3\times}F_{1+} - F_{1\times}F_{3+}}{F_{2+}F_{3\times} - F_{2\times}F_{3+}} , \qquad (3.5a)$$

$$\zeta(\theta,\phi) = \frac{F_{1\times}F_{2+} - F_{2\times}F_{1+}}{F_{2+}F_{3\times} - F_{2\times}F_{3+}} . \qquad (3.5b)$$

It is clear that of the two functions T_J only the one which is constructed from the true direction (A or B) will exactly reproduce $R_1(t)$. This enables one to discriminate the real source location from the spurious one.

If we now drop our initial assumption of knowing the relative time delays, we can still regard the function

$$T(t,\theta,\phi) \equiv \eta(\theta,\phi)R_2[t+\tau_{12}(\theta,\phi)]$$
$$+ \zeta(\theta,\phi)R_3[t+\tau_{13}(\theta,\phi)]$$

as a two-parameter family of templates where the angles (θ,ϕ) are the parameters. Since we know that for the correct source location (θ,ϕ) the template $T(t,\theta,\phi)$ will uniquely reproduce the output $R_1(t)$, the search for the correct time delays can be performed by minimizing the following function (least-squares-fit method):

$$L(\theta,\phi) = \int_{-\infty}^{+\infty} [R_1(t) - T(t,\theta,\phi)]^2 dt . \qquad (3.6)$$

Note that the minimum of the function $L(\theta,\phi)$ is exactly equal to zero. We point out that the method here developed for locating the source works for any

gravitational-wave burst, independently of the time dependence of the wave's two amplitudes $h_+(t)$, $h_\times(t)$.

Consider the functions $\eta(\theta,\phi)$ and $\zeta(\theta,\phi)$ given in Eq. (3.5). The common denominator $F_{2+}F_{3\times} - F_{2\times}F_{3+}$ could vanish for certain source locations. For these source directions the template $T(t,\tau_{12},\tau_{13})$ will be ill defined. In order to avoid this problem we define a new least-squares integrand as follows:

$$I(\theta,\phi,t) = K_1(\theta,\phi)R_1(t) + K_2(\theta,\phi)R_2(t+\tau_{12})$$
$$+ K_3(\theta,\phi)R_3(t+\tau_{13}) , \qquad (3.7)$$

where

$$K_1(\theta,\phi) = F_{2+}F_{3\times} - F_{2\times}F_{3+} , \qquad (3.8a)$$

$$K_2(\theta,\phi) = F_{3+}F_{1\times} - F_{3\times}F_{1+} , \qquad (3.8b)$$

$$K_3(\theta,\phi) = F_{1+}F_{2\times} - F_{1\times}F_{2+} . \qquad (3.8c)$$

The square of this $I(\theta,\phi,t)$ is readily shown to be K_1^2 times the integrand of Eq. (3.6); and, as a result, the integral

$$L(\theta,\phi) = \int_{-\infty}^{+\infty} I^2(\theta,\phi,t) dt \qquad (3.9)$$

like Eq. (3.6) takes on its minimum value (zero) when (θ,ϕ) is the true direction to the source. This $L(\theta,\phi)$ has the advantage over the one defined by Eq. (3.6) that it is well-defined everywhere and it is totally symmetric under permutations of the detector indices $\{1, 2, 3\}$. The symmetry of $L(\theta,\phi)$ under the permutation of the detector indices can be proven in the following way.

Given three detectors there are three relative time delays τ_{12}, τ_{13}, and τ_{23} which are linearly dependent:

$$\tau_{13} = \tau_{12} + \tau_{23} . \qquad (3.10)$$

When a permutation of the detector indices is applied to the integral, the explicit angular functions $K_1(\theta,\phi)$, $K_2(\theta,\phi)$, $K_3(\theta,\phi)$ and the detector responses $R_1(t)$, $R_2(t)$, $R_3(t)$ interchange properly to preserve the integrand. However, the arguments of the detector responses do not immediately permute to the correct order. This can be resolved by using Eq. (3.10), the fact that the integral is invariant under time translations and the fact that the relative time delays change sign under transposition of the detector indices.

Once the source direction has been determined by minimizing the integral given by Eq. (3.9), the waveforms of the gravitational wave can be solved for using Eqs. (3.3a), (3.3b). Note that since we have three responses and only two independent waveforms, there are three distinct, seemingly equivalent ways for reconstructing each of the waveforms:

$$h_+(t) = \frac{F_{3\times}R_2(t+\tau_{12}) - F_{2\times}R_3(t+\tau_{13})}{K_1}$$
$$= \frac{F_{1\times}R_3(t+\tau_{13}) - F_{3\times}R_1(t)}{K_2}$$
$$= \frac{F_{2\times}R_1(t) - F_{1\times}R_2(t+\tau_{12})}{K_3} , \qquad (3.11)$$

$$h_\times(t) = \frac{F_{2+}R_3(t+\tau_{13}) - F_{3+}R_2(t+\tau_{12})}{K_1}$$

$$= \frac{F_{3+}R_1(t) - F_{1+}R_3(t+\tau_{13})}{K_2}$$

$$= \frac{F_{1+}R_2(t+\tau_{12}) - F_{2+}R_1(t)}{K_3} \ . \tag{3.12}$$

The functions K_1, K_2, and K_3 can vanish for particular source directions making the expressions for $h_+(t)$ and $h_\times(t)$ involving that angular function ill defined. For detectors that are not in the same plane and with arms not parallel to each other, all three angular functions can simultaneously vanish only at one point.

IV. LEAST-SQUARES METHOD FOR NOISY DETECTOR RESPONSES

In the case of three real detectors the three response functions [which we now denote $R_{1\Lambda}(t)$, $R_{2\Lambda}(t)$, and $R_{3\Lambda}(t)$] will contain noise as well as the signal:

$$R_{1\Lambda}(t) = F_{1+}(\theta,\phi)h_+(t) + F_{1\times}(\theta,\phi)h_\times(t) + \Lambda_1(t) \ , \tag{4.1a}$$

$$R_{2\Lambda}(t+\tau_{12}) = F_{2+}(\theta,\phi)h_+(t) + F_{2\times}(\theta,\phi)h_\times(t)$$
$$+ \Lambda_2(t+\tau_{12}) \ , \tag{4.1b}$$

$$R_{3\Lambda}(t+\tau_{13}) = F_{3+}(\theta,\phi)h_+(t) + F_{3\times}(\theta,\phi)h_\times(t)$$
$$+ \Lambda_3(t+\tau_{13}) \ . \tag{4.1c}$$

Here $\Lambda_1(t)$, $\Lambda_2(t)$, and $\Lambda_3(t)$ are random processes representing the noise in each detector. We assume that these processes are not correlated either with each other or with the signal. We also assume that these are stationary random processes with a Gaussian distribution.

We define a new least-squares integrand $I_\Lambda(\theta,\phi,t)$ in the following manner:

$$I_\Lambda(\theta,\phi,t) = K_1(\theta,\phi)R_{1\Lambda}(t) + K_2(\theta,\phi)R_{2\Lambda}(t+\tau_{12})$$
$$+ K_3(\theta,\phi)R_{3\Lambda}(t+\tau_{13}) \ , \tag{4.2}$$

where the functions K_1, K_2, and K_3 are as defined in Eqs. (3.8a), (3.8b), and (3.8c); $\tau_{12} = \tau_{12}(\theta,\phi)$ and $\tau_{13} = \tau_{13}(\theta,\phi)$ are defined by Eq. (3.2). The new least-squares function $L_\Lambda(\theta,\phi)$ is defined as

$$L_\Lambda(\theta,\phi) = \frac{1}{\Delta t}\int_{t_0}^{t_1} I_\Lambda^2(\theta,\phi,t)dt \ , \tag{4.3}$$

where $\Delta t = t_1 - t_0$. The time interval (t_0,t_1) is chosen in such a way that it contains the gravitational-wave pulse for each trial source location under consideration and it is not any longer than necessary. We will discuss the choice of the integration interval later in this section.

The least-squares function $L_\Lambda(\theta,\phi)$ can be expressed as

$$L_\Lambda(\theta,\phi) = L(\theta,\phi) + \frac{1}{\Delta t}\int_{t_0}^{t_1}[K_1(\theta,\phi)\Lambda_1(t) + K_2(\theta,\phi)\Lambda_2(t+\tau_{12}) + K_3(\theta,\phi)\Lambda_3(t+\tau_{13})]^2 dt$$

$$+ \frac{2}{\Delta t}\int_{t_0}^{t_1} I(\theta,\phi,t)[K_1(\theta,\phi)\Lambda_1(t) + K_2(\theta,\phi)\Lambda_2(t+\tau_{12}) + K_3(\theta,\phi)\Lambda_3(t+\tau_{13})]dt \ , \tag{4.4}$$

where $L(\theta,\phi)$ is given by

$$L(\theta,\phi) = \frac{1}{\Delta t}\int_{t_0}^{t_1} I^2(\theta,\phi,t)dt \ . \tag{4.5}$$

The function $I(\theta,\phi,t)$ is

$$I(\theta,\phi,t) = K_1(\theta,\phi)R_1(t) + K_2(\theta,\phi)R_2(t+\tau_{12})$$
$$+ K_3(\theta,\phi)R_3(t+\tau_{13}) \tag{4.6}$$

and the functions $R_1(t)$, $R_2(t+\tau_{12})$, $R_3(t+\tau_{13})$ are the noise-free responses.

We minimize $L_\Lambda(\theta,\phi)$ to find the direction to the source. For the correct source direction (θ_s,ϕ_s), the function $L(\theta_s,\phi_s)$ and the cross term in Eq. (4.4) will vanish leaving only the pure noise term to contribute to the minimized function:

$$L_\Lambda(\theta_s,\phi_s) = \frac{1}{\Delta t}\int_{t_0}^{t_1}\{K_1(\theta_s,\phi_s)\Lambda_1(t)$$
$$+ K_2(\theta_s,\phi_s)\Lambda_2[t+\tau_{12}(\theta_s,\phi_s)]$$
$$+ K_3(\theta_s,\phi_s)\Lambda_3[t+\tau_{13}(\theta_s,\phi_s)]\}^2 dt \ . \tag{4.7}$$

Note that when the noise amplitudes are reduced to zero, this value goes to zero as well, matching the noise-free least-squares function. At any other point (θ,ϕ) the function $L(\theta,\phi)$ is greater than zero and the pure-noise term in Eq. (4.4) is greater than or equal to zero. However the cross term in Eq. (4.4) could be negative leading to the result that the minimum of $L_\Lambda(\theta,\phi)$ may not coincide with the minimum of $L(\theta,\phi)$. This causes the method to miss the correct source direction and to produce an incorrect result. The error in determining the source direction will depend on the signal-to-noise ratio in general.

We point out that the least-squares function defined by Eq. (4.3) does not correspond to the standard least-squares function with imprecise data:

$$\text{standard least-squares function} = \sum_{i=1}^N \frac{(x_i - \rho_i)^2}{2\sigma_i^2} \ , \tag{4.8}$$

where x_i are noisy discrete data (numbers, not functions of time) with standard errors σ_i, and ρ_i is the theoretical function to be fitted to the noisy data. Note that the standard least-squares function is normalized by the root-mean-squared (rms) noise level σ_i, but the least-squares function $L_\Lambda(\theta,\phi)$ given by Eq. (4.3) does not have

such a normalizing factor. We will now give an argument that motivates inserting such a normalizing factor into $L_\Lambda(\theta,\phi)$.

Equation (4.3) can be written as

$$L_\Lambda(\theta,\phi) = \frac{1}{\Delta t} \int_{t_0}^{t_1} \{[K_1\Lambda_1(t) + K_2\Lambda_2(t+\tau_{12})$$

$$+ K_3\Lambda_3(t+\tau_{13})]$$

$$+ K_1R_1(t) + K_2R_2(t+\tau_{12})$$

$$+ K_3R_3(t+\tau_{13})\}^2 dt , \qquad (4.9)$$

where we have formally grouped the noise terms together. We can interpret the terms in this equation in the following manner:

$$T'(t,\theta,\phi) \equiv -K_1R_1(t) - K_2R_2(t+\tau_{12}) - K_3R_3(t+\tau_{13})$$

is analogous to the theoretical fit function in the standard least-squares formula;

$$K_1\Lambda_1(t) + K_2\Lambda_2(t+\tau_{12}) + K_3\Lambda_3(t+\tau_{13})$$

is analogous to the noise that is contaminating the data. These data are identically equal to zero in our case since the theoretical fit function $T'(t,\theta,\phi)$ vanishes at the source location.

Consider a source location (θ_s,ϕ_s). Assume that the time interval (t_0,t_1) is subdivided into N equal-length, small intervals. Define $t_i = t_0 + i(t_1-t_0)/N$ where i is an integer in the interval $[0,N]$. The noisy datum

$$d_i(\theta_s,\phi_s) = K_1\Lambda_1(t_i) + K_2\Lambda_2(t_i+\tau_{12}) + K_3\Lambda_3(t_i+\tau_{13})$$

at a particular time t_i is a linear combination of uncorrelated Gaussian random processes $\Lambda_j(t_i)$ with zero mean and with variances σ_j^2 where $j=1,2,3$. Using a well-known result,[22] we deduce that the probability distribution p of $d_i(\theta_s,\phi_s)$ is also a Gaussian distribution with zero mean and with variance $K_1^2\sigma_1^2 + K_2^2\sigma_2^2 + K_3^2\sigma_3^2$; its analytic expression is given by

$$p(d_i(\theta_s,\phi_s)) = \exp\left[-\frac{1}{2}\frac{d_i(\theta_s,\phi_s)^2}{K_1^2\sigma_1^2 + K_2^2\sigma_2^2 + K_3^2\sigma_3^2}\right] . \quad (4.10)$$

Since the theoretical fit function $T'(t_i,\theta_s,\phi_s)$ is zero, the noisy datum $d_i(\theta_s,\phi_s)$ is normally (Gaussian) distributed around the theoretical fit function at the source location. At any other point in the sky (θ,ϕ), the noisy datum $d_i(\theta,\phi)$ is normally distributed around the mean value $T'(t_i,\theta,\phi)$. Hence, the probability density of the datum $d_i(\theta,\phi)$ fitting the mean $T'(t_i,\theta,\phi)$ is given by

$$p(d_i(\theta,\phi)) = \exp\left[-\frac{1}{2}\frac{[d_i(\theta,\phi)-T'(t_i,\theta,\phi)]^2}{K_1^2\sigma_1^2 + K_2^2\sigma_2^2 + K_3^2\sigma_3^2}\right] . \quad (4.11)$$

The probability of the entire set of noisy data $d_i(\theta,\phi)$, $i=0,N$ fitting the theoretical fit function $T'(t_i,\theta,\phi)$, $i=0,N$ at the corresponding times within a constant accuracy $\Delta\Lambda'$ (i.e., $|[d_i(\theta,\phi)-T'(t_i,\theta,\phi)]| \le \Delta\Lambda'/2$) is given by

$$P(\theta,\phi) = \prod_{i=0}^{N}\exp\left[-\frac{1}{2}\frac{[d_i(\theta,\phi)-T'(t_i,\theta,\phi)]^2}{K_1^2\sigma_1^2 + K_2^2\sigma_2^2 + K_3^2\sigma_3^2}\right]\Delta\Lambda' .$$

$$(4.12)$$

When the point (θ,ϕ) is far away from the source location, the noisy data will not have the same mean as the theoretical fit function causing a reduction in the probability given in Eq. (4.12). This probability attains a maximum when the point under consideration is near the source location for large signal-to-noise ratios. Maximizing this probability is equivalent to minimizing the negative of its logarithm:

$$-\ln(P) = \sum_{i=0}^{N}\frac{1}{2}\frac{[d_i(\theta,\phi)-T'(t_i,\theta,\phi)]^2}{K_1^2\sigma_1^2 + K_2^2\sigma_2^2 + K_3^2\sigma_3^2} - N\ln(\Delta\Lambda') .$$

$$(4.13)$$

Since N and $\Delta\Lambda'$ are constants, minimizing Eq. (4.13) is equivalent to minimizing a new least-squares function $L'_\Lambda(\theta,\phi)$ defined with a normalizing noise factor as

$$L'_\Lambda(\theta,\phi) = \frac{1}{\Delta t}\int_{t_0}^{t_1}\frac{I_\Lambda^2(\theta,\phi,t)}{K_1^2\sigma_1^2 + K_2^2\sigma_2^2 + K_3^2\sigma_3^2}dt . \quad (4.14)$$

Note that the least-squares function $L'_\Lambda(\theta,\phi)$ given in Eq. (4.14) is completely symmetric under permutations of detector indices. It is this least-squares function that we will use as the basis of our method for determining the source locations.

One can try to minimize the least-squares function $L'_\Lambda(\theta,\phi)$ in terms of the angles (θ,ϕ) or one can express the angles in terms of the trial time delays τ_{12}, τ_{13} and perform the minimization using the time delays directly. Note that the two time delays give two possible source locations. Hence, the minimization has to be performed locally in a neighborhood of each point. The resulting two minima are then compared with each other to decide on the correct source location. The errors in the two relative time delays τ_{12} and τ_{13} are related to the angular errors in the source location $\Delta\theta$, $\Delta\phi$ by the linear relations

$$\Delta\tau_{12} = \mathbf{r}_{12}\cdot\left[\frac{\partial\mathbf{n}}{\partial\theta}\Delta\theta + \frac{\partial\mathbf{n}}{\partial\phi}\Delta\phi\right] , \quad (4.15)$$

$$\Delta\tau_{13} = \mathbf{r}_{13}\cdot\left[\frac{\partial\mathbf{n}}{\partial\theta}\Delta\theta + \frac{\partial\mathbf{n}}{\partial\phi}\Delta\phi\right] , \quad (4.16)$$

where $\mathbf{r}_{12}$ and $\mathbf{r}_{13}$ are the separation vectors between sites 1,2 and 1,3 respectively. The vector $\mathbf{n}$ is the direction of propagation of the gravitational wave as defined in Sec. II. Equations (4.15) and (4.16) imply that the errors in the relative time delays and the angular resolution are optimized in conjunction. Therefore, the two different implementations of the minimization procedure described above are equivalent.

In the absence of noise the integrand $I(\theta,\phi,t)$ in Eq. (3.9) is nonzero only in a finite time interval. This follows from the fact that for a finite-duration gravity wave the detector responses are finite duration pulses. The length of this interval depends on the angles θ and ϕ since the

relative trial time delays are functions of them. In this noise-free case, it is easy to compute the length of this time interval because the starting times and the durations of the individual responses are known. Note that the durations of the responses are all equal since they are determined by $h_+(t)$ and $h_\times(t)$, but the shapes of the responses are different.

When the noise is present, it is no longer possible to identify the starting times and the durations of the responses precisely. They can only be determined with a statistical accuracy. In this case the interval of integration (t_0, t_1) has to be finite because if it is unnecessarily large the noise will be integrated causing a reduction in the overall signal-to-noise ratio in the search for the correct (θ, ϕ). The starting and ending times of the pulses will have to be determined using a threshold criterion. Since the durations of the pulses are theoretically equal, a good guess for the duration of the pulses can be obtained, in cases where the amplitudes of the responses are nearly the same, by averaging the individual durations obtained by the threshold criterion. The interval of integration determined using the threshold criterion depends on the trial time delays. In the next section we will give an optimal choice for the interval of integration.

Once the source location has been determined, the wave amplitudes $h_+(t)$ and $h_\times(t)$ can be solved for using Eqs. (3.11) and (3.12) with the noise-free responses replaced by the true noisy responses. However, the equalities between different ways of determining a given wave amplitude will not hold since the contributions of noise to each of the terms are different. There is an optimal linear combination of the three equations for each wave amplitude which results in the least amount of root-mean-squared noise in the reconstructed waveform. Consider three distinct reconstructions of $h_+(t)$:

$$h_{1+}(t) = \frac{F_{3\times} R_{2\Lambda}(t+\tau_{12}) - F_{2\times} R_{3\Lambda}(t+\tau_{13})}{K_1}$$
$$= \frac{F_{3\times} R_2(t+\tau_{12}) - F_{2\times} R_3(t+\tau_{13})}{K_1}$$
$$+ \frac{F_{3\times} \Lambda_2(t+\tau_{12}) - F_{2\times} \Lambda_3(t+\tau_{13})}{K_1} , \quad (4.17)$$

$$h_{2+}(t) = \frac{F_{1\times} R_{3\Lambda}(t+\tau_{13}) - F_{3\times} R_{1\Lambda}(t)}{K_2}$$
$$= \frac{F_{1\times} R_3(t+\tau_{13}) - F_{3\times} R_1(t)}{K_2}$$
$$+ \frac{F_{1\times} \Lambda_3(t+\tau_{13}) - F_{3\times} \Lambda_1(t)}{K_2} , \quad (4.18)$$

$$h_{3+}(t) = \frac{F_{2\times} R_{1\Lambda}(t) - F_{1\times} R_{2\Lambda}(t+\tau_{12})}{K_3}$$
$$= \frac{F_{2\times} R_1(t) - F_{1\times} R_2(t+\tau_{12})}{K_3}$$
$$+ \frac{F_{2\times} \Lambda_1(t) - F_{1\times} \Lambda_2(t+\tau_{12})}{K_3} , \quad (4.19)$$

where we have formally separated the contributions of the noise from the noise-free waveforms. Let the optimal linear combination $h_{\text{opt}+}(t)$ which gives the least amount of noise in the reconstructed waveform be

$$h_{\text{opt}+}(t) = a_+(\theta, \phi) h_{1+}(t) + b_+(\theta, \phi) h_{2+}(t)$$
$$+ c_+(\theta, \phi) h_{3+}(t) , \quad (4.20)$$

where

$$a_+(\theta, \phi) + b_+(\theta, \phi) + c_+(\theta, \phi) = 1 , \quad (4.21)$$

since $h_{\text{opt}+}(t)$ should reduce to the noise-free waveform $h_+(t)$ when the noise amplitudes are reduced to zero. We define the root-mean-squared error δh_+ in the reconstructed waveform as

$$\delta h_+ = \left[\frac{1}{\Delta t} \int_{t_0}^{t_1} [h_{\text{opt}+}(t) - h_+(t)]^2 \, dt \right]^{1/2} . \quad (4.22)$$

We minimize this expression with respect to $a_+(\theta, \phi)$, $b_+(\theta, \phi)$, and $c_+(\theta, \phi)$ subject to the constraint given by Eq. (4.21) to obtain three linear equations for them; only two of these equations are linearly independent. We choose one of these coefficients to be a free parameter and express the others in terms of it and the angular functions $F_{i\times}$ and K_i. When the optimally reconstructed waveform $h_{\text{opt}+}(t)$ is expressed in terms of the noisy detector responses $R_{1\Lambda}(t)$, $R_{2\Lambda}(t)$, and $R_{3\Lambda}(t)$ according to Eqs. (4.17), (4.18), and (4.19) using the coefficients $a_+(\theta, \phi)$, $b_+(\theta, \phi)$, and $c_+(\theta, \phi)$ derived above, the dependence on the free parameter cancels out, resulting in a unique optimal reconstruction.

The same argument can be applied in computing the optimal linear combination $h_{\text{opt}\times}(t)$ for the other waveform $h_\times(t)$. The analytic forms of the coefficients $a_+, b_+, c_+, a_\times, b_\times, c_\times$ in these linear combinations are given in Appendix C. [Note that the formula (4.22) and its analog for $\delta h_\times$ give the errors in the reconstructed waveforms solely due to the noise in the detectors. The errors in the determination of the source location will also contribute to the errors in the reconstructed waveforms. Their effect is given by Eqs. (6.9)–(6.11).]

V. A NEAR-OPTIMAL FILTER FOR THE LEAST-SQUARES FUNCTION

The accuracy of the source location determined by minimizing the least-squares function given in Eq. (4.14) depends on the magnitude of the noise terms in that equation. If the contribution of these terms to the least-squares integral can be reduced by filtering then this accuracy will improve.

A linear filter is a map which relates its output to its input as defined by[23]

$$O(t) = \int_{-\infty}^{+\infty} \Phi(t') J(t - t') dt' \quad (5.1)$$

or equivalently

$$O(t) = \int_{-\infty}^{+\infty} \Phi(t - t') J(t') dt' , \quad (5.2)$$

where the output $O(t)$ is obtained from the input $J(t)$

through linear operations with coefficients $\Phi(t)$. In what follows we call the function $\Phi(t)$ the "filter." The filtering operation can also be performed in the frequency domain. The equivalent form of Eqs. (5.1), (5.2) in the frequency domain is

$$\tilde{O}(\omega) = \tilde{\Phi}(\omega)\tilde{J}(\omega) \tag{5.3}$$

and

$$O(t) = \frac{1}{2\pi} \int_{-\infty}^{+\infty} e^{i\omega t} \tilde{\Phi}(\omega)\tilde{J}(\omega) d\omega \ . \tag{5.4}$$

If the noise-free form $Q(t)$ of the noisy input signal $J(t)$ is known, then the "optimal filter," i.e., the filter which maximizes the signal-to-noise ratio at the output $O(t)$ is given by[23]

$$\tilde{\Phi}(\omega) = \frac{\tilde{Q}^*(\omega)}{S_\Lambda(\omega)} c_0 e^{-i\omega t_p} \ . \tag{5.5}$$

Here $\tilde{\Phi}(\omega)$ is the Fourier transform of the filter $\Phi(t)$,

$$\tilde{\Phi}(\omega) = \int_{-\infty}^{+\infty} e^{-i\omega t} \Phi(t) dt \ , \tag{5.6}$$

and its inverse is

$$\Phi(t) = \frac{1}{2\pi} \int_{-\infty}^{+\infty} e^{i\omega t} \tilde{\Phi}(\omega) d\omega \ ; \tag{5.7}$$

$\tilde{Q}^*(\omega)$ is the complex conjugate of the Fourier transform of the noise-free form of the input signal $Q(t)$; $S_\Lambda(\omega)$ is the spectral density of the random process $\Lambda(t)$ which represents the noise; c_0 is an arbitrary complex constant; t_p is the time at which the signal-to-noise ratio is maximum; and the factor $e^{-i\omega t_p}$ serves only to move the maximum signal in $O(t)$ from $t = 0$ back to its location in the input, $t = t_p$.

This optimal filter does not preserve the form of the input signal. This can be seen in the following way: Assume that the noise in the input signal is white so that $S_\Lambda(\omega)$ is a constant. Then choose the arbitrary constant c_0 in the filter [Eq. (5.5)] to be equal to the spectral density of the noise. The filter then becomes

$$\tilde{\Phi}(\omega) = \tilde{Q}^*(\omega) e^{-i\omega t_p} \ . \tag{5.8}$$

Now, choose $t_p = 0$ and assume that the input signal $J(t)$ is free of noise. Then $\tilde{Q}^*(\omega) = \tilde{J}^*(\omega)$ and the filtered function $O(t)$ becomes

$$O(t) = \frac{1}{2\pi} \int_{-\infty}^{+\infty} e^{i\omega t} \tilde{J}^*(\omega)\tilde{J}(\omega) d\omega \ , \tag{5.9}$$

which is equal to the autocorrelation of the input signal $J(t)$:

$$O(t) = \int_{-\infty}^{+\infty} J(t')J(t + t') dt' \ . \tag{5.10}$$

It is clear from this equation that the output function $O(t)$ cannot have the same form as the input function $J(t)$ in general. In particular it is easy to prove that if the input function has a finite duration d_0 then the autocorrelation has the duration $2d_0$ (Ref. 24).

The filter mentioned above is optimal in the sense that it maximizes the signal-to-noise ratio at its output. There

are other optimal filters. In particular, the filter that minimizes the difference between the output signal and the noise-free signal is given by[25]

$$\tilde{\Phi}(\omega) = \frac{|\tilde{Q}(\omega)|^2}{|\tilde{Q}(\omega)|^2 + S_\Lambda(\omega)} \ , \tag{5.11}$$

where $\tilde{Q}(\omega)$ is the Fourier transform of the noise-free signal and $S_\Lambda(\omega)$ is the spectral density of the noise.

When the form of the input signal is not known both of the filters described above are unrealizable. However, there are methods which enable one to construct a "near-optimal" filter.[25]

These methods rely on the fact that the spectrum of the signal is distinguishable from that of the noise. If this assumption is true then one can approximate a noise-free signal spectrum by extrapolating the part of the power spectrum of the noisy signal where the signal is dominant to the other parts of the frequency range. Similarly, one can obtain an approximate full noise spectrum by either extrapolating the spectrum of noise to the frequency range where the signal is dominant or by simply computing the spectrum of the noise when the signal is absent. Since we are dealing with finite duration bursts the latter will be used in our method. Note that since the optimal filter (5.5) is obtained through an extremization procedure, the errors in the determination of the optimal filter result in second-order differences in the performance of this filter. This means that a fairly crudely

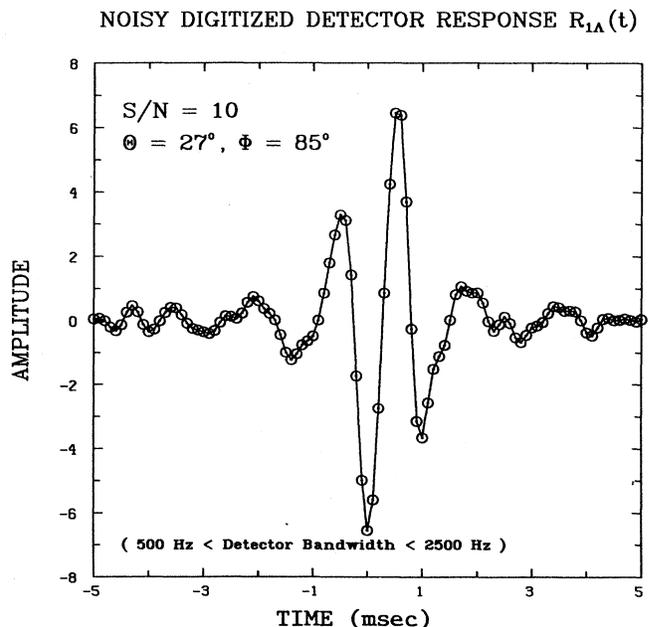NOISY DIGITIZED DETECTOR RESPONSE $R_{1\Lambda}(t)$

FIG. 7. The noisy digitized response for the east-coast detector in the receiver configuration as in Fig. 3. The source is assumed to be at the indicated location and the overall signal-to-noise ratio is 10. The two amplitudes of the incoming gravitational wave are shown in Figs. 16(a) and 16(b). The symbols ⊙ mark the digitized data points.
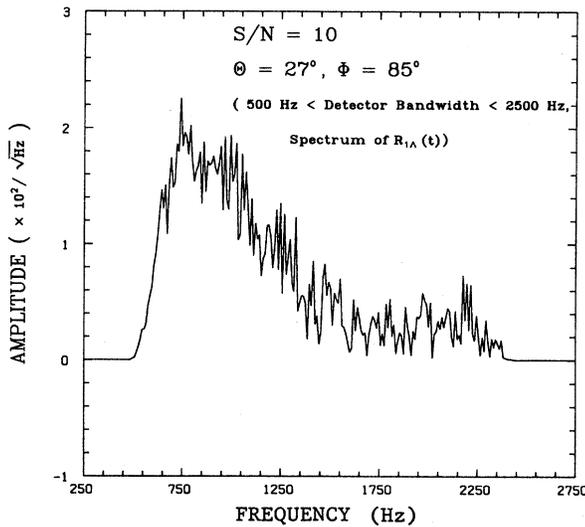
SPECTRUM OF THE DIGITIZED NOISY DETECTOR RESPONSE

FIG. 8. The square root of the suitably normalized power spectrum of the noisy response given in Fig. 7.

COMBED RESPONSE IN THE TIME DOMAIN FOR R_{1A} (t)
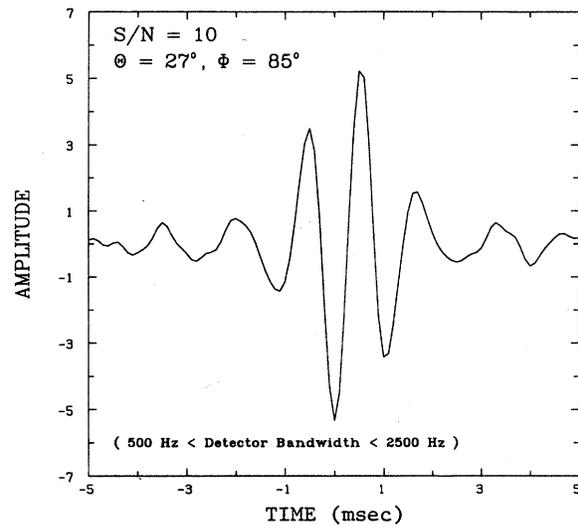
FIG. 10. The corresponding time domain function to the combed spectrum of Fig. 9.

determined optimal filter can still perform well.

If the spectrum of the signal is indistinguishable from that of the noise except by its amplitude in the total bandwidth under consideration, the near optimal filter will not supply any noise suppression. In this case the "unfiltered" method described in the previous section should be used.

In our implementation of the near-optimal filter, we choose the filter that maximizes the signal-to-noise ratio at the output of the filter as described by Eq. (5.5). We

will now describe the procedure to determine the near optimal filter for a sample noisy detector response from a single detector (in this case detector 1). As an example, $R_{1A}(t)$ might have the form shown in Fig. 7. We first compute the spectral density $S_{1A}(\omega)$ for "pure" noise $\Lambda_1(t)$ from a section of the data which does not contain the signal. The power spectrum of the noisy signal is then computed (Fig. 8). The amplitude in each frequency bin
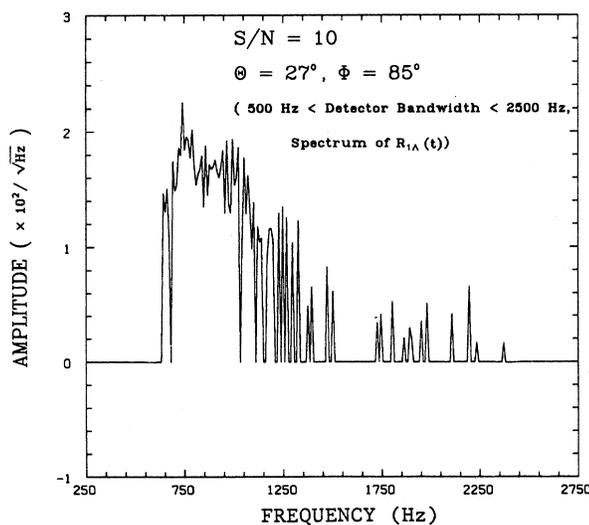
SPECTRUM OF THE COMBED NOISY DETECTOR RESPONSE

FIG. 9. The spectrum shown in Fig. 8 after it has passed through the comb filter.
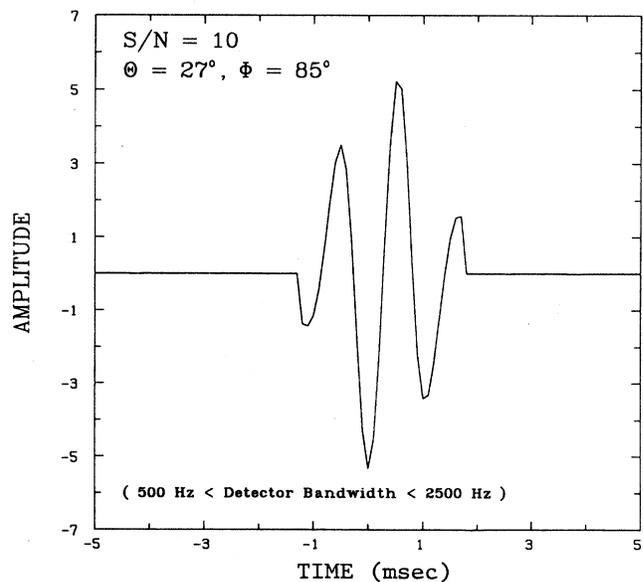
NEAR OPTIMAL FILTER FOR R_{1A} (t)

FIG. 11. The near optimal filter for the noisy response $R_{1A}(t)$ as shown in Fig. 7 obtained from the function shown in Fig. 10 by a threshold operation in the time domain.

in the power spectrum of the noisy signal is compared to the amplitude in the corresponding bin in the sample spectrum of the noise. If this amplitude is smaller than a certain multiple of the corresponding amplitude in the noise spectrum, then the corresponding frequency bins in the real and imaginary parts of the Fourier transform of the signal are set to zero. If it is larger, the corresponding bins in the real and imaginary parts of the Fourier transform of the signal are left unchanged. The power spectrum of the resulting "combed" signal is shown in Fig. 9. This combed signal is then transformed back to the time domain (Fig. 10). A threshold criterion is applied to the resulting signal setting to zero the external parts that are below the threshold value. The output of this operation is our near-optimal filter $Q(t)$ as shown in Fig. 11. We finally apply this filter to the original signal as described in Eqs. (5.4), (5.5) and the resulting filtered detector response is shown in Fig. 12.

We note that the detector responses for widely separated detectors on Earth do not have similar shapes (Fig. 13). This implies that the near-optimal filter derived for one of them is not in general near-optimal for the others. If each of the responses were filtered with its own near optimal filter then the time-delay information would be altered since different filters have different time delays. This would cause the method described in the previous section to break down.

The solution to this problem can be obtained by observing the fact that the least-squares function $I_\Lambda(\theta,\phi,t)$ as given in Eq. (4.2) should be filtered instead of the individual detector responses, since the source location is determined by minimizing the integral of $I_\Lambda^2(\theta,\phi,t)$.

To derive the near-optimal filter for $I_\Lambda(\theta,\phi,t)$ we proceed in the following manner: Let $\tilde{\Phi}_1(\omega)$, $\tilde{\Phi}_2(\omega)$, and $\tilde{\Phi}_3(\omega)$ be the near-optimal filters in the frequency domain for the detector responses $R_{1\Lambda}(t)$, $R_{2\Lambda}(t)$, and $R_{3\Lambda}(t)$, respectively. Because of the linearity of the filter one can easily prove that the near-optimal filter for the function given by Eq. (4.2) is a linear combination of the near optimal filters for the individual responses. If we define $\tilde{\Phi}_I(\omega)$ to be the near-optimal filter in the frequency domain for the function given by Eq. (4.2), we get

$$\tilde{\Phi}_I(\omega) = \frac{K_1 S_{1\Lambda}(\omega)\tilde{\Phi}_1(\omega)}{K_1^2 S_{1\Lambda}(\omega) + K_2^2 S_{2\Lambda}(\omega) + K_3^2 S_{3\Lambda}(\omega)}$$
$$+ \frac{K_2 S_{2\Lambda}(\omega)\tilde{\Phi}_2(\omega)}{K_1^2 S_{1\Lambda}(\omega) + K_2^2 S_{2\Lambda}(\omega) + K_3^2 S_{3\Lambda}(\omega)}$$
$$+ \frac{K_3 S_{3\Lambda}(\omega)\tilde{\Phi}_3(\omega)}{K_1^2 S_{1\Lambda}(\omega) + K_2^2 S_{2\Lambda}(\omega) + K_3^2 S_{3\Lambda}(\omega)} , \quad (5.12)$$

where $S_{1\Lambda}(\omega)$, $S_{2\Lambda}(\omega)$, and $S_{3\Lambda}(\omega)$ are the spectral densities of the noise processes $\Lambda_1(t)$, $\Lambda_2(t)$, and $\Lambda_3(t)$, respectively. Note that when we multiply the filter given by Eq. (5.12) by the Fourier transform of Eq. (4.2) and inverse Fourier transform the result, we obtain nine different terms which represent filtered responses of the detectors. More specifically, the near-optimally-filtered version of
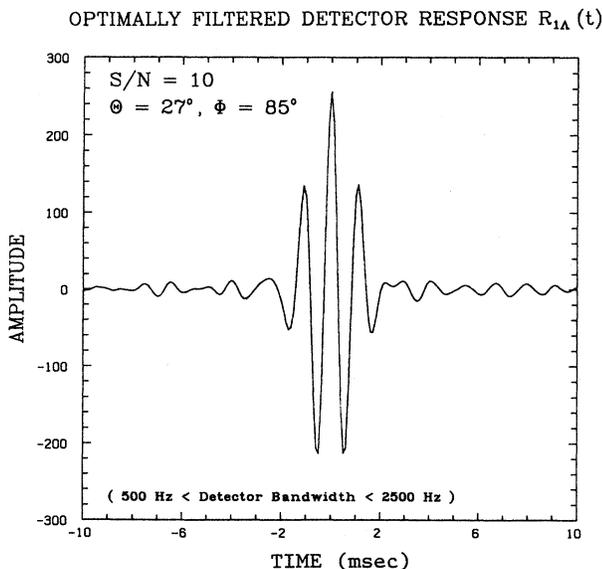
OPTIMALLY FILTERED DETECTOR RESPONSE $R_{1\Lambda}$ (t)

FIG. 12. The optimally filtered noisy response corresponding to $R_{1\Lambda}(t)$ shown in Fig. 7 filtered with the filter shown in Fig. 11.

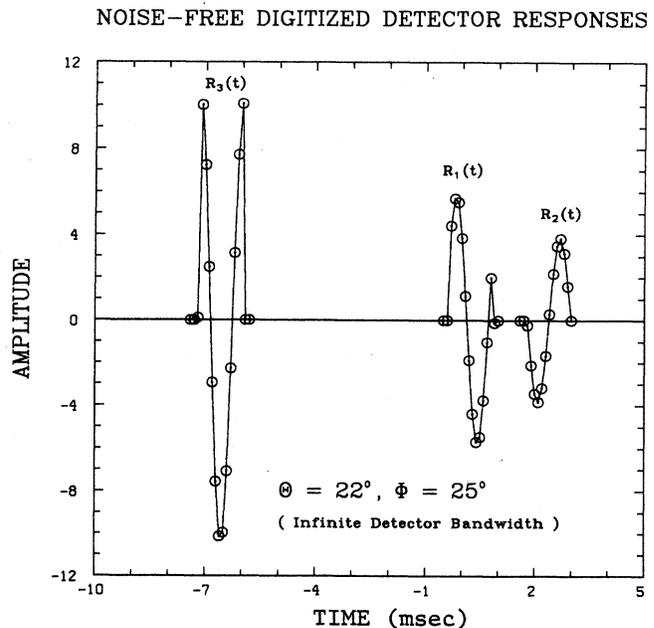NOISE−FREE DIGITIZED DETECTOR RESPONSES

FIG. 13. The noise-free detector responses in the detector configuration as in Fig. 3 illustrating the difference of the shapes of the functions as well as the relative time delays. The symbols ⊙ mark the digitized data points.

$I_\Lambda(\theta,\phi,t)$ is

$$C(\theta,\phi,t)=\frac{1}{2\pi}\int_{-\infty}^{+\infty}[K_1\tilde{R}_{1\Lambda}(\omega)+K_2\tilde{R}_{2\Lambda}(\omega)e^{i\omega\tau_{12}}+K_3\tilde{R}_{3\Lambda}(\omega)e^{i\omega\tau_{13}}]\tilde{\Phi}_I(\omega)e^{i\omega t}d\omega$$

$$=\frac{1}{2\pi}\int_{-\infty}^{+\infty}[K_1\tilde{R}_{1\Lambda}(\omega)+K_2\tilde{R}_{2\Lambda}(\omega)e^{i\omega\tau_{12}}+K_3\tilde{R}_{3\Lambda}(\omega)e^{i\omega\tau_{13}}]$$

$$\times\frac{K_1S_{1\Lambda}(\omega)\tilde{\Phi}_1(\omega)+K_2S_{2\Lambda}(\omega)\tilde{\Phi}_2(\omega)+K_3S_{3\Lambda}(\omega)\tilde{\Phi}_3(\omega)}{K_1^2S_{1\Lambda}(\omega)+K_2^2S_{2\Lambda}(\omega)+K_3^2S_{3\Lambda}(\omega)}e^{i\omega t}d\omega \ . \tag{5.13}$$

Expanding the terms out, we obtain

$$C(\theta,\phi,t)=\frac{1}{2\pi}\left[K_1^2\int_{-\infty}^{+\infty}\frac{\tilde{R}_{1\Lambda}(\omega)S_{1\Lambda}(\omega)\tilde{\Phi}_1(\omega)}{G(\theta,\phi,\omega)}e^{i\omega t}d\omega+K_1K_2\int_{-\infty}^{+\infty}\frac{\tilde{R}_{1\Lambda}(\omega)S_{2\Lambda}(\omega)\tilde{\Phi}_2(\omega)}{G(\theta,\phi,\omega)}e^{i\omega t}d\omega\right.$$

$$+K_1K_3\int_{-\infty}^{+\infty}\frac{\tilde{R}_{1\Lambda}(\omega)S_{3\Lambda}(\omega)\tilde{\Phi}_3(\omega)}{G(\theta,\phi,\omega)}e^{i\omega t}d\omega+K_1K_2\int_{-\infty}^{+\infty}\frac{\tilde{R}_{2\Lambda}(\omega)S_{1\Lambda}(\omega)\tilde{\Phi}_1(\omega)}{G(\theta,\phi,\omega)}e^{i\omega(t+\tau_{12})}d\omega$$

$$+K_2^2\int_{-\infty}^{+\infty}\frac{\tilde{R}_{2\Lambda}(\omega)S_{2\Lambda}(\omega)\tilde{\Phi}_2(\omega)}{G(\theta,\phi,\omega)}e^{i\omega(t+\tau_{12})}d\omega+K_2K_3\int_{-\infty}^{+\infty}\frac{\tilde{R}_{2\Lambda}(\omega)S_{3\Lambda}(\omega)\tilde{\Phi}_3(\omega)}{G(\theta,\phi,\omega)}e^{i\omega(t+\tau_{12})}d\omega$$

$$+K_1K_3\int_{-\infty}^{+\infty}\frac{\tilde{R}_{3\Lambda}(\omega)S_{1\Lambda}(\omega)\tilde{\Phi}_1(\omega)}{G(\theta,\phi,\omega)}e^{i\omega(t+\tau_{13})}d\omega+K_2K_3\int_{-\infty}^{+\infty}\frac{\tilde{R}_{3\Lambda}(\omega)S_{2\Lambda}(\omega)\tilde{\Phi}_2(\omega)}{G(\theta,\phi,\omega)}e^{i\omega(t+\tau_{13})}d\omega$$

$$\left.+K_3^2\int_{-\infty}^{+\infty}\frac{\tilde{R}_{3\Lambda}(\omega)S_{3\Lambda}(\omega)\tilde{\Phi}_3(\omega)}{G(\theta,\phi,\omega)}e^{i\omega(t+\tau_{13})}d\omega\right] \ , \tag{5.14}$$

where

$$G(\theta,\phi,\omega)=K_1^2S_{1\Lambda}(\omega)+K_2^2S_{2\Lambda}(\omega)+K_3^2S_{3\Lambda}(\omega) \ .$$

In terms of the nearly noise-free waveforms $Q_i(t)$, $i=1,2,3$ obtained using our near-optimal filter determination procedure, the near-optimal filters $\tilde{\Phi}_i(\omega)$, $i=1,2,3$ become

$$\tilde{\Phi}_1(\omega)=\frac{\tilde{Q}_1^*(\omega)}{S_{1\Lambda}(\omega)} \ , \tag{5.15}$$

$$\tilde{\Phi}_2(\omega)=\frac{\tilde{Q}_2^*(\omega)}{S_{2\Lambda}(\omega)}e^{-i\omega\tau_{12}} \ , \tag{5.16}$$

$$\tilde{\Phi}_3(\omega)=\frac{\tilde{Q}_3^*(\omega)}{S_{3\Lambda}(\omega)}e^{-i\omega\tau_{13}} \ . \tag{5.17}$$

After substituting Eqs. (5.15)–(5.17) in Eq. (5.14), consider a typical term in the resulting equation:

$$V_{3\Lambda}^{(2)}(\theta,\phi,t)=\frac{1}{2\pi}\int_{-\infty}^{+\infty}\frac{\tilde{R}_{3\Lambda}(\omega)\tilde{Q}_2^*(\omega)}{G(\theta,\phi,\omega)}e^{i\omega(t+\tau_{13}-\tau_{12})}d\omega \ , \tag{5.18}$$

where $V_{3\Lambda}^{(2)}(\theta,\phi,t)$ is the response $R_{3\Lambda}$ filtered with the filter Φ_2. We consider three cases. (i) The spectral densities of the noise in the detectors are constants (possibly different). In this case, the function

$$G(\theta,\phi)=K_1^2S_{1\Lambda}+K_2^2S_{2\Lambda}+K_3^2S_{3\Lambda}$$

is independent of the frequency and it can be factored out of the integral in Eq. (5.18). (ii) The spectral densities of the noise in the detectors are the same, but they are not

constant. In this case, the spectral density $S_\Lambda(\omega)$ can be factored out of the function G and the resulting

$$G(\theta,\phi)=K_1^2+K_2^2+K_3^2$$

can also be factored out of the integral in Eq. (5.18). (iii) The spectral densities of the noise in the detectors are not constant and they are all different. In this case the integral remains unchanged.

In the case (i), the typical term given by Eq. (5.18) can be written as

$$V_{3\Lambda}^{(2)}(\theta,\phi,t)=\frac{1}{G(\theta,\phi)}R_{3\Lambda}^{(2)}(t+\tau_{13}-\tau_{12}) \ ,$$

where $G(\theta,\phi)$ is as given in that case and

$$R_{3\Lambda}^{(2)}(t+\tau_{13}-\tau_{12})$$

$$=\frac{1}{2\pi}\int_{-\infty}^{+\infty}\tilde{R}_{3\Lambda}(\omega)\tilde{Q}_2^*(\omega)e^{i\omega(t+\tau_{13}-\tau_{12})}d\omega \ .$$

In the case (ii), the typical term given by Eq. (5.18) can be written as

$$V_{3\Lambda}^{(2)}(\theta,\phi,t)=\frac{1}{G(\theta,\phi)}R_{3\Lambda}^{(2)}(t+\tau_{13}-\tau_{12}) \ ,$$

where $G(\theta,\phi)$ is as given in that case and

$$R_{3\Lambda}^{(2)}(t+\tau_{13}-\tau_{12})$$

$$=\frac{1}{2\pi}\int_{-\infty}^{+\infty}\frac{\tilde{R}_{3\Lambda}(\omega)\tilde{Q}_2^*(\omega)}{S_\Lambda(\omega)}e^{i\omega(t+\tau_{13}-\tau_{12})}d\omega \ .$$

Note that the definition of $R_{3\Lambda}^{(2)}(t+\tau_{13}-\tau_{12})$ is different

in each case.

In these cases, the function $R_{3\Lambda}^{(2)}(t+\tau_{13}-\tau_{12})$ can be interpreted as the response $R_{3\Lambda}(t)$ filtered with the filter Φ_2 and shifted by the relative time delay $\tau_{13}-\tau_{12}$. Hence each of the frequency domain integrals in the functions $R_{n\Lambda}^{(m)}(t)$, $m,n=1,2,3$, has to be performed only once be-

fore the search for the correct time delays starts. The resulting functions are shifted as required by the relative trial time delays. The point is that the unfiltered responses have to be filtered only once. Then the filtered functions are used in the minimization procedure.

Define $C'(\theta,\phi,t)$ in the cases (i) and (ii) by

$$C'(\theta,\phi,t)=\frac{1}{G(\theta,\phi)}[K_1^2 R_{1\Lambda}^{(1)}(t)+K_2^2 R_{2\Lambda}^{(2)}(t)+K_3^2 R_{3\Lambda}^{(3)}(t)+K_1 K_2 R_{2\Lambda}^{(1)}(t+\tau_{12})+K_1 K_2 R_{1\Lambda}^{(2)}(t-\tau_{12})+K_1 K_3 R_{3\Lambda}^{(1)}(t+\tau_{13})$$

$$+K_1 K_3 R_{1\Lambda}^{(3)}(t-\tau_{13})+K_2 K_3 R_{3\Lambda}^{(2)}(t+\tau_{13}-\tau_{12})+K_2 K_3 R_{2\Lambda}^{(3)}(t-\tau_{13}+\tau_{12})]\ . \tag{5.19}$$

In terms of this function $C'(\theta,\phi,t)$, the near-optimally-filtered least-squares integral $L_\Lambda''(\theta,\phi)$ becomes

$$L_\Lambda''(\theta,\phi)=\frac{1}{\Delta t}\int_{t_0}^{t_1} C'^2(\theta,\phi,t)dt\ . \tag{5.20}$$

The advantage of this procedure is that we do not have to perform inverse Fourier transforms for each combination of time delays during the search because the exponential factors containing the trial time delays in the filter functions correspond to time-shifted filtered functions.

In the case (iii), the factorization of the angular functions from the frequency domain integrals cannot be accomplished in general. The filter still functions as described; however, an inverse Fourier transform has to be performed at each step in the search for the optimal time delays making the filtering procedure computationally more expensive. The least-squares integral $L_\Lambda''(\theta,\phi)$ retains its form given in Eq. (5.20), but the integrand $C'(\theta,\phi,t)$ becomes

$$C'(\theta,\phi,t)=K_1^2 V_{1\Lambda}^{(1)}(\theta,\phi,t)+K_2^2 V_{2\Lambda}^{(2)}(\theta,\phi,t)+K_3^2 V_{3\Lambda}^{(3)}(\theta,\phi,t)+K_1 K_2 V_{2\Lambda}^{(1)}(\theta,\phi,t)+K_1 K_2 V_{1\Lambda}^{(2)}(\theta,\phi,t)$$

$$+K_1 K_3 V_{3\Lambda}^{(1)}(\theta,\phi,t)+K_1 K_3 V_{1\Lambda}^{(3)}(\theta,\phi,t)+K_2 K_3 V_{3\Lambda}^{(2)}(\theta,\phi,t)+K_2 K_3 V_{2\Lambda}^{(3)}(\theta,\phi,t)\ .$$

In the following, we will compute the effect of the near optimal filtering process on the value of the least-squares function $L_\Lambda''(\theta_s,\phi_s)$ at the source location (θ_s,ϕ_s). This value is used in the next section to derive the estimates for the angular errors $(\Delta\theta,\Delta\phi)$ in the source location.

The near optimal filter described above is made out of three operations: The first one is the combing operation in the frequency domain; the second is the threshold operation in the time domain and the subsequent Fourier transform to the frequency domain; the third consists of the multiplication of the Fourier transform of the noisy signal with the function obtained in the first two operations, the division of the resulting function by the spectral density of the noise, and the subsequent inverse Fourier transform back to the time domain. The first operation can be represented mathematically in terms of a function $\tilde{Z}_1(\omega)$ which has a constant value when the power spectrum of the original signal at the frequency ω is above a certain multiple of the corresponding noise spectrum at the same frequency and it has the value 0 when the opposite condition holds. It is normalized in the frequency domain in the following way:

$$\int_{\omega_0}^{\omega_1}\tilde{Z}_1(\omega)d\omega=g\ ,$$

where g is the ratio of the total range of frequencies (bandwidth) in which $\tilde{Z}_1(\omega)\neq 0$ to the full band of integration, $\omega_1-\omega_0$. The combing operation is then simply multiplication of the Fourier transform of the original signal by the function $\tilde{Z}_1(\omega)$ in the frequency domain. The resulting function is then transformed back to the time domain where a threshold operation is performed on it. This threshold operation can be represented by a multiplication with a rectangular window with height 1 when the function is above the threshold value and height 0 when the opposite condition holds. The last multiplication with the rectangular window can be represented by a convolution in the frequency domain. Hence, the function $\tilde{U}(\theta,\phi,\omega)$ which corresponds to the function $\tilde{Q}(\omega)$ in Eq. (5.5) is given in the frequency domain by the expression

$$\tilde{U}(\theta,\phi,\omega)=\int_{-\infty}^{+\infty}\tilde{Z}_2(\omega-\omega')\tilde{Z}_1(\omega')\tilde{I}_\Lambda(\theta,\phi,\omega')d\omega'\ , \tag{5.21}$$

where $\tilde{I}_\Lambda(\theta,\phi,\omega)$ is the Fourier transform of the function $I_\Lambda(\theta,\phi,t)$ given in Eq. (4.2) and $\tilde{Z}_2(\omega)$ is the Fourier transform of the window function described above. The filtered function $\tilde{C}'(\theta,\phi,\omega)$ becomes

$$\tilde{C}'(\theta,\phi,\omega)=\tilde{I}_\Lambda(\theta,\phi,\omega)\frac{\tilde{U}^*(\theta,\phi,\omega)}{G(\theta,\phi,\omega)}\ . \tag{5.22}$$

Since $\tilde{I}_\Lambda(\theta,\phi,\omega)=\tilde{I}(\theta,\phi,\omega)+\tilde{M}_\Lambda(\theta,\phi,\omega)$ where $\tilde{I}(\theta,\phi,\omega)$ is the Fourier transform of the expression given in Eq. (3.7) and

$$\tilde{M}_\Lambda(\theta,\phi,\omega)=K_1(\theta,\phi)\tilde{\Lambda}_1(\omega)+K_2(\theta,\phi)\tilde{\Lambda}_2(\omega)+K_3(\theta,\phi)\tilde{\Lambda}_3(\omega)\ , \tag{5.23}$$

we obtain

$$\tilde{C}'(\theta,\phi,\omega) = \frac{\tilde{I}(\theta,\phi,\omega) + \tilde{M}_\Lambda(\theta,\phi,\omega)}{G(\theta,\phi,\omega)} \int_{-\infty}^{+\infty} \tilde{Z}_2^*(\omega-\omega')\tilde{Z}_1^*(\omega')[\tilde{I}^*(\theta,\phi,\omega') + \tilde{M}_\Lambda^*(\theta,\phi,\omega')]d\omega' \ . \tag{5.24}$$

Note that at the correct source location (θ_s,ϕ_s) the function $I(\theta_s,\phi_s,t)=0$. As a result, Eq. (5.24) gives

$$\tilde{C}'(\theta_s,\phi_s,\omega) = \frac{\tilde{M}_\Lambda(\theta_s,\phi_s,\omega)}{G(\theta_s,\phi_s,\omega)} \int_{-\infty}^{+\infty} \tilde{Z}_2^*(\omega-\omega')\tilde{Z}_1^*(\omega')\tilde{M}_\Lambda^*(\theta_s,\phi_s,\omega')d\omega' \ . \tag{5.25}$$

The corresponding least-squares-integrand function in the time domain is

$$C'(\theta_s,\phi_s,t) = \frac{1}{2\pi} \int_{-\infty}^{+\infty} \frac{\tilde{M}_\Lambda(\theta_s,\phi_s,\omega)}{G(\theta_s,\phi_s,\omega)} \int_{-\infty}^{+\infty} \tilde{Z}_2^*(\omega-\omega')\tilde{Z}_1^*(\omega')\tilde{M}_\Lambda^*(\theta_s,\phi_s,\omega')d\omega' e^{i\omega t}d\omega \ . \tag{5.26}$$

Eq. (5.26) can be rearranged to give

$$C'(\theta_s,\phi_s,t) = \frac{1}{2\pi} \int_{-\infty}^{+\infty}\int_{-\infty}^{+\infty} \frac{\tilde{M}_\Lambda(\theta_s,\phi_s,\omega)}{G(\theta_s,\phi_s,\omega)} \tilde{Z}_2^*(\omega-\omega')\tilde{Z}_1^*(\omega')\tilde{M}_\Lambda^*(\theta_s,\phi_s,\omega')e^{i\omega t}d\omega'd\omega \ . \tag{5.27}$$

Since all signals under consideration except $\tilde{Z}_2^*(\omega)$ are band-limited, we get

$$C'(\theta_s,\phi_s,t) = \frac{1}{2\pi} \int_{\omega_0}^{\omega_1}\int_{\omega_0}^{\omega_1} \frac{\tilde{M}_\Lambda(\theta_s,\phi_s,\omega)}{G(\theta_s,\phi_s,\omega)} \tilde{Z}_2^*(\omega-\omega')\tilde{Z}_1^*(\omega')\tilde{M}_\Lambda^*(\theta_s,\phi_s,\omega')e^{i\omega t}d\omega'd\omega$$

$$\leq \frac{1}{2\pi} \int_{\omega_0}^{\omega_1}\int_{\omega_0}^{\omega_1} \left| \frac{\tilde{M}_\Lambda(\theta_s,\phi_s,\omega)}{G(\theta_s,\phi_s,\omega)} \tilde{Z}_2^*(\omega-\omega')\tilde{Z}_1^*(\omega')\tilde{M}_\Lambda^*(\theta_s,\phi_s,\omega')e^{i\omega t} \right| d\omega'd\omega$$

$$\leq \frac{1}{2\pi} \int_{\omega_0}^{\omega_1}\int_{\omega_0}^{\omega_1} \left| \frac{\tilde{M}_\Lambda(\theta_s,\phi_s,\omega)}{G(\theta_s,\phi_s,\omega)} \tilde{M}_\Lambda^*(\theta_s,\phi_s,\omega') \right| |\tilde{Z}_2^*(\omega-\omega')||\tilde{Z}_1^*(\omega')|d\omega'd\omega \ , \tag{5.28}$$

where ω_0 and ω_1 are the limits of the passed band. Note that

$$\left| \frac{\tilde{M}_\Lambda(\theta_s,\phi_s,\omega)}{G(\theta_s,\phi_s,\omega)} \tilde{M}_\Lambda^*(\theta_s,\phi_s,\omega') \right| \leq \left| \frac{G_{max}(\theta_s,\phi_s,\omega)}{G_{min}(\theta_s,\phi_s,\omega)} \right| = u \ ,$$

where subscripts max and min refer to the minimum and the maximum values attained by the spectral density $G(\theta_s,\phi_s,\omega)$ in the band $\omega_0 \leq \omega \leq \omega_1$. u is 1 for white noise. Using the definition of $\tilde{Z}_1(\omega)$ we see that

$$|\tilde{Z}_1^*(\omega)| \leq \frac{g}{\omega_1-\omega_0} \ .$$

Since $Z_2(t)$ is a rectangular window with unit height and width $\Delta t = t_1 - t_0$, we get

$$|\tilde{Z}_2^*(\omega-\omega')| = \left| \frac{\sin[(\omega-\omega')\Delta t/2]}{(\omega-\omega')\Delta t/2} \right| \Delta t \leq \Delta t \ .$$

Substituting these results in Eq. (5.28), we obtain

$$C'(\theta_s,\phi_s,t) \leq \frac{1}{2\pi} ug\Delta\omega\Delta t \ , \tag{5.29}$$

where $\Delta\omega = \omega_1 - \omega_0$. Note that for Gaussian white noise, for the realistic bandwidths and pulse durations and for a reasonable threshold setting g, $C'(\theta_s,\phi_s,t) < 1$. Using Eq. (5.20), we get

$$L_\Lambda''(\theta_s,\phi_s) < 1 \ . \tag{5.30}$$

This result will be used in the next section to derive the estimate of the errors in the computed source location for the filtered least-squares function.

We will use the linear optimal filter described by Eq. (5.5) in this section. The reason for this is that the filter described by Eq. (5.11) is much more expensive computationally than (5.5). The filter (5.11) must be computed for each combination of trial time delays and then an inverse Fourier transform has to be performed in order to compute the value of the function $L_\Lambda''(\theta,\phi)$ at each (θ,ϕ). Note that we cannot perform the decomposition of the filter (5.11) in terms of the individual filters of the noisy responses as we did for the optimal filter described by Eq. (5.5) since the filter $\tilde{\Phi}(\omega)$ described by Eq. (5.11) is nonlinear.

The construction of the near optimal filter chosen above is not unique. An alternate method for realizing the filter (5.5) is to "smooth" the power spectrum of the noisy signal in the frequency band where the signal is stronger than the noise and to use the resulting "smooth" function as the filter for the responses. This procedure should be performed carefully to ensure that the filter thus obtained corresponds to a real function in the time domain. Then, the method of filtering chosen above can be used to construct the filtered least-squares function. One way to build such a filter is as follows: Consider the noisy signal in the frequency domain. Since the response

$R_\Lambda(t)$ is real in the time domain, its Fourier transform satisfies the condition $\widetilde{R}_\Lambda(\omega)=\widetilde{R}_\Lambda^*(-\omega)$. This implies that the real part and the imaginary part of $\widetilde{R}_\Lambda(\omega)$ satisfy

$$\text{Re}[\widetilde{R}_\Lambda(\omega)]=\text{Re}[\widetilde{R}_\Lambda(-\omega)],$$

$$\text{Im}[\widetilde{R}_\Lambda(\omega)]=-\text{Im}[\widetilde{R}_\Lambda(-\omega)] .$$

First, one smoothes the positive frequency section of the power spectrum of the signal. One way to do this is to treat the positive-frequency section of the power spectrum as a signal itself and to apply a low-pass filter to it. Other standard smoothing methods will also work. Let $\widetilde{P}(\omega)$ be the amplitude in the smoothed power spectrum at the frequency ω. Consider the real and the imaginary parts of the original signal at the same frequency. Let

$$a=|\text{Re}[\widetilde{R}_\Lambda(\omega)]|/|\text{Im}[\widetilde{R}_\Lambda(\omega)]| ,$$

$$b=\text{sgn}\{\text{Re}[\widetilde{R}_\Lambda(\omega)]\}, \quad d=\text{sgn}\{\text{Im}[\widetilde{R}_\Lambda(\omega)]\} .$$

Construct the new real and imaginary parts of the filter for positive frequencies in the following way:

$$\text{Re}[\widetilde{U}(\omega)]=b\left[\frac{a^2\widetilde{P}(\omega)}{1+a^2}\right]^{1/2} ,$$

$$\text{Im}[\widetilde{U}(\omega)]=d\left[\frac{\widetilde{P}(\omega)}{1+a^2}\right]^{1/2} .$$

The negative frequency part of the filter $\widetilde{U}(\omega)$ is computed according to the symmetry equations given above. This new filter $\widetilde{U}(\omega)$ has $\widetilde{P}(\omega)$ as its power spectrum amplitude at the frequency ω and its real and imaginary parts have the same phase relationship to each other as in the original signal. By its construction, this filter is a real function in the time domain. Note that the function $\widetilde{U}(\omega)$ is not necessarily smooth, but its power spectrum $\widetilde{P}(\omega)$ is smooth by construction.

Up to this point, intervals of integration are chosen by a threshold criterion. One may argue that by choosing a function of time which multiplies the least-squares integrand and vanishes beyond the "optimal" limits of integration, one can improve the signal-to-noise ratio in the least-squares function. Such an optimal "cutoff" function may not be a rectangular window with constant height.

We will now argue that the optimal cutoff function is a rectangular window whose extent is determined by the threshold criteria described in this section. If the cutoff function has any other shape, then finding the optimal shape corresponds to applying yet another optimal filter

to the minimized function which is already as optimally filtered as possible. This will not give anything new. It is also easy to deduce that any cutoff function whose duration exceeds the duration of our rectangular window will simply add more noise to the minimized function without improving the signal-to-noise ratio. Hence the rectangular window with unit height and with duration equal to the one obtained by the method described in the previous section is the optimal cutoff function with this near-optimal filter.

VI. THE ESTIMATES OF ERRORS

Consider the unfiltered least-squares function $L'_\Lambda(\theta,\phi)$ as described in Sec. IV [Eq. (4.14)]. Since we expect our solution to be near the actual source location for a good signal-to-noise ratio, we assume the least-squares function to be well approximated by a quadratic form in the neighborhood of the minimum as follows:

$$L'_\Lambda(\theta,\phi)\simeq L'_\Lambda(\theta_m,\phi_m)+\tfrac{1}{2}(\theta-\theta_m,\phi-\phi_m)\overleftrightarrow{H}'_m\begin{bmatrix}\theta-\theta_m\\\phi-\phi_m\end{bmatrix} ,$$

(6.1)

where $\overleftrightarrow{H}'_m$ is the Hessian matrix of $L'_\Lambda(\theta,\phi)$ evaluated at (θ_m,ϕ_m). The explicit form of this $\overleftrightarrow{H}'_m$ is given in Section A of Appendix B.

The Hessian matrix $\overleftrightarrow{H}'_m$ is formed out of the second derivatives of the function $L'_\Lambda(\theta,\phi)$ evaluated at the minimum and it contains information about the shape of the minimized function in the neighborhood of the minimum. Note that since $L'_\Lambda(\theta_m,\phi_m)$ is positive and $L'_\Lambda(\theta,\phi)$ is larger than the minimum value, the quadratic form

$$\tfrac{1}{2}(\theta-\theta_m,\phi-\phi_m)\overleftrightarrow{H}'_m\begin{bmatrix}\theta-\theta_m\\\phi-\phi_m\end{bmatrix}=L'_\Lambda(\theta,\phi)-L'_\Lambda(\theta_m,\phi_m)$$

(6.2)

is positive definite. Therefore, the shape of the function given by Eq. (6.1) is an elliptical paraboloid in a neighborhood of the minimum. Since we assumed a good signal-to-noise ratio, the actual source location will be in this neighborhood somewhere on the paraboloid. As the signal-to-noise ratio approaches infinity, the minimum will move to the actual source location. The quadratic form given by Eq. (6.1) is not diagonal in general. If it is diagonalized, its eigenvalues describe the curvature of the paraboloid along its principal directions and this provides an estimate of the errors caused by the noise.

At the actual source location (θ_s,ϕ_s) the value of the least-squares function $L'_\Lambda(\theta,\phi)$ is given by

$$L'_\Lambda(\theta_s,\phi_s)=\frac{1}{\Delta t}\int_{t_0}^{t_1}\frac{[K_1\Lambda_1(t)+K_2\Lambda_2(t+\tau_{12})+K_3\Lambda_3(t+\tau_{13})]^2}{K_1^2\sigma_1^2+K_2^2\sigma_2^2+K_3^2\sigma_3^2}dt , \tag{6.3}$$

where the functions K_1, K_2, K_3, τ_{12}, and τ_{13} are evaluated at the source location (θ_s,ϕ_s). Note that the value of this $L'_\Lambda(\theta_s,\phi_s)$ is

$$L'_\Lambda(\theta_s,\phi_s)=\lim_{T\to\infty}\frac{1}{T}\int_{-T/2}^{+T/2}\frac{[K_1\Lambda_1(t)+K_2\Lambda_2(t+\tau_{12})+K_3\Lambda_3(t+\tau_{13})]^2}{K_1^2\sigma_1^2+K_2^2\sigma_2^2+K_3^2\sigma_3^2}dt=1 . \tag{6.4}$$

Since the bandwidth of the detector outputs is limited, the relaxation time for the random processes $\Lambda_j(t)$, $j=1,2,3$, as seen through the limited bandwidth is equal to the period of the highest frequency in the band. If the time interval Δt is large compared to this relaxation time (as will be the case in the simulations in the next section), the actual value of $L'_\Lambda(\theta_s,\phi_s)$ will be close to unity.

Assuming that the actual source location (θ_s,ϕ_s) is in a small neighborhood of the minimum (θ_m,ϕ_m) of $L'_\Lambda(\theta,\phi)$ so that the expansion given by Eq. (6.1) is valid, we obtain

$$L'_\Lambda(\theta_s,\phi_s)\simeq L'_\Lambda(\theta_m,\phi_m)$$
$$+\tfrac{1}{2}(\theta_s-\theta_m,\phi_s-\phi_m)\overleftrightarrow{H}'_m\begin{bmatrix}\theta_s-\theta_m\\ \phi_s-\phi_m\end{bmatrix}. \quad (6.5)$$

Substituting 1 for $L'_\Lambda(\theta_s,\phi_s)$, we get

$$\tfrac{1}{2}(\theta_s-\theta_m,\phi_s-\phi_m)\overleftrightarrow{H}'_m\begin{bmatrix}\theta_s-\theta_m\\ \phi_s-\phi_m\end{bmatrix}=1-L'_\Lambda(\theta_m,\phi_m).$$
$$(6.6)$$

This is a quadratic equation for the errors $(\theta_s-\theta_m,\phi_s-\phi_m)$ with coefficients specified at the minimum point (θ_m,ϕ_m). We diagonalize the Hessian matrix to solve this equation.

The diagonalized Hessian is obtained by transferring to a new coordinate system which is determined by the eigenvectors of the Hessian. In this coordinate system (x_1,x_2) Eq. (6.6) becomes

$$\frac{(x_{1s}-x_{1m})^2}{(1/\lambda_+)}+\frac{(x_{2s}-x_{2m})^2}{(1/\lambda_-)}=1-L'_\Lambda(x_{1m},x_{2m}),\quad(6.7)$$

where λ_+ and λ_- are the eigenvalues of the Hessian. Note that the radii of curvature along the principal directions are given by the inverse square roots of the eigenvalues. The estimated errors in the original coordinate system (θ,ϕ) will in general be a linear combination of these radii. The explicit expressions for the angular errors $\Delta\theta$ and $\Delta\phi$ in terms of the Hessian are given in Appendix D. We point out that the estimated errors will get smaller as the noise level vanishes since the minimum $L'_\Lambda(\theta_m,\phi_m)$ approaches 1.

The analysis carried out above also holds for the filtered least-squares function defined in Sec. V. However, because of the results obtained in Sec. V [Eq. (5.30)], Eq. (6.6) takes the following form:

$$\tfrac{1}{2}(\theta_s-\theta_m,\phi_s-\phi_m)\overleftrightarrow{H}''_m\begin{bmatrix}\theta_s-\theta_m\\ \phi_s-\phi_m\end{bmatrix}=Y-L''_\Lambda(\theta_m,\phi_m),$$
$$(6.8)$$

where $\overleftrightarrow{H}''_m$ is the Hessian matrix of $L''_\Lambda(\theta,\phi)$ evaluated at the point (θ_m,ϕ_m) (see Appendix B 2) and $Y=L''_\Lambda(\theta_s,\phi_s)$ is smaller than 1.

In the absence of noise, the least-squares function can still be expressed in quadratic form near its minimum. The radii of curvature for the paraboloid which represents the noise-free least-squares function in a neigh-

borhood of the minimum value are smaller than the radii of curvature of the paraboloid which represents the noisy least-squares function in a neighborhood of its minimum. As the signal-to-noise ratio gets lower, the paraboloid opens up making the minimum less well defined. Therefore, the eigenvalues of the Hessian $\overleftrightarrow{H}''_m$ are larger than the eigenvalues of the Hessian $\overleftrightarrow{H}'_m$ if the filtering improves the signal-to-noise ratio.

As the signal-to-noise ratio increases, the minimum point of the paraboloid moves towards the actual source location which is at the value 1 for the unfiltered least-squares function and at the value Y for the filtered one. The estimated errors are proportional to the ratio of the difference between the values of the least-squares function at the actual source location and at the minimum, and the eigenvalues of the Hessian. Hence, we deduce that the estimated errors will be smaller for the filtered least-squares function in general. The actual elements of the Hessian are different for the two cases. Their explicit forms are given in Appendix B. A method for computing the probability distributions of the errors in the angles (θ,ϕ) is given in Appendix D.

If the signal-to-noise ratio is too low, the estimated errors given above may not be accurate. The reason for this is that as the signal-to-noise ratio gets lower the radii of curvature of the paraboloid defined by Eq. (6.7) grow larger making the minimum of the paraboloid harder to locate. Eventually, the minimization method will not be able to discriminate between the correct source direction and its mirror image with respect to the plane defined by the positions of the detectors; and the computed minimum may end up in the neighborhood of either point with equal probability. Note that with four detectors this difficulty is less pronounced since one will be able to perform the minimization around the approximate source location determined by using three independent relative time delays. We will examine this case in a future paper.

The errors $\Delta\theta$, $\Delta\phi$ in the determination of the source direction and the noise $\Lambda_j(t)$ in the detector responses $R_{j\Lambda}(t)$ will induce inaccuracies in the reconstructed gravitational waveforms $h_{\mathrm{opt}+}(t)$ and $h_{\mathrm{opt}\times}(t)$. Since these waveforms are functions of time, the errors in them are functions of time as well. Using Eqs. (4.17)–(4.19) and the corresponding equations for $h_\times(t)$ we get the following expressions for the error functions $\Delta h_{\mathrm{opt}+}(t)$ and $\Delta h_{\mathrm{opt}\times}(t)$:

$$\Delta h_{\mathrm{opt}+}(t)=\sum_{i=1}^{3}[\mu_{i+}(\theta,\phi,\Delta\theta,\Delta\phi)R_{i\Lambda}(t+\xi_i)$$
$$+\epsilon_{i+}(\theta,\phi,\Delta\theta,\Delta\phi)\dot{R}_{i\Lambda}(t+\xi_i)],\quad(6.9)$$

$$\Delta h_{\mathrm{opt}\times}(t)=\sum_{i=1}^{3}[\mu_{i\times}(\theta,\phi,\Delta\theta,\Delta\phi)R_{i\Lambda}(t+\xi_i)$$
$$+\epsilon_{i\times}(\theta,\phi,\Delta\theta,\Delta\phi)\dot{R}_{i\Lambda}(t+\xi_i)].\quad(6.10)$$

The angular functions μ_{i+},ϵ_{i+} and $\mu_{i\times},\epsilon_{i\times}$ are determined by the optimal choice of the reconstruction formula for the waveforms. The function ξ_i is the appropriate time delay for the response used. These functions are evaluated at the computed source direction which mini-

mizes the appropriate least-squares function. The explicit form of these functions are given in Appendix C. $\dot{R}_{i\Lambda}(t)$ is the time derivative of the noisy response $R_{i\Lambda}(t)$.

Finally, one can also define a measure of the inaccuracies in the functions $h_{\text{opt}+}(t)$ and $h_{\text{opt}\times}(t)$ in the following way:

$$\sigma_+^2 = \frac{1}{\Delta t_{ab}} \int_{t_a}^{t_b} \Delta h_{\text{opt}+}^2(t)dt \ , \tag{6.11a}$$

$$\sigma_\times^2 = \frac{1}{\Delta t_{ab}} \int_{t_a}^{t_b} \Delta h_{\text{opt}\times}^2(t)dt \ , \tag{6.11b}$$

where the integration range $\Delta t_{ab} = t_b - t_a$ is the common domain of definition of the noisy responses $R_{i\Lambda}(t)$, $i = 1,2,3$. Note that Eqs. (6.9)–(6.11) include both the errors due to the noise in the detectors and the errors in the determination of the source location.

VII. THE NUMERICAL IMPLEMENTATION

A. Simulation of the gravitational-wave signal

Once the detectors are built and operating, data from them will be kept in digitized form because of the ease of storage and manipulation. The algorithm described in this section assumes that the data are presented in this form. Because of the present unavailability of the data from wide-band gravitational wave detectors containing pulses with signal-to-noise ratios larger than 1, the incoming gravitational wave and the responses of the detectors have to be simulated in order to test the performance of the method described above. The simulation involves the construction of the continuous waveforms $h_+(t)$, $h_\times(t)$, the computation of the angular functions and the relative time delays related to the simulated source position, and the simulation of the instrument noise which gets added to the incoming noiseless waveforms. In addition, any other parameter of the receiving instrument which affects the responses has to be included. In our simulations we assume idealized detectors which are characterized by the formalism given in Sec. II and by the spectrum of their noise. Our idealized detectors are assumed to have two arms with identical length along two orthogonal directions. We assume that the noise in the receivers is Gaussian and white and their spectral densities are the same for all three detectors. Note that our filtered method works when the noise is not white and the spectral densities are different for the three detectors, since its derivation was carried out with arbitrary spectral densities. The numerical implementations are different for the cases (i), (ii), and (iii) described in Sec. V.

In our simulations, the detector responses are digitized with a sampling rate of 10 kHz. The "continuous" signal is simulated by a digitized waveform sampled at 80 kHz and spline fitted to produce the values between the sampling points. The clock for the continuous signal is not synchronized with the clocks which digitize the receiver responses. A random phase shift is added to the receiver digitization clocks relative to the continuous signal clock when the receiver responses are digitized. The receiver clocks are synchronized with each other.

In the simulations, the signal is constructed from two functions $h_+(t)$ and $h_\times(t)$. In one set of simulations, we use a one-cycle, circularly polarized sinusoid: $h_+(t) = A\sqrt{2}\cos(\omega t)$ and $h_\times(t) = A\sqrt{2}\sin(\omega t)$, $0 \le \omega t \le 2\pi$ where t is measured by the continuous signal clock. The frequency ω of these waveforms is randomly selected to place the largest frequency component of the wave at an arbitrary location in the frequency band under consideration. The waveforms are normalized so that the root-mean-squared amplitude for each of them is A.

The "continuous" receiver responses $R_j(t)$ are then constructed from these waveforms using Eqs. (3.1a)–(3.1c) with appropriately chosen angular functions and relative time delays which correspond to the simulated source location. These noise-free $R_j(t)$ are shown, for the above choice of $h_+(t)$ and $h_\times(t)$ and for a specific choice of detectors and source locations, in Fig. 13. The Gaussian white noise in each receiver is simulated by a normally distributed deviate with zero mean and unit variance.[26] This noise is added to the "continuous" signal at each tick of the clock for the "continuous" signal [Eqs. (4.1a)–(4.1c)]. This noisy digitized signal is then fitted by cubic splines to supply the values between the sampling points.

Since the root-mean-squared amplitude of the signal in an optimally oriented detector is A, this case can be thought of as having a signal-to-noise ratio

$$\frac{S}{N} \equiv \frac{A}{\sigma} \ , \tag{7.1}$$

where σ^2 is the variance of the Gaussian deviate described above. It is instructive to reexpress our definition (7.1) of signal-to-noise ratio in terms of the (white) spectral density of the detectors' noise S_h. Denote by $2f_{\max}$ the sampling frequency (80 kHz) used in our noise-generating procedure—so $f_{\max} = 40$ kHz is the highest frequency present in the noise. Then, because $\int_0^\infty S_h df = \sigma^2$, the spectral density of the noise is $S_h = \sigma^2/f_{\max}$; and thus our definition (7.1) is equivalent to

$$\frac{S}{N} = \frac{A}{\sqrt{S_h f_{\max}}} \ . \tag{7.2}$$

Figure 14 shows the spectral density S_h of the noise used in our simulations.

Having constructed the noisy "continuous" receiver responses $R_{j\Lambda}(t)$, we then filter them with a band-pass filter that has relatively sharp cutoffs at 500 Hz and 2500 Hz (Fig. 15). This filtering operation can be interpreted in two ways. First, the actual gravitational wave detectors are band-limited devices. The noise level rises at low frequencies due to seismic noise and other factors reducing the sensitivity and the dynamic range of the instrument. At high frequencies the resonances in the mechanical and electrical parts of the receiver servo system limit the dynamic range well before the photon counting noise becomes dominant. A high frequency cutoff is also needed to limit the data acquisition rate to a manageable level. We choose the cutoffs described above to correspond to the current operating band of a typical
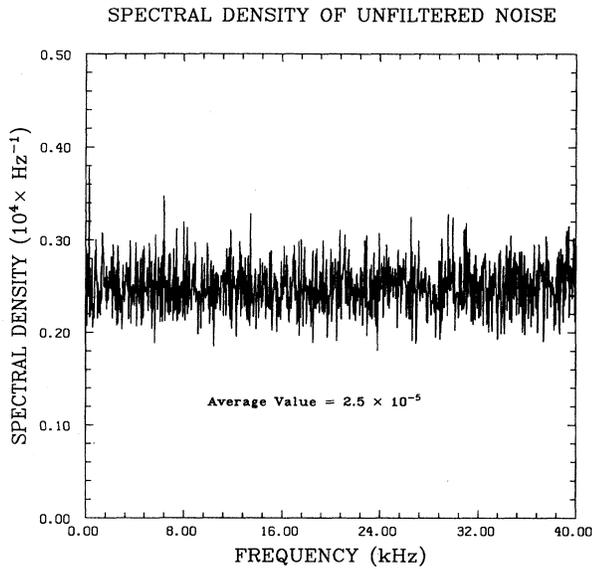
SPECTRAL DENSITY OF UNFILTERED NOISE

FIG. 14. The spectral density of the unfiltered noise used in the simulations.

laser interferometric gravitational wave detector proto-type.[8−10,12,27] Second, another way to interpret this band-pass filtering is to regard it as a preliminary filter in our method. The band-limited wave amplitudes $h_+(t)$ and $h_\times(t)$ of the two polarizations of the incoming gravitational waves are shown in Figs. 16(a) and 16(b).
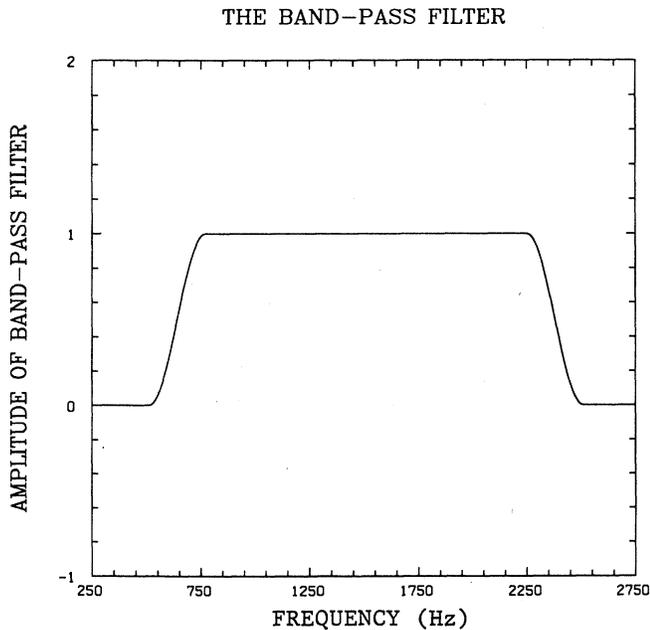
THE BAND−PASS FILTER

FIG. 15. The band-pass filter in the frequency domain. This filter is applied to every noisy response.

Often one encounters, for a broadband signal such as ours, an alternative definition of the signal-to-noise ratio:

$$\left[\frac{S}{N}\right]_{\text{alternative}} = \frac{A}{\sqrt{S_h \Delta f_{\text{band-pass}}}}$$

$$= \left[\frac{f_{\max}}{\Delta f_{\text{band-pass}}}\right]^{1/2} \frac{S}{N} \simeq (20)^{1/2} \frac{S}{N} . \quad (7.3)$$

Here $\Delta f_{\text{band-pass}} = 2$ kHz is the width of our band-pass filter. For example, this alternative definition is a good approximation to the more sophisticated one used by Thorne [Eq. (29) of Ref. 2]. Thus, our simulations, which entail $S/N = 10$ for an optimally oriented detector according to our definition, actually entail a larger $(S/N)_{\text{alternative}} \simeq 45$ for an optimally oriented detector according to the alternative definition. For a random orientation of the detector relative to the source, the signal-to-noise ratio will be reduced from these values by roughly a factor 2.

After the "continuous" detector responses are band-pass filtered, they are digitized at the rate of 10 kHz with synchronized receiver clocks. The minimum sampling rate for a signal whose largest frequency component is at ~ 2500 Hz is 5 kHz.[28] We choose to sample at twice the minimum rate to be able to perform fast reconstruction of the receiver responses from the digitized points without causing an excessive distortion in the reconstructed responses. We will discuss this choice in more detail when we address the reconstruction problem later in the following subsection.

In order to test the waveform independence of our method we also used a somewhat arbitrary waveform in another set of simulations. The band-pass filtered incoming waveforms $h_+(t)$ and $h_\times(t)$ corresponding to this wave are shown in Figs. 16(c) and 16(d). In this case, each wave amplitude is normalized in the manner described above. By contrast, with our previous $h_+(t)$ and $h_\times(t)$, these "arbitrary" $h_+(t)$ and $h_\times(t)$ are not related to each other by a simple phase shift; i.e., this wave does not have a well-defined polarization.

The simulation of the continuous signal is done in a subroutine of the main program that implements our method. This subroutine is written in such a manner as to provide digitized detector responses to the main program when given a source location, and it does not share any other information with the main program. Then the main program calls our method to get the computed source location and the reconstructed waveforms. The sets of Figs. 17–19 show contour plots of the maximum response amplitudes of the detectors for a given source location, as functions of the source location in the coordinate system described in Sec. II. Note that this coordinate system depends on the set of detectors under consideration. Hence a given source location corresponds to different coordinate angles for different sets of detectors. Compare these figures with the ones in sets 3–5 showing the geometric antenna patterns.

B. Reconstruction of the "continuous" signal

Since the responses of the detectors are kept in digitized form, the band-limited "continuous" responses have to be constructed out of them in order to be able to search for the correct time delays which are noninteger multiples of the sampling period in general. The sampling theorem governs the parameters of the digitization. It states that if a continuous function of time $h(t)$ is band limited, i.e., its Fourier transform vanishes above a cer-
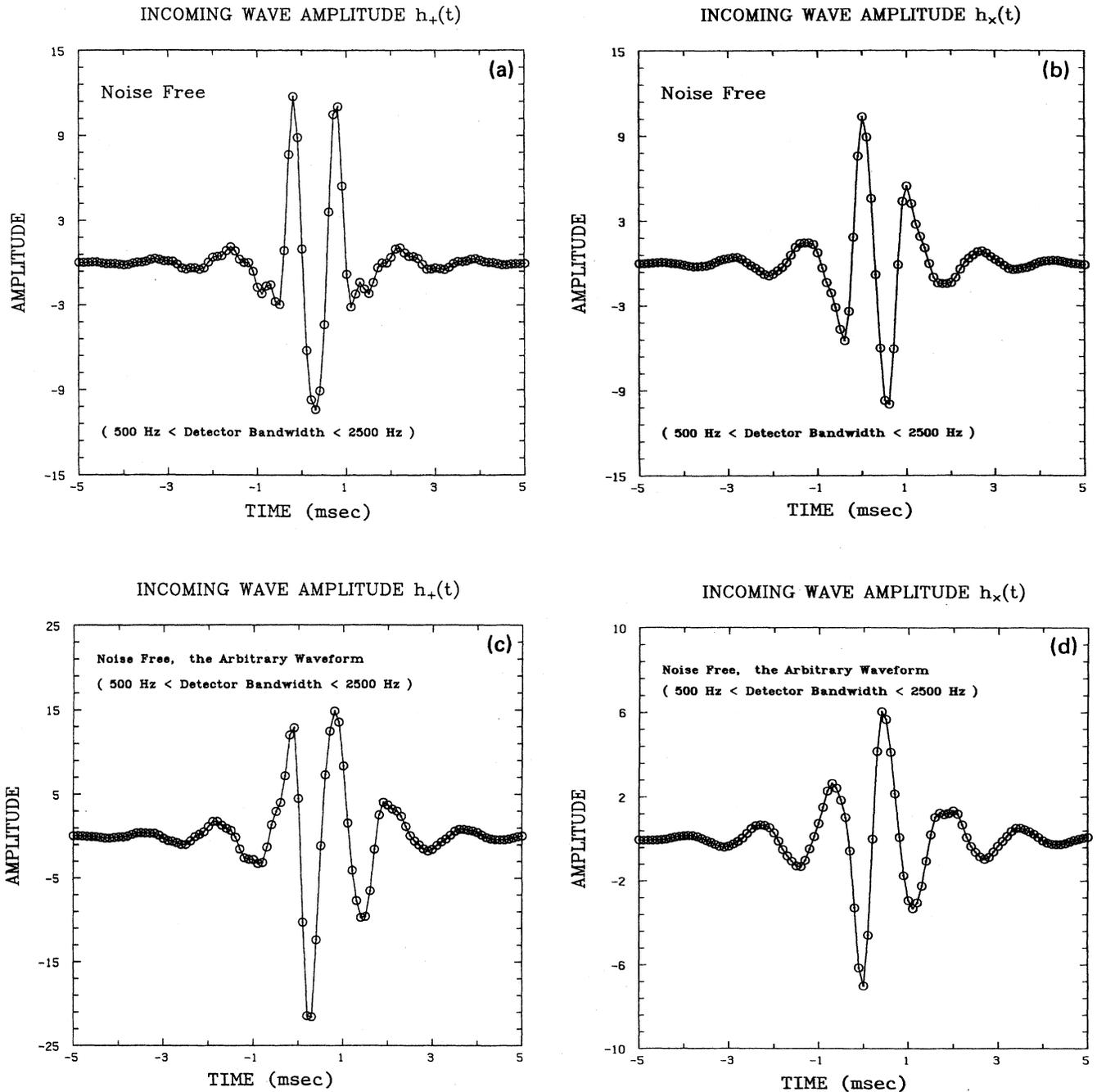
INCOMING WAVE AMPLITUDE $h_+(t)$

INCOMING WAVE AMPLITUDE $h_\times(t)$

INCOMING WAVE AMPLITUDE $h_+(t)$

INCOMING WAVE AMPLITUDE $h_\times(t)$

FIG. 16. The incoming band-limited wave amplitudes (a) $h_+(t)$ and (b) $h_\times(t)$ for single cycle, circularly polarized, sinusoidal pulses and the incoming band-limited wave amplitudes (c) $h_+(t)$ and (d) $h_\times(t)$ for an arbitrarily chosen nonsinusoidal waveform. The symbols ⊙ mark the digitized data points.
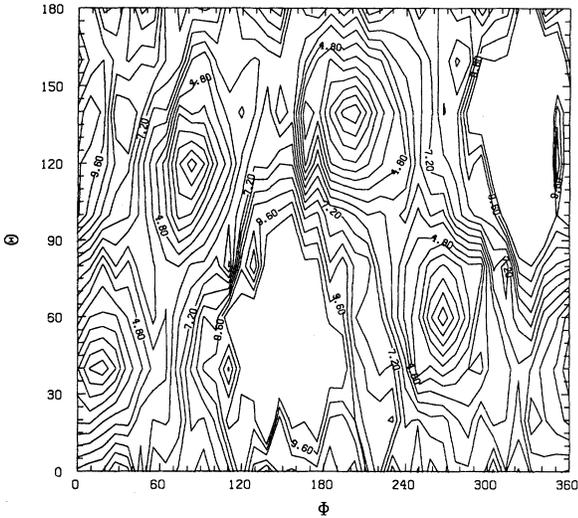
tain cutoff frequency f_c, then the function can be uniquely determined from a knowledge of its sampled values $\hat{h}(t)$:

$$\hat{h}(t) = \sum_{n=-\infty}^{+\infty} h(nT)\delta(t-nT) , \qquad (7.4)$$

where $T = 1/(2f_c)$. Note that the sampling frequency has to be at least twice the cutoff frequency; otherwise aliasing will occur. The reconstructed continuous function $h(t)$ is given by[28]

$$h(t) = T \sum_{n=-\infty}^{+\infty} h(nT)\frac{\sin 2\pi f_c(t-nT)}{\pi(t-nT)} . \qquad (7.5)$$

EASTERN SITE SKYMAP ($h_\times = h_+$, S/N = 10 , α = 72°)

WESTERN SITE SKYMAP ($h_\times = h_+$, S/N = 10 , α = 12°)

GERMANY SKYMAP ($h_\times = h_+$, S/N = 10 , α = 0°)

FIG. 17. The maximum amplitude of the noisy detector responses as a function of the source location (θ,ϕ) for detector configurations described in Fig. 3. The waveforms are single cycles of sinusoids. The amplitude of the waves emitted by the source is assumed to be a constant independent of the source location while the frequency of the pulses are allowed to vary randomly in the range [770 Hz, 2000 Hz]. The realization of the noise is computed to be randomly different for different source locations. The sources are uniformly distributed over the sky and the overall signal-to-noise ratio is 10 as defined in Sec. VII.

Although Eq. (7.5) describes how to construct the continuous function from its sampled values, it is of little use in practical applications where a large number of the values of the function at arbitrary times are required. Since the number N of digitized points is finite in reality, we assume that $h(nT)$ given in Eq. (7.5) is zero for values

of n outside the existing stretch of data and the series given by Eq. (7.5) becomes finite. However, for a typical data run that is just long enough to cover all possible time delays between the detector responses the number N is about 2000 for a sampling rate of 10 kHz. This implies that in order to obtain the value of the continuous

EASTERN SITE SKYMAP ($h_x = h_+$, S/N = 10 , $\alpha = 72°$)
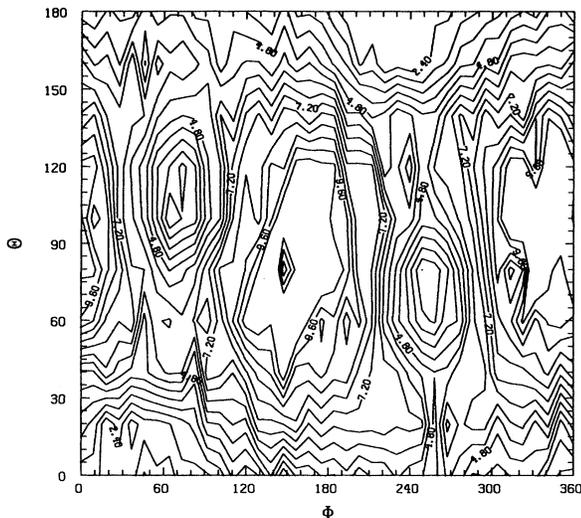
WESTERN SITE SKYMAP ($h_x = h_+$, S/N = 10 , $\alpha = 12°$)
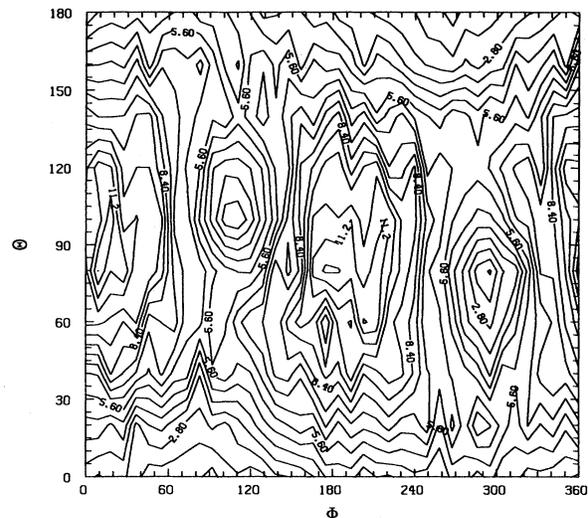
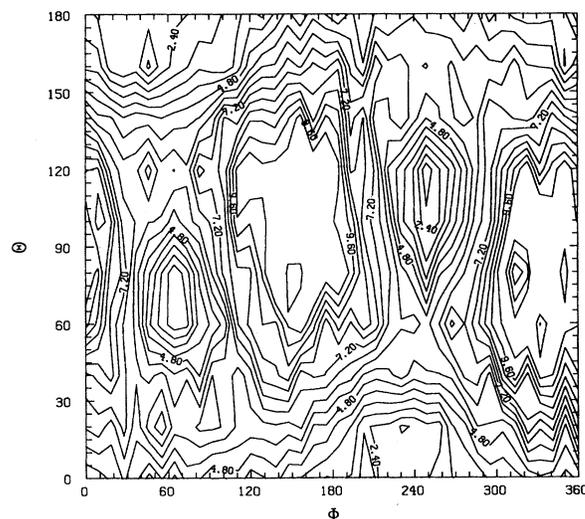AUSTRALIA SKYMAP ($h_x = h_+$, S/N = 10 , $\alpha = 76°$)

FIG. 18. The maximum amplitude of the noisy detector responses as a function of the source location (θ, ϕ) for detector configurations described in Fig. 4. The waveforms are single cycles of sinusoids. The amplitude of the waves emitted by the source is assumed to be a constant independent of the source location while the frequency of the pulses are allowed to vary randomly in the range [770 Hz, 2000 Hz]. The realization of the noise is computed to be randomly different for different source locations. The sources are uniformly distributed over the sky and the overall signal-to-noise ratio is 10 as defined in Sec. VII.

responses at a given time t a large number of trigonometric functions has to be computed. These facts make the direct use of Eq. (7.5) prohibitively expensive in implementing the method described in Secs. IV and V. The main reason for the computational cost is the requirement that the least-squares function must be computed for arbitrary time delays and for a large number of iterations in order to converge to the correct source direction. In addition, a numerical integration with possibly variable stepsize has to be performed in order to compute the least-squares function.

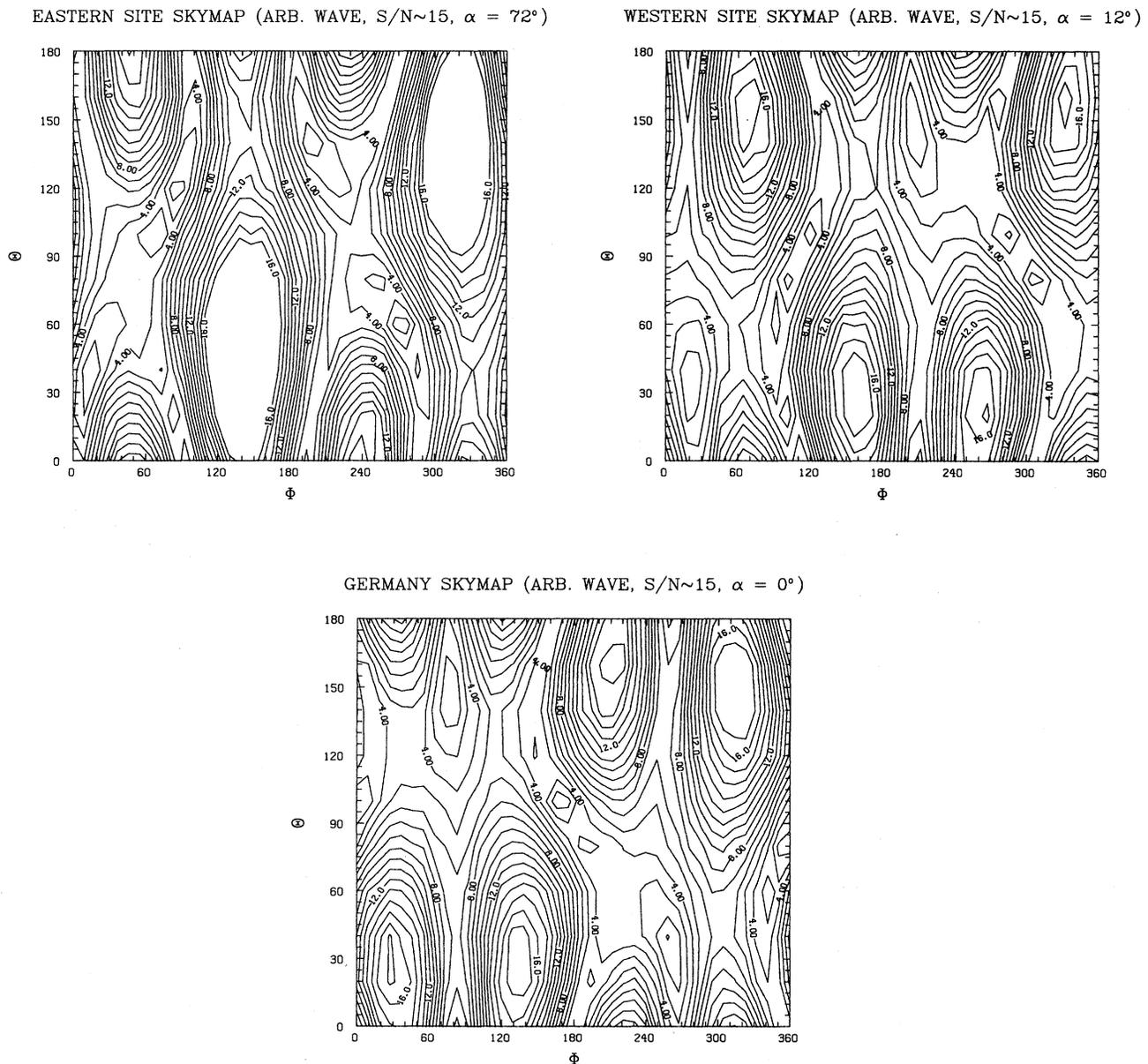An alternate approach to the reconstruction of the

EASTERN SITE SKYMAP (ARB. WAVE, S/N~15, α = 72°)

WESTERN SITE SKYMAP (ARB. WAVE, S/N~15, α = 12°)

GERMANY SKYMAP (ARB. WAVE, S/N~15, α = 0°)

FIG. 19. The maximum amplitude of the noisy detector responses as a function of the source location (θ,ϕ) for detector configurations described in Fig. 3. The waveforms are shown in Figs. 16(c) and 16(d). The root-mean-squared amplitude of the waves emitted by the source is assumed to be a constant independent of the source location. The realization of the noise is computed to be randomly different for different source locations. The sources are uniformly distributed over the sky and the overall signal-to-noise ratio is 15 as defined in Sec. VII.

continuous function is to use polynomial interpolation. If the outputs of the detectors are sampled at an adequate rate and they are band limited, we expect that the interpolated responses will not be too far off from the actual responses. The reason for this is that the signal has to change very rapidly between two consecutive samples in order to differ from the interpolated value significantly. This is not possible since the signal is band limited. The effect of interpolation is to introduce additional noise into the signal as compared to the signal reconstructed according to Eq. (7.5). If the level of this noise is small enough not to affect the accuracy of the method, the interpolation is acceptable. The advantage of the interpolation is that it is much faster computationally. The simplest form of interpolation is the linear interpolation. However this introduces too much noise into the interpolated response because it does not have continuous first derivatives at the sampling points. As we have seen in Sec. VI we need continuous second time derivatives of the responses in order to compute the estimated errors. The simplest choice that satisfies these criteria is the cubic spline interpolation, and we have chosen to implement it. Tests of the errors caused by cubic spline interpolation are discussed in the Sec. VII D.

C. The least-squares function

The least-squares functions are computed according to Eqs. (4.14) or (5.20) depending on whether the unfiltered or filtered version of the method is used. We computed the integrals in the time domain using a constant step integration technique. The step size of the integration was chosen to be a quarter of the sampling time, which gives a good compromise between the accuracy of integration and the time it takes to run the method. We note that the computation of the least-squares function is in the innermost loop of the method; hence the time it takes to complete the search for a given source location is directly proportional to the integration time.

The range of the integration has to be chosen carefully in order to avoid a reduction in accuracy due to the square-integrated noise when the signal is absent. The range of integration depends on the trial time delays. We separate the unsquared integrands given by Eqs. (4.2) and (5.19) into two parts: A template and a fit function. This separation is only employed while determining the integration range for each particular combination of the trial time delays. In the unfiltered case we consider the largest in absolute value of the three terms in Eq. (4.2) as the template, and the sum of the remaining two is taken to be the fit function. In the filtered case we consider the sum of the terms in Eq. (5.19) which do not contain any of the trial time delays as the template and the sum of the remaining terms as the fit function.

The stretch of data is scanned in the direction of increasing time with steps of length equal to the sampling time. When either the absolute value of the template or of the fit function exceeds a certain threshold, that time is taken to be the lower limit of the integration. The scan is then repeated starting from the other end of the stretch in the direction of decreasing time. When the condition

described above is met, that time is taken to be the upper limit of integration. The integration thresholds are chosen to be a certain fraction of the maximum amplitude in the template. The reason for this choice is that if the amplitude in the responses gets too small, the entire stretch of the data is used in the integration possibly leading to an inaccurate source location due to excessive noise contamination. This way the program is robust against the lack of signal in the data and it always produces an answer. The error estimates given in Sec. VI indicate whether the amplitudes are too low to cause a successful source location determination.

D. The minimizer

We minimize the least-squares functions defined by Eq. (4.14) and (5.20) with respect to the relative time delays. For a given pair of time delays there are two mirror image points in our coordinate system. We minimize the least squares function separately for these points. When the minima for the set of points is computed, we compare the values and we take the one which has the smallest value for the least-squares function. In the very unlikely case of equal minima we choose the upper point. In the absence of noise these minima can never be equal. The noise has to conspire to produce this pathological configuration. Since we assume the signal-to-noise ratio is larger than 2.1 $[(S/N)_{\text{alternative}} \simeq 10]$ at each detector, the pathological case never arises. Note that for pulse rates of about once a month and for a digitization rate of 10 kHz, the minimum threshold value for a single detector (for having one false alarm per month due to Gaussian white noise larger than this threshold) is equal to 1.5 times the root-mean-squared noise amplitude $[(S/N)_{\text{alternative}} \simeq 6.6]$. For three separated detectors running in coincidence, the minimum threshold goes down to 1.0 times the root-mean-squared noise amplitude for similar data rates and observation times $[(S/N)_{\text{alternative}} \simeq 4.5]$.[29]

The minimizer needs a starting point which is relatively close to the location of the expected minimum. A simpleminded guess is to compute an arrival time for each of the pulses and subtract the arrival times to get a pair of starting time delays. In the presence of noise, this procedure is not very reliable. An alternative to this approach is to compute a "center of amplitude" for each of the responses which is guaranteed to give a time value within the duration of the pulse. For a given detector response, we apply a threshold criterion to find the approximate starting and the ending times of the pulse. The stretch of data containing the pulse is scanned in the increasing time direction. When the absolute value of the amplitude exceeds a certain threshold we take that time to be the lower limit of the pulse. A similar scan is performed in the opposite direction starting from the other end of the stretch. When the same condition holds, the resulting time is taken to be the upper limit of the pulse. A "center of amplitude" T_{ica} for the pulse is then computed by the following expression:

$$T_{ica} = \frac{\int_{t_{il}}^{t_{iu}} t \, |R_{i\Lambda}(t)| \, dt}{\int_{t_{il}}^{t_{iu}} |R_{i\Lambda}(t)| \, dt} , \quad i = 1, 2, 3 , \qquad (7.6)$$

where t_{il} and t_{iu} are the lower and the upper limits of the pulse $R_{i\Lambda}(t)$, respectively. The initial relative time delays $\tau_{\text{init } 12}$ and $\tau_{\text{init } 13}$ are then computed by

$$\tau_{\text{init } 12} = T_{2\,ca} - T_{1\,ca}, \quad \tau_{\text{init } 13} = T_{3\,ca} - T_{1\,ca} . \qquad (7.7)$$

These initial time delays are not accurate enough to compute the source location. A search has to be performed in an area around this point in the two-dimensional space of trial relative time delays. Due to the complicated nature of the least-squares function in the presence of noise, the standard minimization methods that follow narrow valleys in the minimized function usually cannot reach the minimum if they are started from the point described above. In order to circumvent this problem, we perform an initial grid search in a patch surrounding the crude startup point. We choose a rectangular patch in the space of trial relative time delays. The size of this patch is decided by assuming a certain maximum error in the determination of the "center of amplitude" time delays. We subdivide this patch into small rectangles and we compute the least-squares function at each grid point. We then pick the point with the smallest least-squares value as the next starting point. We note that we compute the least-squares function for both of the mirror image source locations defined by the two trial time delays and we choose the one with the smaller least-squares function at each grid point. The resulting pair of time delays corresponding to the source location with the smallest least-squares value is used as the starting point of the next step of the minimizer. The next stage is a direction set minimization method known as the Powell minimizer.[30,31] This minimizer is run for a constant number of iterations on each of the two candidate source locations defined by the starting pair of relative time delays found by the previous stage of the minimizer and the answers it supplies are compared with each other. The one with the smaller least-squares value is taken to be the computed source location.

The Powell minimizer is an automatically stepping minimizer. This means that it is free to choose any time delay combination while searching for the minimum. If the trial time delays are unconstrained in magnitude, then the minimizer can get a low value by trying very large time delays which push parts of the responses out of the stretch of digitized data since we assume the signal is zero outside that stretch. To prevent this we implement a maximum trial time delay check in the least-squares integral. We estimate the accuracy of the "center of amplitude" algorithm, and we constrain the minimizer to a region in the search space centered around the starting point computed by the "center of amplitude" algorithm. The size of this region is proportional to the estimated accuracies for each coordinate in the search space. If the trial time delays result in a point which is outside this region, the least-squares integral returns a very large value which is not normally computed. This action prevents the minimizer from trying such time delays.

The number of grid points in the initial grid search and the number of iterations in the Powell minimizer are chosen by considering a variety of source locations and instances of noise. Note that in the noise-free case, the Powell minimizer can be run in a mode where it searches for the absolute minimum of the least-squares function which is zero. The number of iterations is left free and the minimizer stops when the computed minimum is in a neighborhood of zero with a specified accuracy. It is possible that in this mode the minimizer may not reach the absolute minimum when it is started from the initial point described above. The program checks for this possibility and refines the grid search to locate the minimum better.

This cannot be done in the noisy case, because the value of the minimum depends on the particular realization of the noise. Running the minimizer with a halting condition that depends on the relative change in the least-squares function (approximate local minimum) is not advised with this function, since it has a large number of such local minima in the presence of noise. The procedure employed above is analogous to integrating differential equations with a given step size. In order to check the answer one runs the integrator with a finer step size and checks whether the answer is stable against such disturbances.

A similar method can be applied in this case by changing the fineness of the grid search and the iteration count of the Powell minimizer. In our program, after the Powell minimizer has located an optimum position for the source, another grid search in a small neighborhood of this location is performed followed by another pass of the Powell minimizer. The answer thus obtained is printed out. The program has provisions of refining this procedure indefinitely. The only limitations to this procedure are the available precision of floating point arithmetic and the time it takes to compute these iterations.

In order to test the algorithm we implemented the noise-free case first. The reasons for this are as follows.

(a) The numerical precision that is necessary can only be decided by actually implementing the method and by running it for a few source locations and waveforms. Since we did not know in advance the absolute value of the difference of the least-squares function for the two mirror image points determined by the same time delays, the only way to test the method is to actually run it.

(b) There is a certain amount of numerical noise introduced by various approximations (cubic splines, time domain integration) made earlier. An estimate of the magnitude of this noise is necessary in order not to confuse it with the actual detector noise.

(c) The nature of the function $L(\theta, \phi)$ has to be examined in order to decide on a minimization strategy and to see how accurately one can locate sources that are placed in arbitrary directions in the sky.

The crude grid-search followed by Powell's algorithm as described above was run on simulated noise-free detector outputs. The standard single precision arithmetic as defined in FORTRAN 77 language (REAL*4) was used which allocated 32 bits per floating point number on the work

stations we used. The program was run for a number of source directions and for a number of detector orientations. The noise introduced by the cubic spline interpolation was found to be completely insignificant as well as the noise introduced by the finite-step time-domain integration. The minimizer was able to locate the source direction within 10^{-5} degrees in each of the two angles which define the source location without an excessive number of iterations.

E. Determination of the wave's parameters

The full test of the method is conducted by running it on simulated noisy detector responses for source locations, uniformly distributed over the sphere, defined by the angles θ, ϕ. The locations of the detectors are chosen to coincide with detector sites for large scale laser interferometric gravitational wave receivers considered in various proposals.[8-12] We assume that there are two detectors in the United States of America located on the east coast and the west coast. As a detector location in Europe, we choose a site in southern Germany which represents an average location for the future large scale interferometers planned by the British, the Italian-French and the German groups. To evaluate the effects of a longer baseline we also include a receiver located in Western Australia. The precise locations and the orientations of these detectors are given in Table I.

The orientations of the detectors are chosen according to the criteria given by Tinto and Schutz.[13,32] We pick the detector on the east coast of the United States of America as the reference detector to explain the optimal orientations. The west-coast detector is then oriented with the east-coast detector in such a way to optimize the mean coincidence probabilities for sources located in the Virgo cluster of galaxies. This alignment is near the optimal alignment for sources randomly distributed in the sky. The European detector is separately aligned with the east-coast detector according to the same criteria. After this procedure, the orientations of the European and the west-coast detector are near optimal when they are considered as a pair.[13] The Australian detector is aligned with the American pair in a similar manner. In order to see the dependence of the method on other possible orientations of the detectors, we also consider a case in which the west coast detector is rotated by 45° from the optimal orientation.

The sources are chosen to lie on a grid defined by the angles θ, ϕ; $0 \leq \theta \leq \pi$, $0 \leq \phi \leq 2\pi$ and the grid steps are $\pi/10$ in the angle θ, $\pi/20$ in the angle ϕ resulting in 400 grid points on the sphere. The number of points on the grid is limited to 400 because of the computational time limits imposed by the speed of the computing machinery we used. The amplitudes A of the waves emitted by the sources are assumed to be a constant independent of the source location while the frequencies $\omega/2\pi$ of the pulses are allowed to vary randomly in the range [770 Hz, 2000 Hz]. The realization of the noise is computed to be randomly different for different source locations.

In certain directions in the sky, the signal-to-noise ratio for a given receiver falls below the threshold value of 2.1 [$(S/N)_{\text{alternative}} = 10$] due to the variations in the antenna pattern. Such points are removed from the simulation since our method does not always converge to the correct source location in these cases. The number of such directions is less than 10% of the total number of source locations considered.

As a test of the adequacy of the source location grid, we run the method with a 10 times finer grid restricted to one quarter of the whole sphere. The answers are in agreement with the main results. We also run the method for three different values of the optimally oriented signal-to-noise ratio: 10, 30, 50 [or $(S/N)_{\text{alternative}} \simeq 45$, 135, 225]. For larger values of the signal-to-noise ratio the number of source locations which gave poor amplitudes is considerably reduced since the large signal-to-noise ratio compensates for the unfavorable antenna response. The program failed to find the location of the source in about 2% of all the source locations which produced larger than threshold amplitudes in all three detector responses. An analysis of such points will be given in the next subsection. We note that the initial thresholds in the program were set before the program started and the program automatically selected to alter them for the source locations under consideration in a given simulation without human intervention or a prior knowledge of the source locations and amplitudes. The filters in the program usually start with a threshold value which is certain to be too high and lower it in a smooth fashion in such a way that the maximum amplitude of the filtered pulse is not less than 75% of the maximum amplitude of the unfiltered pulse.

The reconstruction of the two independent wave amplitudes of the gravitational-wave $h_+(t)$ and $h_\times(t)$ is performed after the source location is computed, according to the algorithm described at the end of Sec. IV and in Appendix C.

F. Analysis of failed points

As mentioned above, the program failed to find the correct source location in about 2% of the trial source locations which resulted in above-threshold amplitudes in all three detectors. The failure was marked by the fact that the actual error in the source location was of the order of 20° in either of the angles θ, ϕ. The reason for this is determined to be the following: Although the Powell minimizer is restricted to try time delays that are within the initial delay range mentioned above, it can still try time delays which will lead it out of the range of the initial crude grid search. If the minimizer is not able to get back into this range because of the nature of the particular instance of noise, it falls into the next local minimum which does not correspond to the correct source location. A further restriction of the minimizer to the range of the prior grid search caused the minimizer to converge to the correct source location.

G. Computing resources, precision, and timing

The program was run on several different brands of computers with various speeds and precision. The computers used were Cray X-MP/48, Masscomp MC-5500,
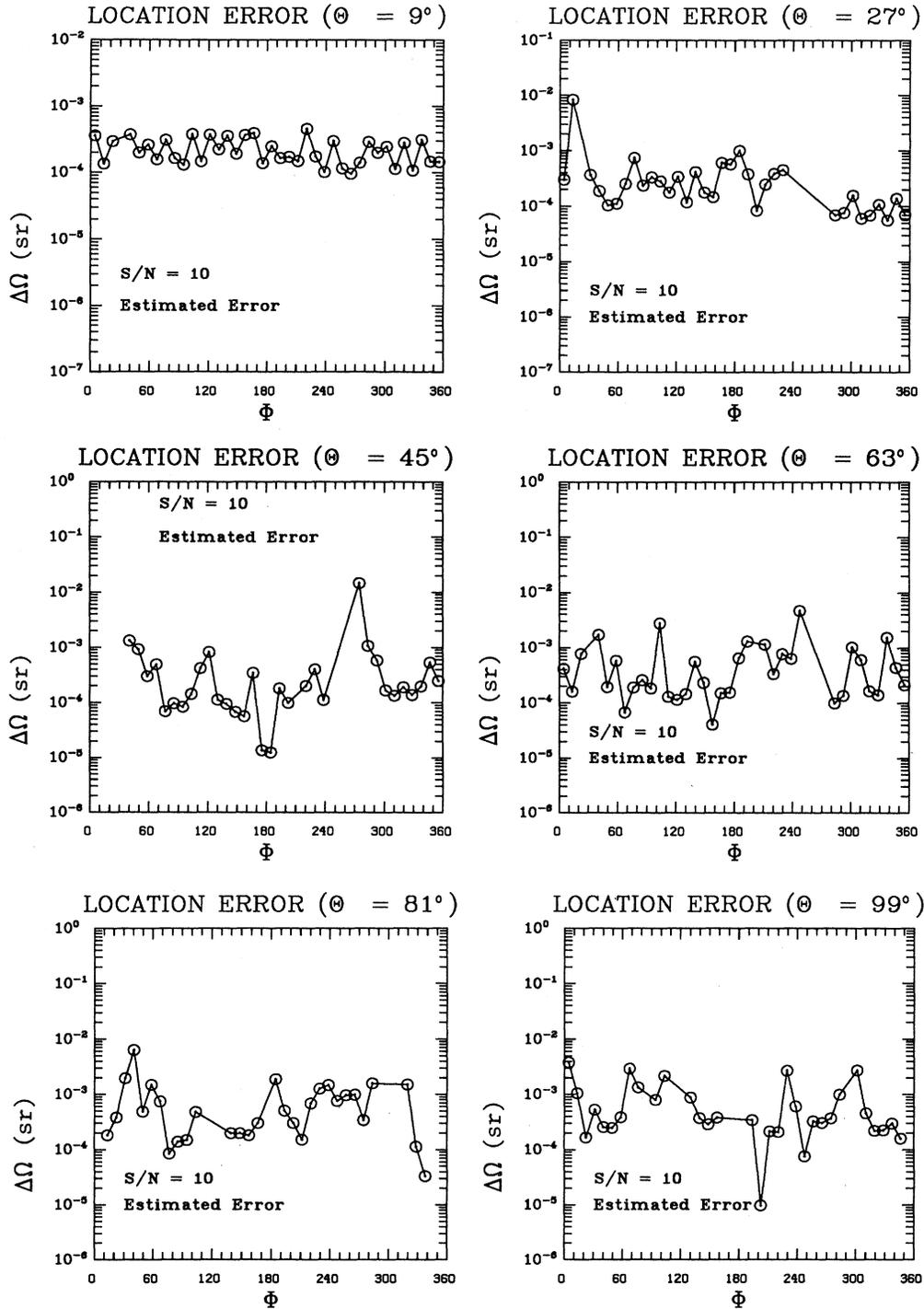
FIG. 20. The estimated error $\Delta\Omega_{est}$ [Eq. (8.1a)] and the actual error $\Delta\Omega_{act}$ [Eq. (8.2)] in the source location as functions of (θ, ϕ). The detector configuration is described in Fig. 3. The waveforms are single cycles of sinusoids. The amplitude of the waves emitted by the source is assumed to be a constant independent of the source location while the frequency of the pulses are allowed to vary randomly in the range [770 Hz, 2000 Hz]. The realization of the noise is computed to be randomly different for different source locations. The sources are uniformly distributed over the sky and the signal-to-noise ratio is 10 as defined in Sec. VII. The symbols ⊙ mark the simulated source locations. A line is drawn through them to emphasize the sequential order of the simulated points. The source locations which produced maximum detector responses below a threshold of 2.1 times the root-mean-squared noise level are not displayed.
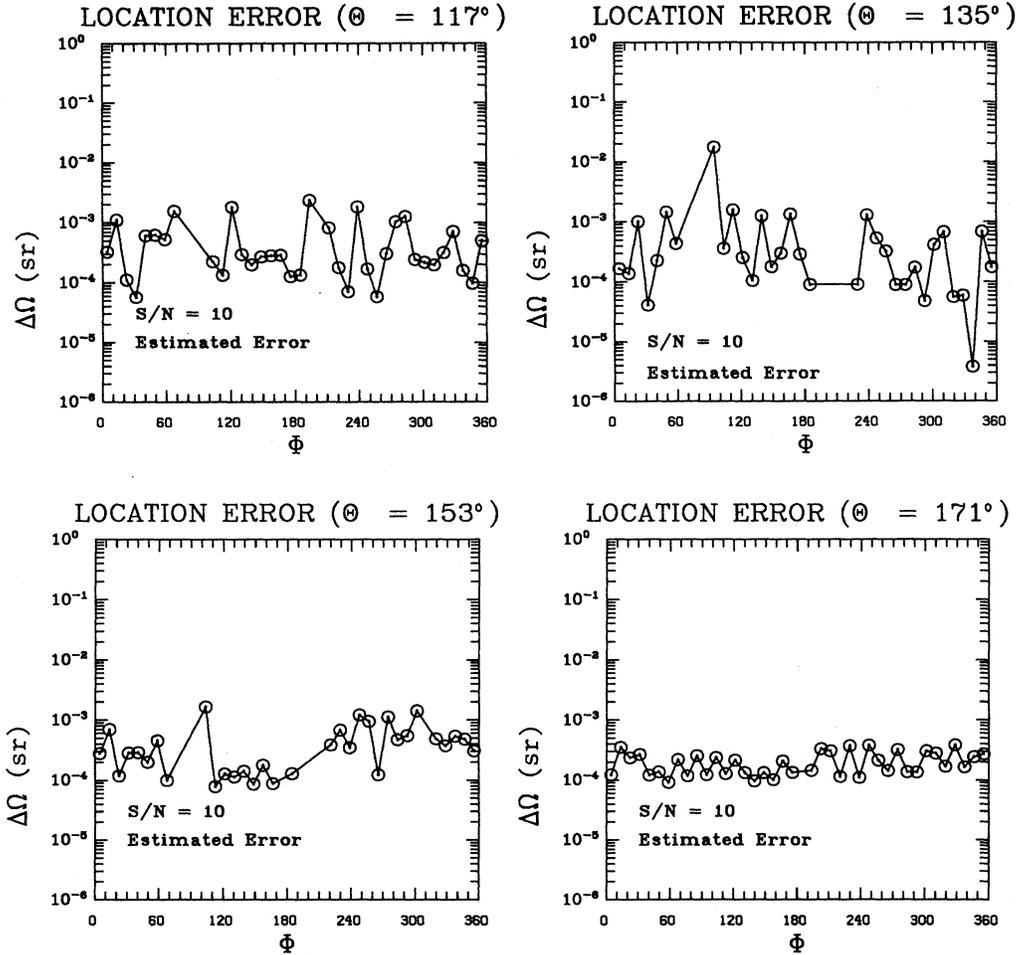
FIG. 20. (*Continued*).

Ridge 3200, Sun 3/50, Sun 3/160, Sun 4/160, and Sun 4/260 in alphabetical order. The noise-free program was developed on the Ridge. The noisy algorithm was developed on the Masscomp and the Suns. All of the simulations were run on the Suns in single precision. The program was then ported to the Cray and vectorized. The resulting code was run on the Cray in Cray single precision which had twice as many digits as the Suns for two full simulations: one optimally filtered and one unfiltered. The same program which ran on the Cray was then run on the Suns to check the effects of the precision difference between the two computers. No significant difference in the accuracy of the source location determination was observed.

On the Sun 4/260, the average time to determine one source location was 15 min for the unfiltered algorithm and 30 min for the filtered algorithm. The Cray was found to be 70 to 100 times faster than this work station.

VIII. RESULTS

The sets of Figs. 20–23 summarize the estimated and the actual errors in the source location for the simula-

tions mentioned above. The estimated errors are computed using the formulas given in Sec. VI. The actual errors are computed by comparing the simulated source location to the computed one. Note that the errors in the source location in these figures are expressed in terms of the solid angle $\Delta\Omega$.

The estimated error $\Delta\Omega_{est}$ is taken to be the area of the ellipse defined by Eq. (6.6) in the unfiltered case and by Eq. (6.8) in the near-optimally-filtered case. The expression for the area of this ellipse in the unfiltered case is

$$\Delta\Omega_{est} = \pi \frac{1 - L'_\Lambda(\theta_m, \phi_m)}{(\lambda_+ \lambda_-)^{1/2}} . \qquad (8.1a)$$

Here λ_+ and λ_- are the eigenvalues of the Hessian of the least-squares function $L'_\Lambda(\theta, \phi)$ evaluated at the minimum point (θ_m, ϕ_m) [Eqs. (6.7) and (D6)]. In the near-optimally-filtered case, Eq. (8.1a) becomes

$$\Delta\Omega_{est} = \pi \frac{1 - L''_\Lambda(\theta_m, \phi_m)}{(\lambda'_+ \lambda'_-)^{1/2}} , \qquad (8.1b)$$

where λ'_+ and λ'_- are the eigenvalues of the Hessian of

FIG. 20. (*Continued*).

LOCATION ERROR (Θ = 117°)   LOCATION ERROR (Θ = 135°)

LOCATION ERROR (Θ = 153°)   LOCATION ERROR (Θ = 171°)
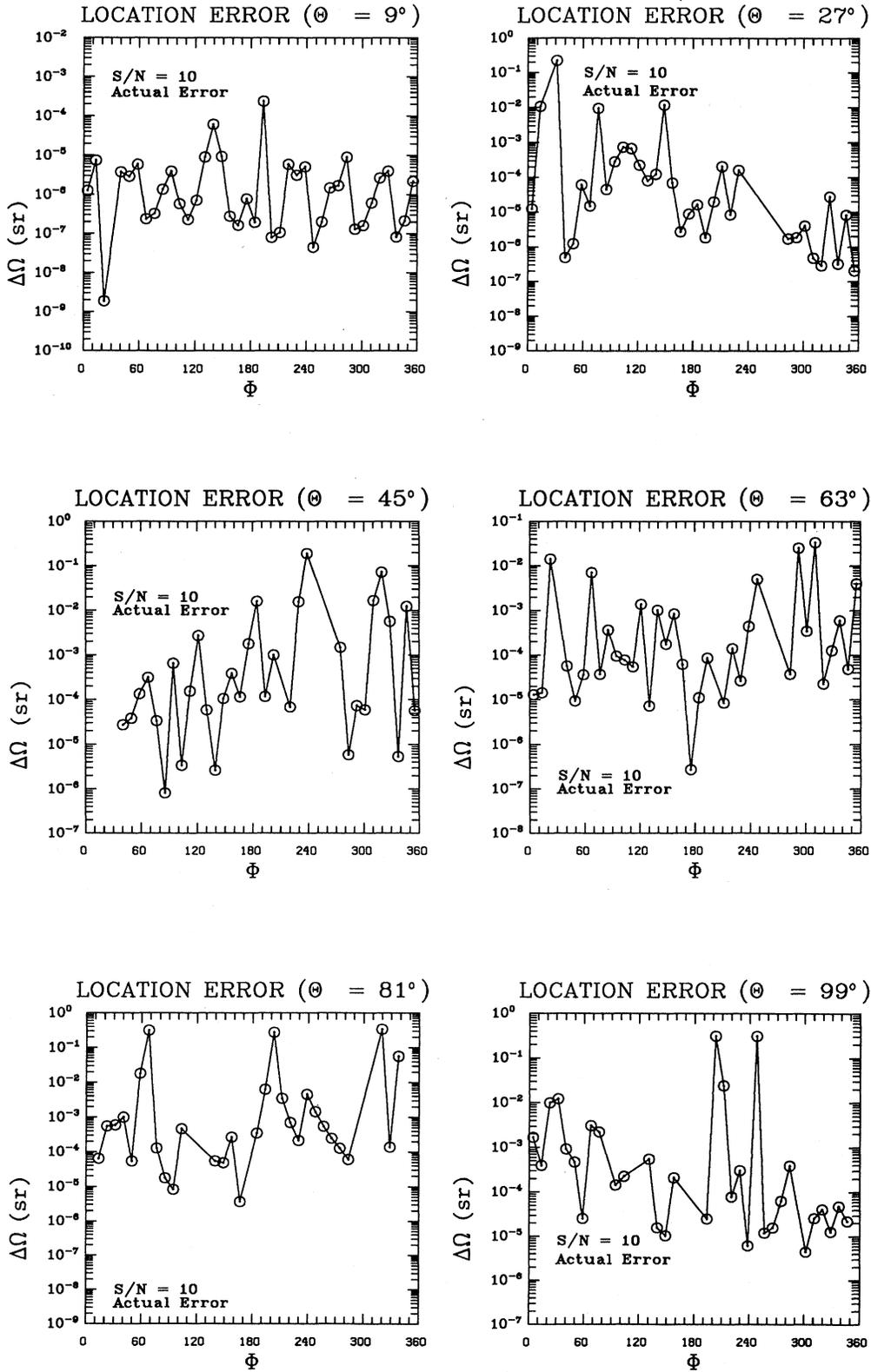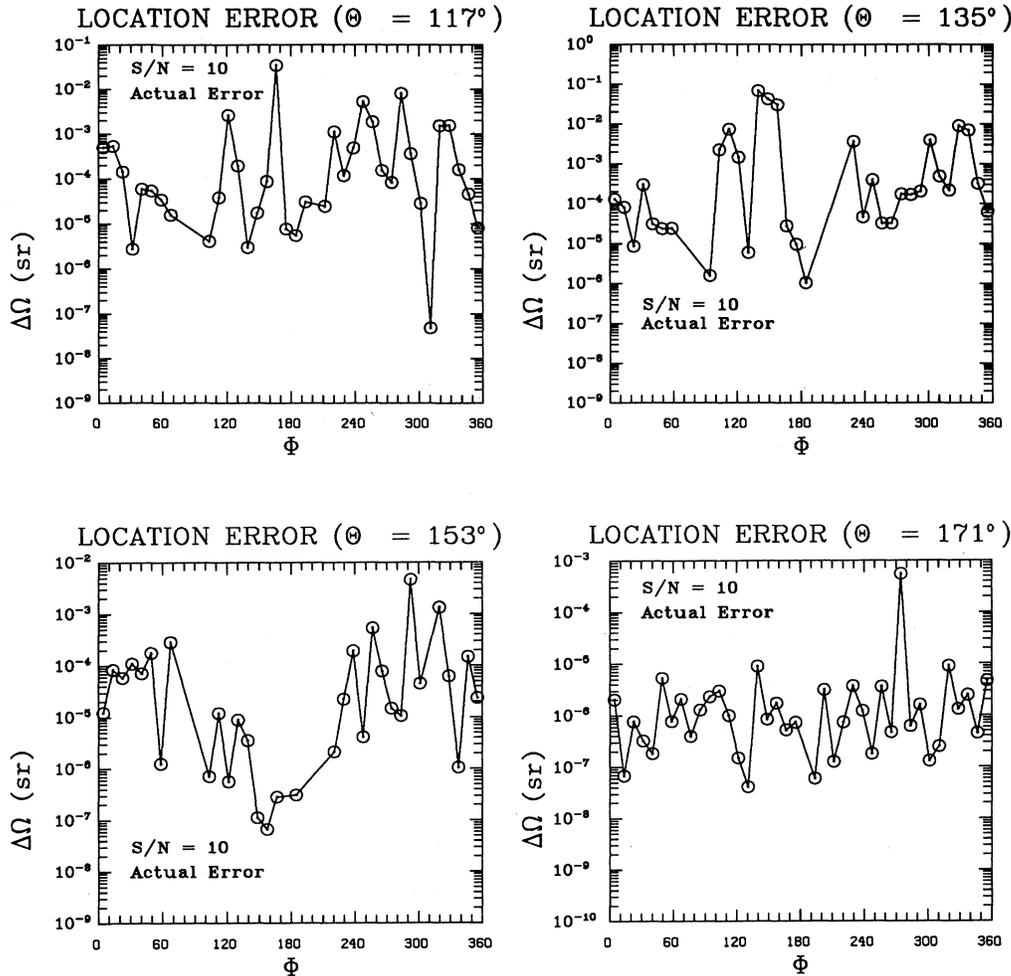
FIG. 20. (*Continued*).

the least-squares function $L''_\Lambda(\theta,\phi)$ evaluated at the minimum point (θ_m,ϕ_m).

The actual error $\Delta\Omega_{act}$ is computed using the formula

$$\Delta\Omega_{act} = \pi[(\theta_{comp}-\theta_{act})^2 + \sin^2(\theta_{act})(\phi_{comp}-\phi_{act})^2] \, ,$$

(8.2)

where θ_{comp}, ϕ_{comp} are the computed source coordinates; θ_{act}, ϕ_{act} are the actual source coordinates. Equation (8.2) gives the area of the circle on the unit sphere centered on the actual source location with radius equal to the length of the difference vector between the computed and the actual source locations. We assume that the computed source location is likely to fall anywhere in this circle with different realizations of the simulated noise for a given signal-to-noise ratio.

The plots in each set of figures show the error in the source location $\Delta\Omega$—estimated or actual—as a function of the coordinate angle ϕ and for a particular coordinate angle θ. The symbol $\odot$ marks the points we have in the simulation. Lines are drawn through them to aid in distinguishing the ordering.

We see that for a signal-to-noise ratio of at least 2.1 $[(S/N)_{alternative} \simeq 10]$ in each detector, the average actual error given by the unfiltered method is about 1×10^{-4} sr, while the filtered case gives a location error of 1×10^{-5} sr. The estimated errors are 5 to 10 times larger than the actual ones in the unfiltered case and the filtered method produces tighter error estimates. The errors decrease as the signal-to-noise ratio increases. The rotated detector and the change in the waveform do not alter these results significantly. [This insensitivity to detector rotation is what one should expect in our case of circularly polarized waves [Figs. 16(a), 16(b)] or the arbitrary wave [Figs. 16(c), 16(d)]. For linearly polarized waves there would probably be a sensitivity to rotation. However, we have not explored this case.] There is a slight decrease in the errors when a longer baseline is used.

The errors quoted above are in good agreement with the approximate geometric formula for the error in the source location in terms of the uncertainties in the time delays $\Delta\tau_{12}$, $\Delta\tau_{13}$ and the area A of the triangle defined by the detector locations:[33]
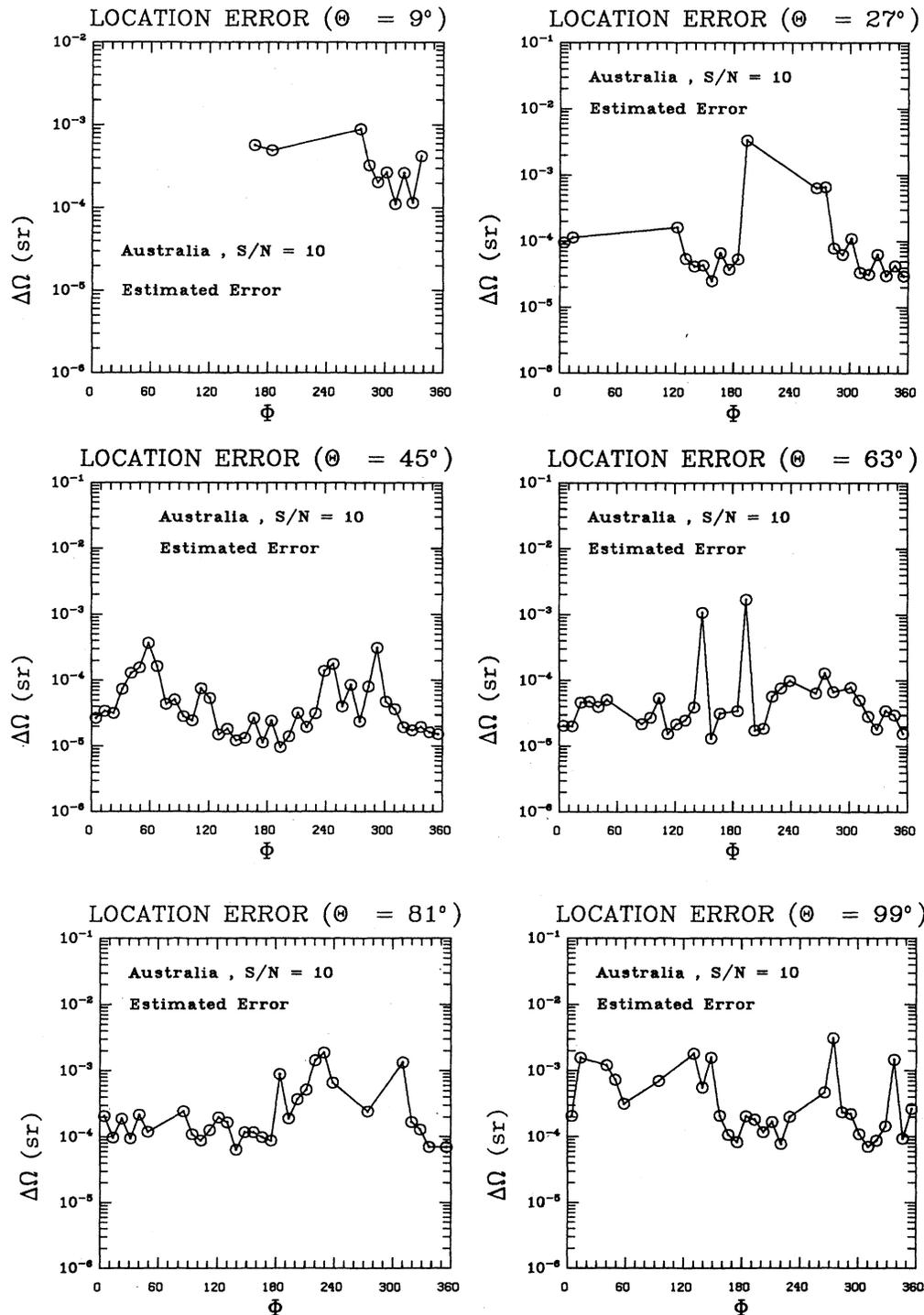
FIG. 21. The estimated error $\Delta\Omega_{est}$ [Eq. (8.1a)] and the actual error $\Delta\Omega_{act}$ [Eq. (8.2)] in the source location as functions of (θ,ϕ). The detector configuration is described in Fig. 4. The waveforms are single cycles of sinusoids. The amplitude of the waves emitted by the source is assumed to be a constant independent of the source location while the frequency of the pulses are allowed vary randomly in the range [770 Hz, 2000 Hz]. The realization of the noise is computed to be randomly different for different source locations. The sources are uniformly distributed over the sky and the signal-to-noise ratio is 10 as defined in Sec. VII. The symbols ⊙ mark the simulated source locations. A line is drawn through them to emphasize the sequential order of the simulated points. The source locations which produced maximum detector responses below a threshold of 2.1 times the root-mean-squared noise level are not displayed.
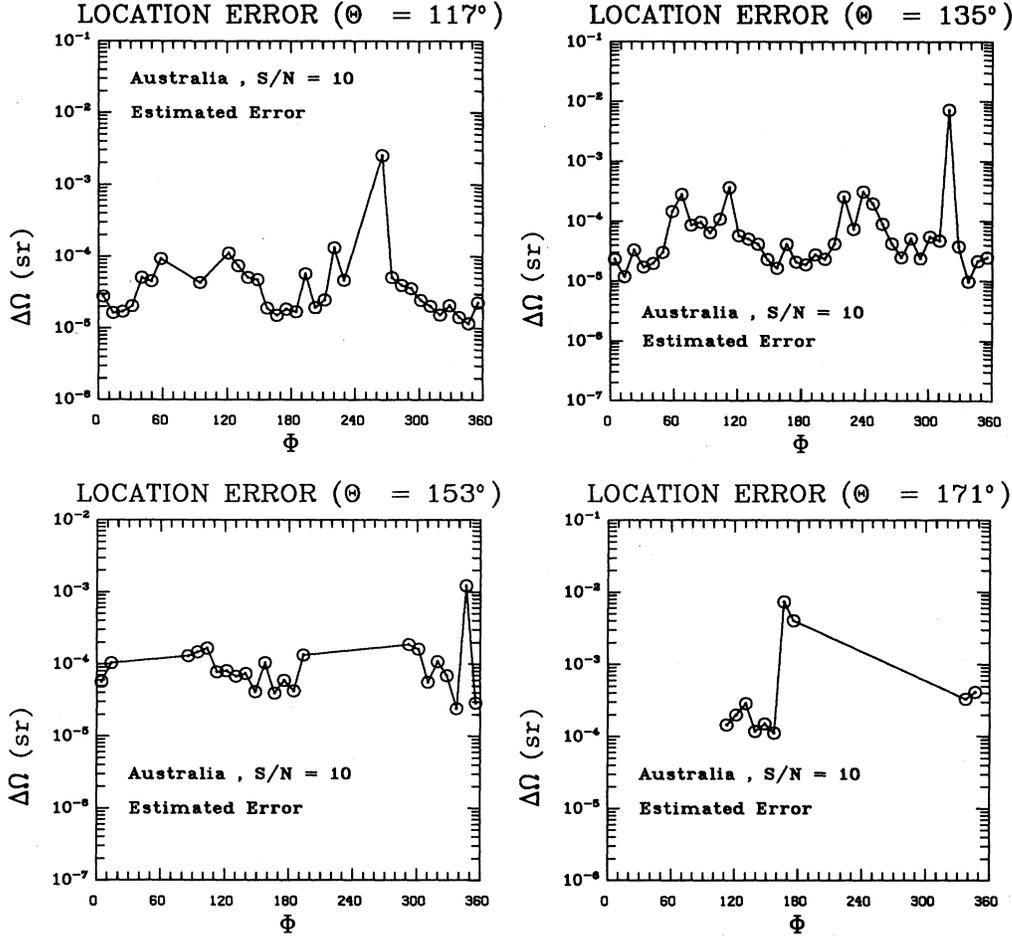
LOCATION ERROR (Θ = 117°)

Australia , S/N = 10
Estimated Error

$\Delta\Omega$ (sr)

Φ

LOCATION ERROR (Θ = 135°)

Australia , S/N = 10
Estimated Error

$\Delta\Omega$ (sr)

Φ

LOCATION ERROR (Θ = 153°)

Australia , S/N = 10
Estimated Error

$\Delta\Omega$ (sr)

Φ

LOCATION ERROR (Θ = 171°)

Australia , S/N = 10
Estimated Error

$\Delta\Omega$ (sr)

Φ

FIG. 21. (Continued).

$$\Delta\Omega = \frac{2c^2 \Delta\tau_{12} \Delta\tau_{13}}{A\cos\theta} . \tag{8.3}$$

Here θ is the angle between the source direction and the normal to the plane of the three detectors. The uncertainities in the time delays are related to the signal-to-noise ratio $(S/N)_{\text{alternative}}$ and the dominant frequency f_0 in the signal in the following manner:[33,34]

$$\Delta\tau_{12,13} = \frac{1}{\pi f_0 (S/N)_{\text{alternative}}} , \tag{8.4}$$

where we assume that the bandwidth of the signal is equal to the dominant frequency in the signal as in a supernova burst.

In our simulations the dominant frequency f_0 is about 1 kHz, the alternative signal-to-noise ratio in each detector is about 20, the typical value $\cos\theta = 0.5$ and the bandwidth of the signal is about 1 kHz. The area of the triangle spanned by the detectors is about 0.2 of the square of the radius of the Earth. Substituting these numbers in Eqs. (8.3), (8.4) we obtain $\Delta\Omega \simeq 1 \times 10^{-5}$ sr.

By combining Eqs. (8.3) and (8.4), we get

$$\Delta\Omega = \frac{2c^2}{\pi^2 A\cos\theta f_0^2 (S/N)_{\text{alternative}}^2} . \tag{8.5}$$

If a burst has a lower dominant frequency f_0, then its bandwidth will also be lower. In our method, all integrations are performed in the bandwidth of the signal in order to maximize the signal-to-noise ratio. Since the alternative signal-to-noise ratio $(S/N)_{\text{alternative}}$, for white noise and fixed wave amplitude A, is inversely proportional to the square root of the bandwidth of the bandpass filter used, we deduce that the error $\Delta\Omega$ in the source location is inversely proportional to the dominant frequency of the signal.

It is possible that the strongest signals that will be seen by the future generation of gravitational wave detectors will have a dominant frequency and bandwidth of about 100 Hz. This implies that the error $\Delta\Omega$ in the source location will be 10 times worse than those quoted above if the noise is white and the amplitude is fixed. For the weakest detectable signals, $(S/N)_{\text{alternative}} \simeq 6.6$ at any frequency, $\Delta\Omega$ will be 100 times worse for $f_0 = 100$ Hz than for $f_0 = 1000$ Hz.
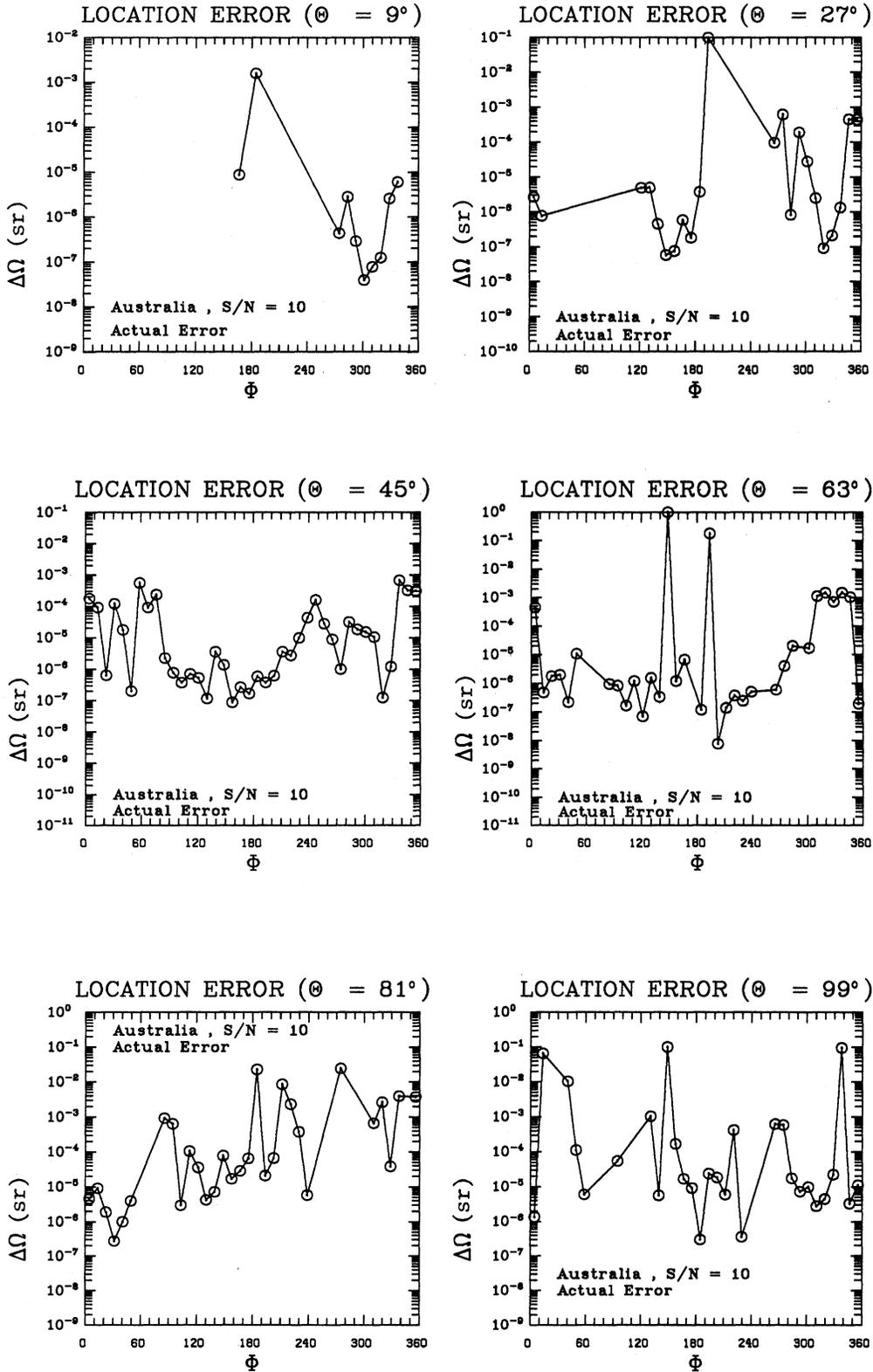
YEKTA GÜRSEL AND MASSIMO TINTO

FIG. 21. (Continued).

LOCATION ERROR (Θ = 117°)

LOCATION ERROR (Θ = 135°)

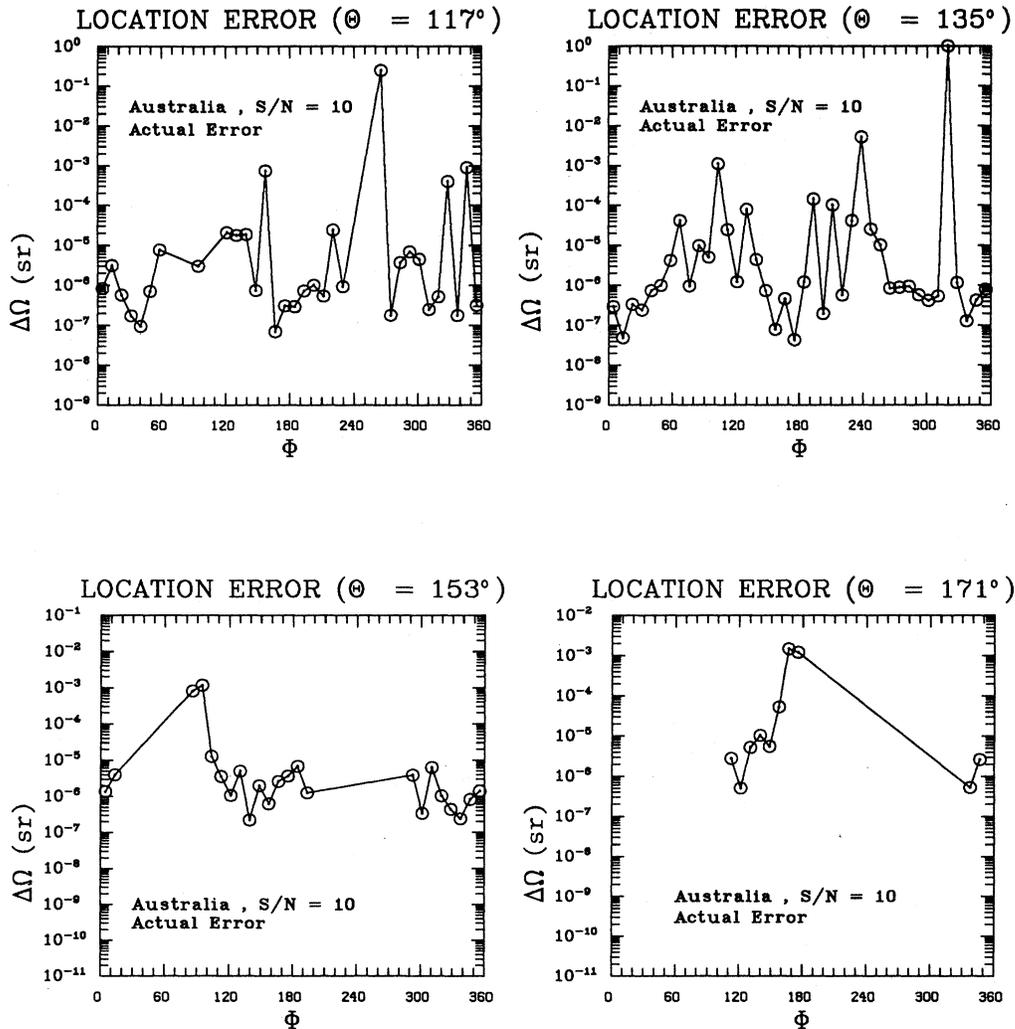LOCATION ERROR (Θ = 153°)

LOCATION ERROR (Θ = 171°)

FIG. 21. (Continued).

If the waveform of the burst is known, as in the case of coalescing compact binaries, the frequency dependence derived above for the error $\Delta\Omega$ no longer holds as pointed out by Schutz.[34] An improvement in the error $\Delta\Omega$ can be obtained by using a specially tailored interferometer for lower frequencies, and the error decreases as the frequency decreases. We will evaluate the performance of our method for signals from coalescing compact binaries in a forthcoming paper.

We show a particular case of optimal waveform reconstruction in Figs. 24(a) and 24(b). The incoming waveforms are shown in Figs. 16(a) and 16(b).

IX. CONCLUSIONS

We have developed a method for solving the inverse problem for gravitational-wave bursts. The method is capable of computing the source direction and the wave's two amplitudes and it is insensitive to the actual

waveforms. We show that for networks of three detectors widely separated on the Earth (whose locations and orientations are given in Table I), for signals with a dominant frequency and bandwidth of 1 kHz and for a signal-to-noise ratio of at least 2.1 $[(S/N)_{\text{alternative}} = 10]$ in each detector, it can locate the source direction within 1×10^{-5} sr. Signal-to-noise ratios significantly lower than 2.1 result in the loss of discrimination between the mirror-image directions determined by the correct relative time delays. For signal-to-noise ratios lower than 1 the method completely loses its resolution.

In this paper we considered only short bursts of gravitational radiation. In a forthcoming paper we will analyze signals with characteristic signatures and longer durations. Examples of such sources include coalescing compact binaries, quasi-normal-mode radiation from pulsating black holes and brehmsstrahlung from colliding black holes. These signals contain information about their sources which can be extracted from the waveforms;
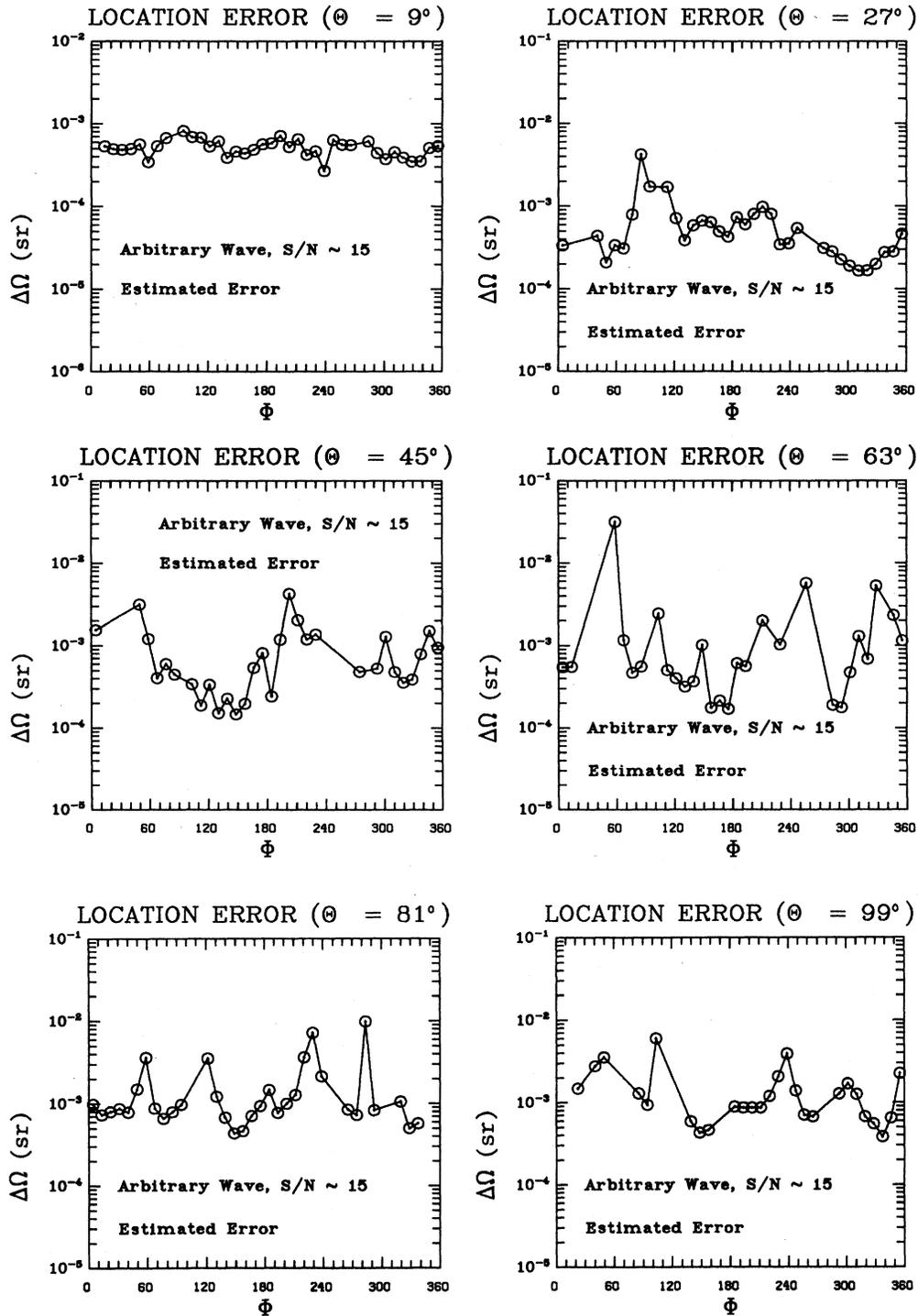
LOCATION ERROR ($\Theta = 9°$)

LOCATION ERROR ($\Theta = 27°$)

Arbitrary Wave, S/N ~ 15

Estimated Error

LOCATION ERROR ($\Theta = 45°$)

Arbitrary Wave, S/N ~ 15

Estimated Error

LOCATION ERROR ($\Theta = 63°$)

Arbitrary Wave, S/N ~ 15

Estimated Error

LOCATION ERROR ($\Theta = 81°$)

Arbitrary Wave, S/N ~ 15

Estimated Error

LOCATION ERROR ($\Theta = 99°$)

Arbitrary Wave, S/N ~ 15

Estimated Error

FIG. 22. The estimated error $\Delta\Omega_{est}$ [Eq. (8.1a)] and the actual error $\Delta\Omega_{act}$ [Eq. (8.2)] in the source location as functions of (θ, ϕ). The detector configuration is described in Fig. 3. The waveforms are shown in Figs. 16(c) and 16(d). The root-mean-squared amplitude of the waves emitted by the source is assumed to be a constant independent of the source location. The realization of the noise is computed to be randomly different for different source locations. The sources are uniformly distributed over the sky and the signal-to-noise ratio is 15 as defined in Sec. VII. The symbols ⊙ mark the simulated source locations. A line is drawn through them to emphasize the sequential order of the simulated points. The source locations which produced maximum detector responses below a threshold of 2.1 times the root-mean-squared noise level are not displayed.
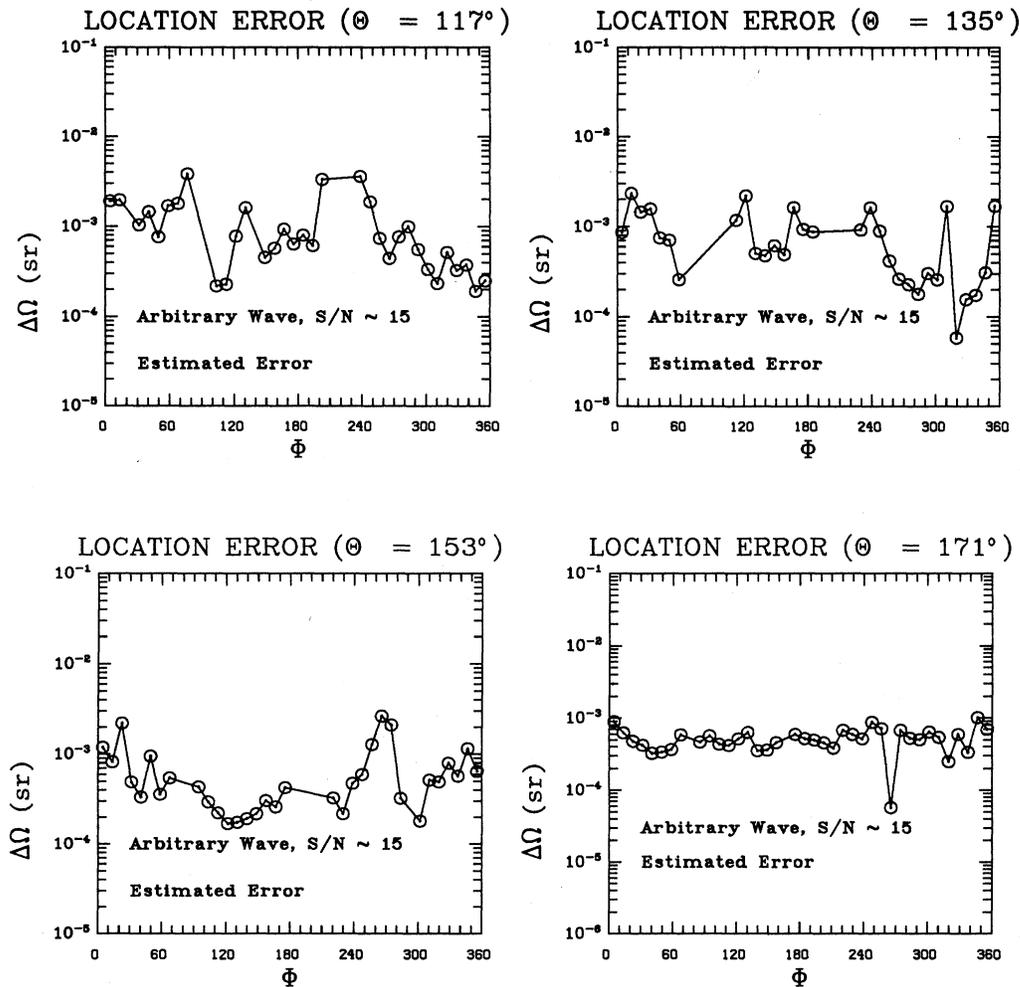
LOCATION ERROR ($\Theta = 117°$)

LOCATION ERROR ($\Theta = 135°$)

LOCATION ERROR ($\Theta = 153°$)

LOCATION ERROR ($\Theta = 171°$)

Arbitrary Wave, S/N ~ 15

Estimated Error

FIG. 22. (*Continued*).

however the limited bandwidth of the instrument alters the shape of the waveform. As the bandwidth of the instruments gets larger, this effect will be diminished. We will also consider the case of four or more wideband gravitational wave detectors running in coincidence. With four or more detectors we will be able to compute the source direction with possibly improved accuracy due to the availability of three or more independent relative time delays.

We plan to extend the method described in this paper to the case of continuous and stochastic signals. Continuous signals originate from pulsars or spinning neutron stars and they are expected to be emitted at well-defined frequencies. The frequency of these signals must be searched for as well as their directions. Since these signals last much longer than a typical data run, the response of a detector is Doppler shifted by the rotation of the earth. This fact raises the computational cost of the search considerably.[35]

LOCATION ERROR (Θ = 9°)

LOCATION ERROR (Θ = 27°)

LOCATION ERROR (Θ = 45°)

LOCATION ERROR (Θ = 63°)

LOCATION ERROR (Θ = 81°)

LOCATION ERROR (Θ = 99°)

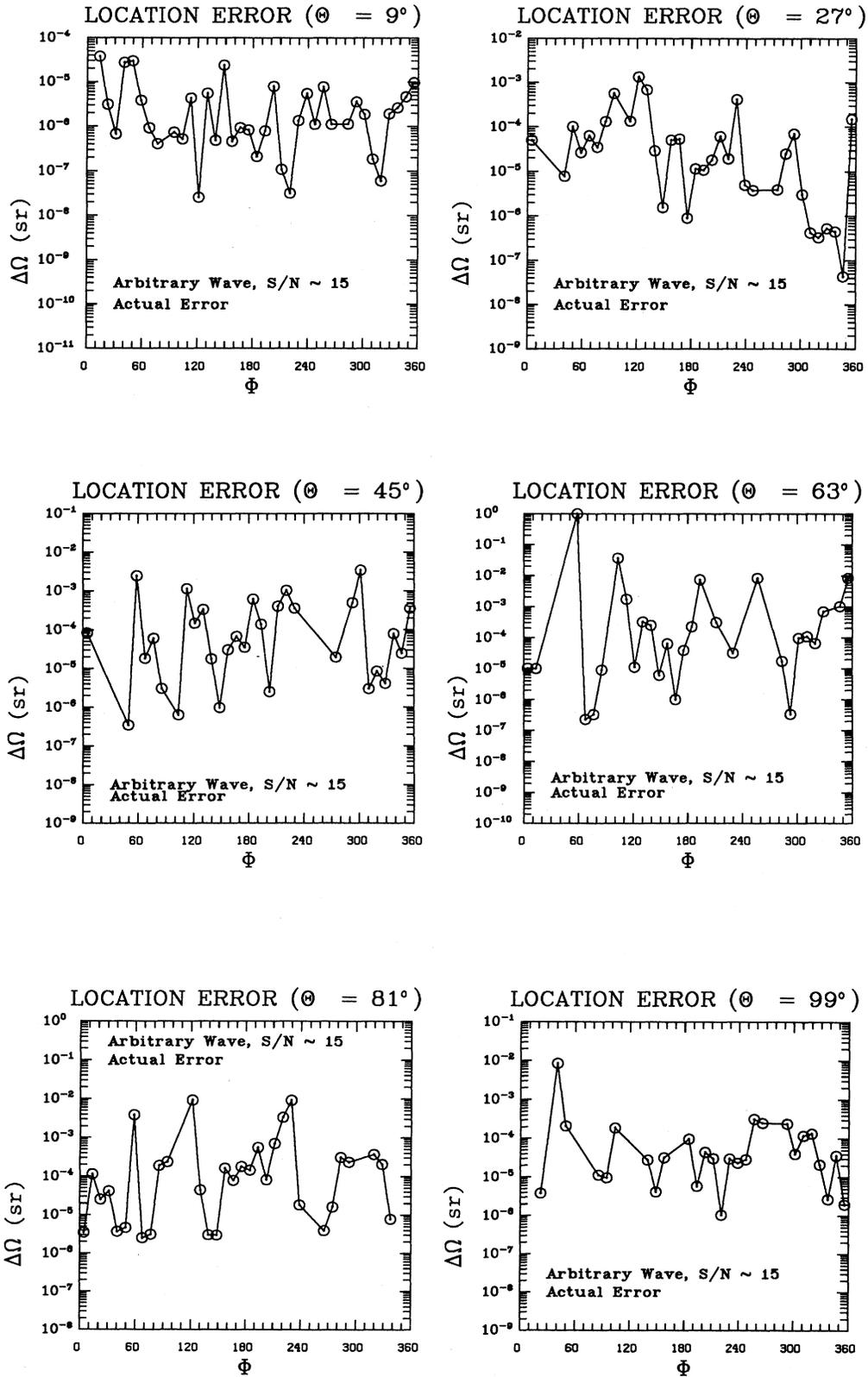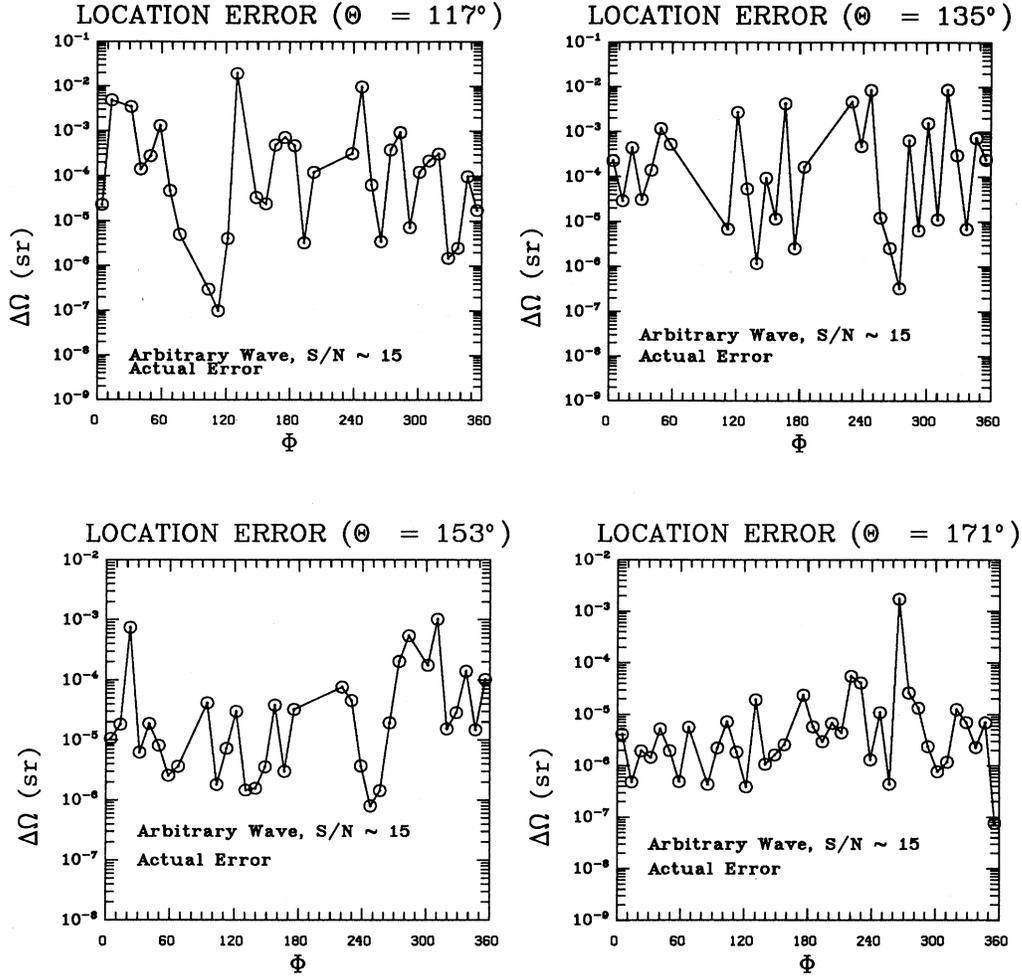Arbitrary Wave, S/N ~ 15
Actual Error

FIG. 22. (Continued).

FIG. 22. (Continued).

were generated using the NCAR graphics library. The text editor GNUEmacs was used in developing the program, in analyzing the results and in writing this paper. We also thank the Theoretical Astrophysics Group at Caltech and the LIGO project for providing some of the computing resources.

APPENDIX A

In this Appendix we derive the explicit expressions for the detectors' beam-pattern functions $F_+(\theta,\phi,\alpha,\beta,\gamma)$ and $F_\times(\theta,\phi,\alpha,\beta,\gamma)$ which are introduced in Sec. II. The location of a chosen detector is given in the form of latitude β and longitude γ in an Earth-based coordinate system (Fig. 2). The orientation of the detector is measured in the plane tangent to the Earth at the detector location and is given as the angle α between the bisector of the arms of the detector and the local east-west direction. The quantities (θ,ϕ) are the Euler angles of the source in a certain coordinate system (x,y,z) with z orthogonal to the plane formed by the detector locations and x along the line from detector 1 to detector 2.

The Earth coordinate system is defined by choosing the x'' axis to lie in the direction of the line passing through the center of the Earth and the intersection of the great circle which passes through Greenwich, England and the equator. The z'' axis is chosen to lie in the direction of the line passing through the center of the Earth and the North Pole. The y'' axis is chosen to form a right-handed Cartesian coordinate system with the x'' and z'' axis.

Let α_I, β_I, γ_I be the angles α, β, γ (defined above) for detector I. In the detectors' coordinates (as defined in Sec. II), consider the following complex null vector:

$$\epsilon = \frac{1}{\sqrt{2}}(\mathbf{e}_{x'} + i\mathbf{e}_{y'}) , \tag{A1}$$

where $\mathbf{e}_{x'}$, $\mathbf{e}_{y'}$ are the unit vectors along the x' and y' axes. The vector ϵ is given by

LOCATION ERROR (Θ = 9°)

Optimally Filtered, S/N = 10
Estimated Error

$\Delta\Omega$ (sr)

Φ

LOCATION ERROR (Θ = 27°)

Optimally Filtered, S/N = 10
Estimated Error

$\Delta\Omega$ (sr)

Φ

LOCATION ERROR (Θ = 45°)

Optimally Filtered, S/N = 10
Estimated Error

$\Delta\Omega$ (sr)

Φ

LOCATION ERROR (Θ = 63°)

Optimally Filtered, S/N = 10
Estimated Error

$\Delta\Omega$ (sr)

Φ

LOCATION ERROR (Θ = 81°)

Optimally Filtered, S/N = 10
Estimated Error

$\Delta\Omega$ (sr)

Φ

LOCATION ERROR (Θ = 99°)

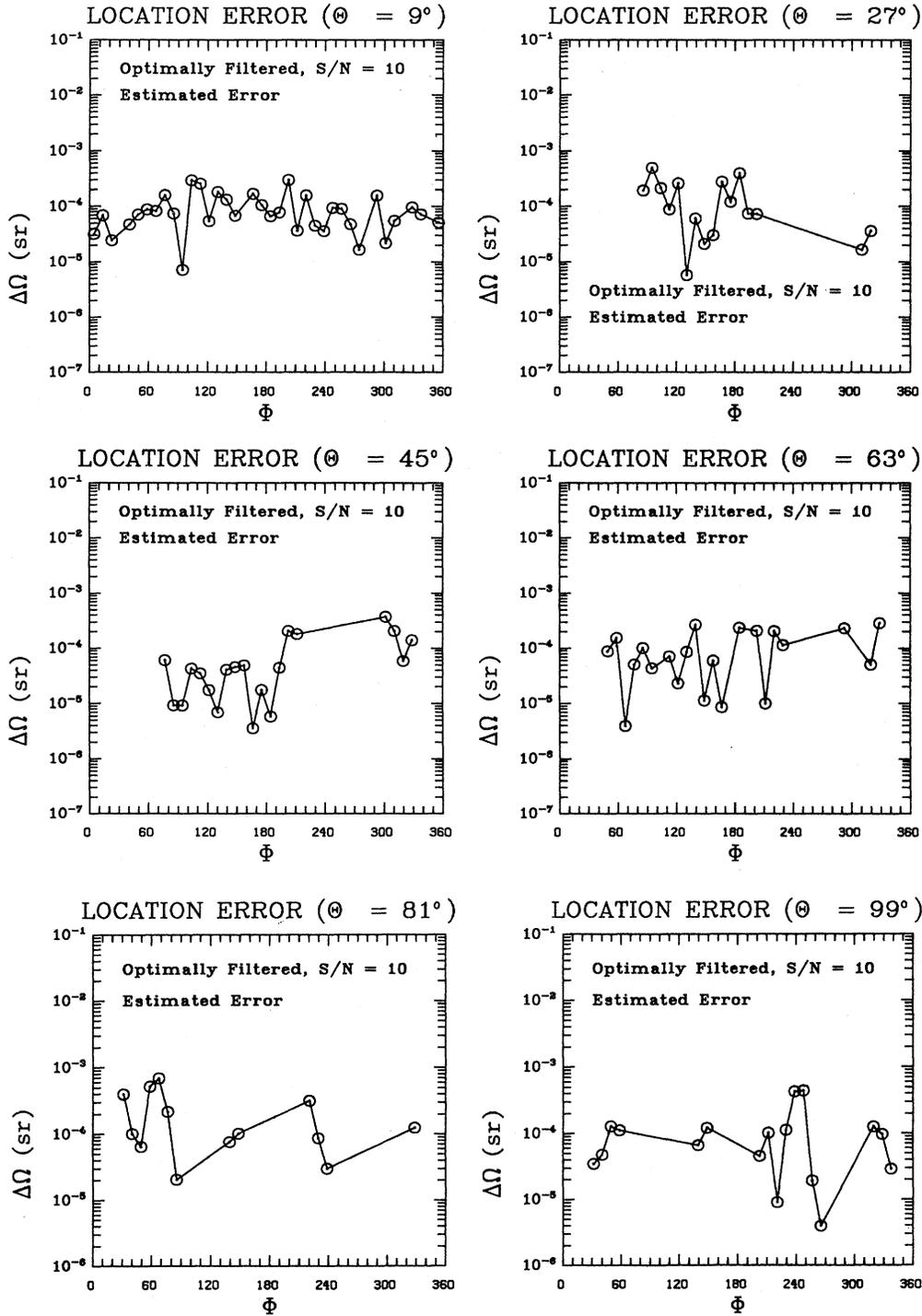Optimally Filtered, S/N = 10
Estimated Error

$\Delta\Omega$ (sr)

Φ

FIG. 23. The estimated error $\Delta\Omega_{est}$ [Eq. (8.1b)] and the actual error $\Delta\Omega_{act}$ [Eq. (8.2)] in the source location as functions of (θ, ϕ) for the near-optimally-filtered simulation. The detector configuration is described in Fig. 3. The waveforms are single cycles of sinusoids. The amplitude of the waves emitted by the source is assumed to be a constant independent of the source location while the frequency of the pulses are allowed to vary randomly in the range [770 Hz, 2000 Hz]. The realization of the noise is computed to be randomly different for different source locations. The sources are uniformly distributed over the sky and the signal-to-noise ratio is 10 as defined in Sec. VII. The symbols ⊙ mark the simulated source locations. A line is drawn through them to emphasize the sequential order of the simulated points. The source locations which produced maximum detector responses below a threshold of 3.6 times the root-mean-squared noise level are not displayed.
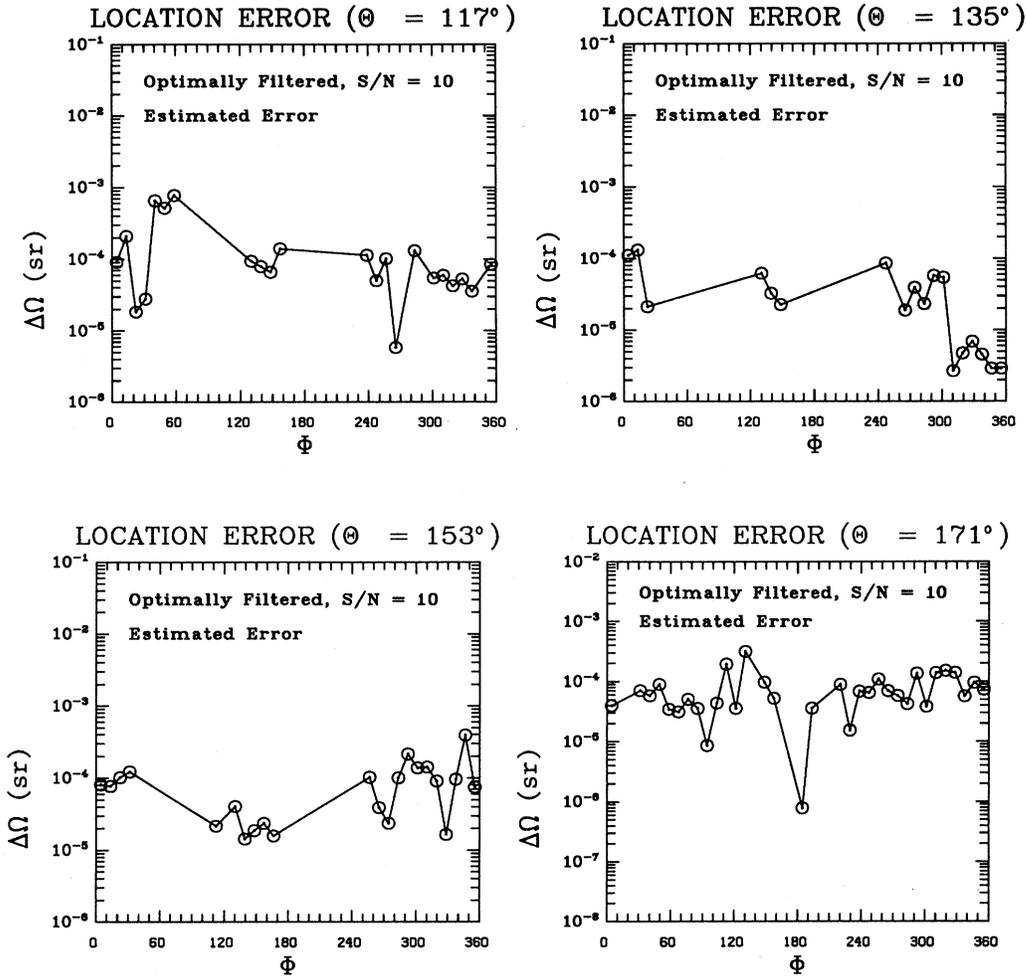
LOCATION ERROR (Θ = 117°)

Optimally Filtered, S/N = 10

Estimated Error

LOCATION ERROR (Θ = 135°)

Optimally Filtered, S/N = 10

Estimated Error

LOCATION ERROR (Θ = 153°)

Optimally Filtered, S/N = 10

Estimated Error

LOCATION ERROR (Θ = 171°)

Optimally Filtered, S/N = 10

Estimated Error

FIG. 23. (*Continued*).

$$\epsilon = \frac{1}{\sqrt{2}}[(-\sin\gamma_I - i\sin\beta_I\cos\gamma_I)\mathbf{e}_{x''}$$

$$+(\cos\gamma_I - i\sin\beta_I\sin\gamma_I)\mathbf{e}_{y''}+(i\cos\beta_I)\mathbf{e}_{z''}]e^{-i\alpha_I} \; .$$

$$\text{(A2)}$$

For an interferometer oriented in such a way that the x' axis bisects the angle between the arms, the detector tensor $\overleftrightarrow{D}^I$ can be written as

$$\overleftrightarrow{D}^I = \sin2\Omega_I(\mathbf{e}_{x'}\otimes\mathbf{e}_{y'}+\mathbf{e}_{y'}\otimes\mathbf{e}_{x'}) \qquad \text{(A3)}$$

Here $2\Omega_I$ is the value of the angle between the arms (usually close to 90°).

In terms of ϵ the detector tensor $\overleftrightarrow{D}^I$ can be written as

$$\overleftrightarrow{D}^I = \sin2\Omega_I\frac{\epsilon\otimes\epsilon-\epsilon^*\otimes\epsilon^*}{i} \; . \qquad \text{(A4)}$$

Let $\mathbf{d}_I$ be the unit vectors pointing from the center of the Earth to detector I. They can be written as

$$\mathbf{d}_I = (\cos\beta_I\cos\gamma_I)\mathbf{e}_{x''}+(\cos\beta_I\sin\gamma_I)\mathbf{e}_{y''}+(\sin\beta_I)\mathbf{e}_{z''} \; .$$

$$\text{(A5)}$$

We will now construct the transformation from the Earth axes (x'',y'',z'') to the common detector axes (x,y,z). Let $\mathbf{f}$ and $\mathbf{g}$ be defined by

$$\mathbf{f} = \frac{\mathbf{d}_1-\mathbf{d}_2}{|\mathbf{d}_1-\mathbf{d}_2|} \; , \qquad \text{(A6)}$$

$$\mathbf{g} = \frac{\mathbf{d}_1-\mathbf{d}_3}{|\mathbf{d}_1-\mathbf{d}_3|} \; . \qquad \text{(A7)}$$

Define the unit vector $\mathbf{o}$ by

$$\mathbf{o} = \frac{\mathbf{f}\times\mathbf{g}}{|\mathbf{f}\times\mathbf{g}|} \; , \qquad \text{(A8)}$$

where we assume in the vector product $\times$ that the order of the vectors $\mathbf{f}$ and $\mathbf{g}$ is chosen in such a way as to make the triad $(\mathbf{f},\mathbf{g},\mathbf{o})$ a right-handed one. We can get the orthonormal right-handed triad $(\mathbf{f},\mathbf{p},\mathbf{o})$ by computing the following vector $\mathbf{p}$:

$$\mathbf{p} = \mathbf{o}\times\mathbf{f} \; . \qquad \text{(A9)}$$

We construct the orthogonal transformation matrix Q_{ij}

LOCATION ERROR ($\Theta = 9°$)

LOCATION ERROR ($\Theta = 27°$)

LOCATION ERROR ($\Theta = 45°$)

LOCATION ERROR ($\Theta = 63°$)

LOCATION ERROR ($\Theta = 81°$)

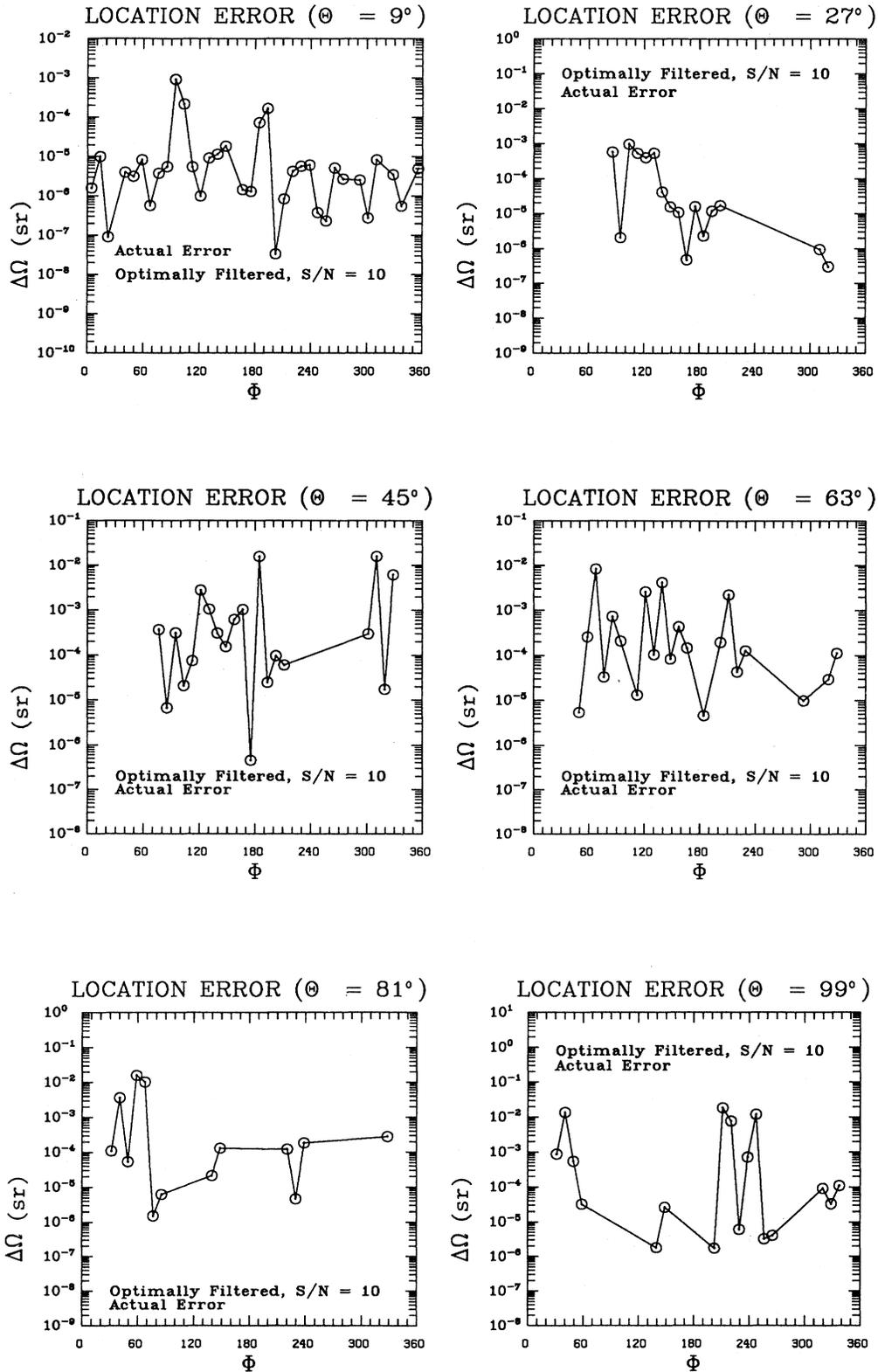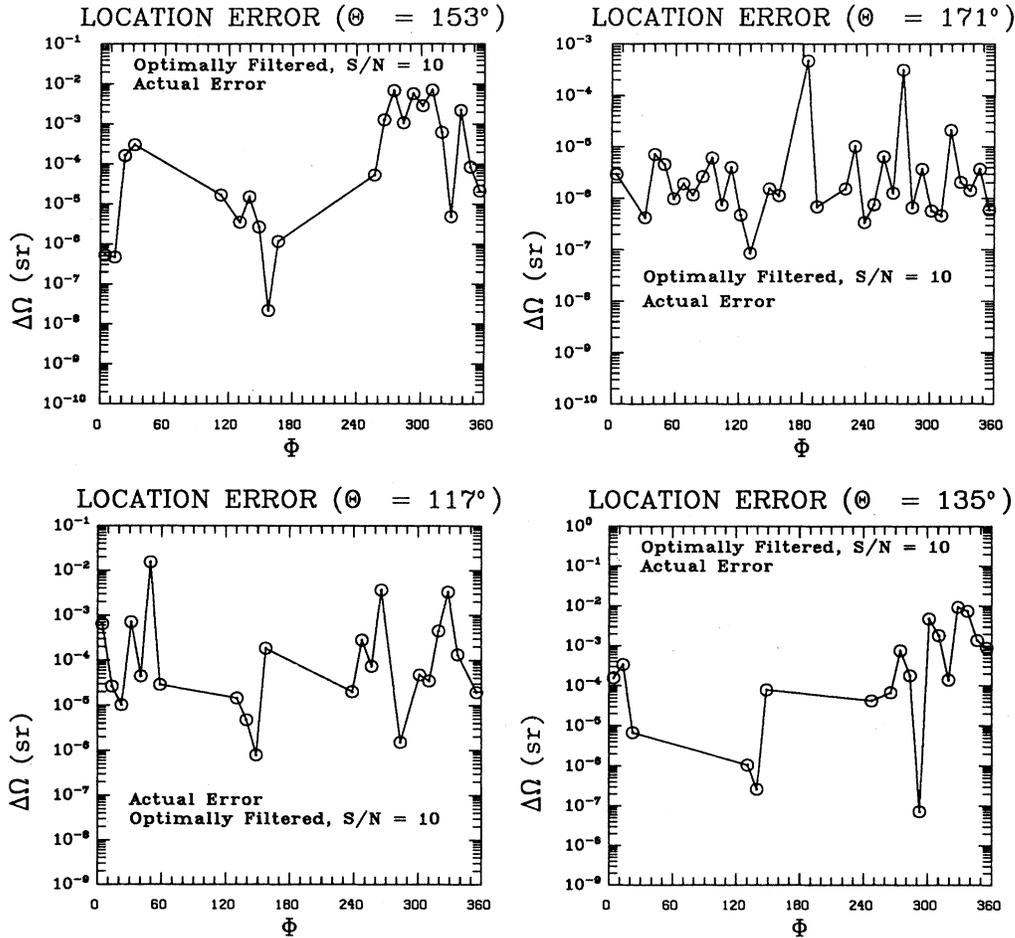LOCATION ERROR ($\Theta = 99°$)

FIG. 23. (*Continued*).

FIG. 23. (*Continued*).

in the following way:

$$Q_{ij} = \begin{bmatrix} f_{x''} & p_{x''} & o_{x''} \\ f_{y''} & p_{y''} & o_{y''} \\ f_{z''} & p_{z''} & o_{z''} \end{bmatrix} . \qquad (A10)$$

Then the functions $F_{I+}(\theta,\phi,\alpha,\beta,\gamma)$ and $F_{I\times}(\theta,\phi,\alpha,\beta,\gamma)$ are given by

$$F_{I+}(\theta,\phi,\alpha,\beta,\gamma) = D_{ij}^I Q_{ik} Q_{jl} \text{Re}(m_k m_l) , \qquad (A11a)$$

$$F_{I\times}(\theta,\phi,\alpha,\beta,\gamma) = D_{ij}^I Q_{ik} Q_{jl} \text{Im}(m_k m_l) , \qquad (A11b)$$

where we have assumed the Einstein summation convention over all repeated indices, and the vector **m** is defined by

$$\mathbf{m} = \frac{1}{\sqrt{2}} [(\cos\phi - i\cos\theta\sin\phi)\mathbf{e}_x$$

$$+ (\sin\phi + i\cos\theta\cos\phi)\mathbf{e}_y + (i\sin\theta)\mathbf{e}_z] . \qquad (A12)$$

By combining the Eqs. (A2) and (A4)–(A12) we obtain the explicit form of $F_{I+}(\theta,\phi,\alpha,\beta,\gamma)$ and $F_{I\times}(\theta,\phi,\alpha,\beta,\gamma)$.

APPENDIX B

In this Appendix, we give the explicit forms of the Hessian matrices for the filtered and the unfiltered methods.

A. The Hessian for the unfiltered method

The Hessian $\overleftrightarrow{H}'_m$ for the unfiltered method is given in terms of the second partial derivatives of the least-squares function $L'_\Lambda(\theta,\phi)$ given in Eq. (4.14) evaluated at the minimum point (θ_m,ϕ_m) where

$$\frac{\partial L'_\Lambda(\theta,\phi)}{\partial \theta}\bigg|_{\theta_m,\phi_m} = \frac{\partial L'_\Lambda(\theta,\phi)}{\partial \phi}\bigg|_{\theta_m,\phi_m} = 0 .$$

The matrix representation of the Hessian is as follows:

$$\overleftrightarrow{H}'_m = \begin{bmatrix} \dfrac{\partial^2 L'_\Lambda(\theta,\phi)}{\partial\theta^2}\bigg|_{\theta_m,\phi_m} & \dfrac{\partial^2 L'_\Lambda(\theta,\phi)}{\partial\theta\,\partial\phi}\bigg|_{\theta_m,\phi_m} \\ \dfrac{\partial^2 L'_\Lambda(\theta,\phi)}{\partial\phi\,\partial\theta}\bigg|_{\theta_m,\phi_m} & \dfrac{\partial^2 L'_\Lambda(\theta,\phi)}{\partial\phi^2}\bigg|_{\theta_m,\phi_m} \end{bmatrix} . \qquad (B1)$$

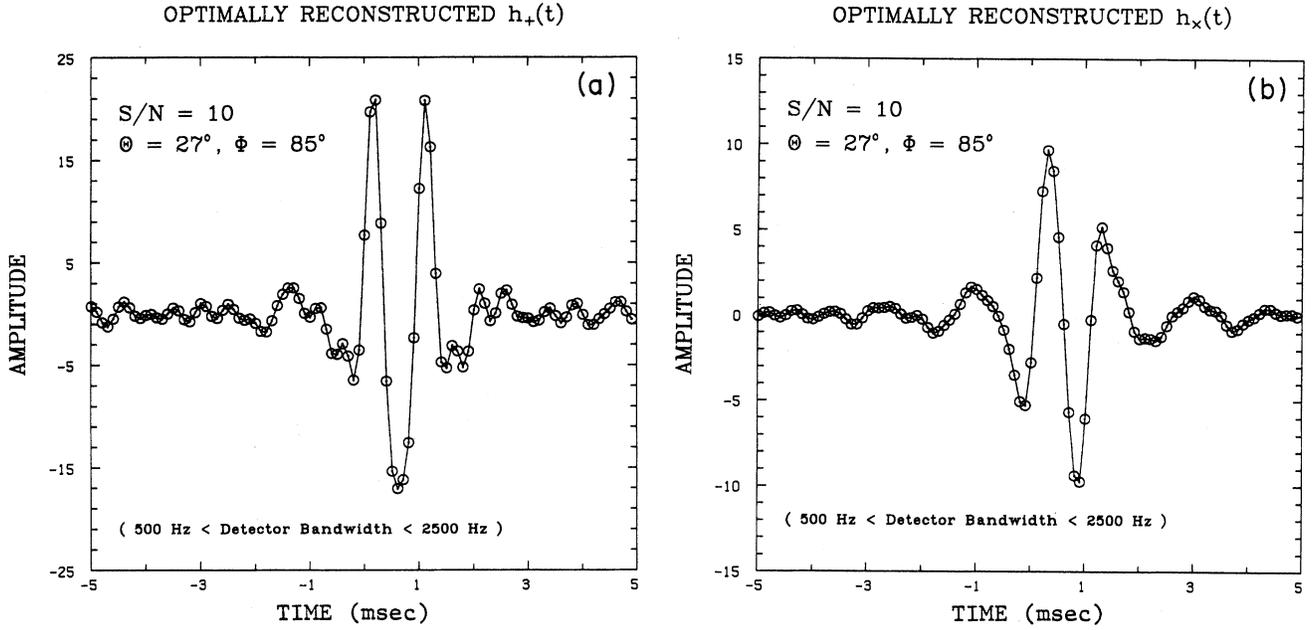The second partial derivatives of $L'_\Lambda(\theta,\phi)$ at the minimum point are given below:

FIG. 24. (a) The optimally reconstructed waveform $h_{\text{opt}+}(t)$; compare with Fig. 16(a). (b) The optimally reconstructed waveform $h_{\text{opt}\times}(t)$; compare with Fig. 16(b). The detector configuration, the coordinate system, and the amplitudes of the incoming gravitational wave are as described in Fig. 3. The source is placed at $(27°, 85°)$. The overall signal-to-noise ratio is 10.

$$\frac{\partial^2 L'_\Lambda(\theta,\phi)}{\partial\theta^2}\bigg|_{\theta_m,\phi_m} = \frac{2}{K_1^2\sigma_1^2 + K_2^2\sigma_2^2 + K_3^2\sigma_3^2}\left\{\frac{1}{\Delta t}\int_{t_0}^{t_1}\left[\left[\frac{\partial I_\Lambda}{\partial\theta}\right]^2 + I_\Lambda\frac{\partial^2 I_\Lambda}{\partial\theta^2}\right]dt\right.$$

$$-L'_\Lambda\left\{\left[\left[\frac{\partial K_1}{\partial\theta}\right]^2 + K_1\frac{\partial^2 K_1}{\partial\theta^2}\right]\sigma_1^2 + \left[\left[\frac{\partial K_2}{\partial\theta}\right]^2 + K_2\frac{\partial^2 K_2}{\partial\theta^2}\right]\sigma_2^2\right.$$

$$\left.\left.+\left[\left[\frac{\partial K_3}{\partial\theta}\right]^2 + K_3\frac{\partial^2 K_3}{\partial\theta^2}\right]\sigma_3^2\right\}\right\}, \tag{B2}$$

$$\frac{\partial^2 L'_\Lambda(\theta,\phi)}{\partial\theta\,\partial\phi}\bigg|_{\theta_m,\phi_m}$$

$$= \frac{2}{K_1^2\sigma_1^2 + K_2^2\sigma_2^2 + K_3^2\sigma_3^2}\left\{\frac{1}{\Delta t}\int_{t_0}^{t_1}\left[\frac{\partial I_\Lambda}{\partial\theta}\frac{\partial I_\Lambda}{\partial\phi} + I_\Lambda\frac{\partial^2 I_\Lambda}{\partial\theta\,\partial\phi}\right]dt\right.$$

$$-L'_\Lambda\left[\left[\frac{\partial K_1}{\partial\theta}\frac{\partial K_1}{\partial\phi} + K_1\frac{\partial^2 K_1}{\partial\theta\,\partial\phi}\right]\sigma_1^2 + \left[\frac{\partial K_2}{\partial\theta}\frac{\partial K_2}{\partial\phi} + K_2\frac{\partial^2 K_2}{\partial\theta\,\partial\phi}\right]\sigma_2^2\right.$$

$$\left.\left.+\left[\frac{\partial K_3}{\partial\theta}\frac{\partial K_3}{\partial\phi} + K_3\frac{\partial^2 K_3}{\partial\theta\,\partial\phi}\right]\sigma_3^2\right]\right\}, \tag{B3}$$

$$\frac{\partial^2 L'_\Lambda(\theta,\phi)}{\partial\phi^2}\bigg|_{\theta_m,\phi_m} = \frac{2}{K_1^2\sigma_1^2 + K_2^2\sigma_2^2 + K_3^2\sigma_3^2}\left[\frac{1}{\Delta t}\int_{t_0}^{t_1}\left[\left[\frac{\partial I_\Lambda}{\partial\phi}\right]^2 + I_\Lambda\frac{\partial^2 I_\Lambda}{\partial\phi^2}\right]dt\right.$$

$$-L'_\Lambda\left\{\left[\left[\frac{\partial K_1}{\partial\phi}\right]^2 + K_1\frac{\partial^2 K_1}{\partial\phi^2}\right]\sigma_1^2 + \left[\left[\frac{\partial K_2}{\partial\phi}\right]^2 + K_2\frac{\partial^2 K_2}{\partial\phi^2}\right]\sigma_2^2\right.$$

$$\left.\left.+\left[\left[\frac{\partial K_3}{\partial\phi}\right]^2 + K_3\frac{\partial^2 K_3}{\partial\phi^2}\right]\sigma_3^2\right\}\right], \tag{B4}$$

where I_Λ is given by Eq. (4.2); K_1, K_2, and K_3 are given in Eqs. (3.8a), (3.8b), and (3.8c); σ_1, σ_2, and σ_3 as in Eq. (4.14). The times t_0, t_1 are the limits of the integration corresponding to the minimum point and $\Delta t = t_1 - t_0$.

The derivatives of I_Λ are given below:

$$\frac{\partial I_\Lambda}{\partial \theta} = \frac{\partial K_1}{\partial \theta} R_{1\Lambda}(t) + \frac{\partial K_2}{\partial \theta} R_{2\Lambda}(t + \tau_{12}) + \frac{\partial K_3}{\partial \theta} R_{3\Lambda}(t + \tau_{13}) + \frac{\partial \tau_{12}}{\partial \theta} K_2 \dot{R}_{2\Lambda}(t + \tau_{12}) + \frac{\partial \tau_{13}}{\partial \theta} K_3 \dot{R}_{3\Lambda}(t + \tau_{13}), \text{ (B5)}$$

$$\frac{\partial I_\Lambda}{\partial \phi} = \frac{\partial K_1}{\partial \phi} R_{1\Lambda}(t) + \frac{\partial K_2}{\partial \phi} R_{2\Lambda}(t + \tau_{12}) + \frac{\partial K_3}{\partial \phi} R_{3\Lambda}(t + \tau_{13}) + \frac{\partial \tau_{12}}{\partial \phi} K_2 \dot{R}_{2\Lambda}(t + \tau_{12}) + \frac{\partial \tau_{13}}{\partial \phi} K_3 \dot{R}_{3\Lambda}(t + \tau_{13}), \text{ (B6)}$$

$$\frac{\partial^2 I_\Lambda}{\partial \theta^2} = \frac{\partial^2 K_1}{\partial \theta^2} R_{1\Lambda}(t) + \frac{\partial^2 K_2}{\partial \theta^2} R_{2\Lambda}(t + \tau_{12}) + \frac{\partial^2 K_3}{\partial \theta^2} R_{3\Lambda}(t + \tau_{13})$$
$$+ \left[2\frac{\partial K_2}{\partial \theta} \frac{\partial \tau_{12}}{\partial \theta} + K_2 \frac{\partial^2 \tau_{12}}{\partial \theta^2} \right] \dot{R}_{2\Lambda}(t + \tau_{12}) + \left[2\frac{\partial K_3}{\partial \theta} \frac{\partial \tau_{13}}{\partial \theta} + K_3 \frac{\partial^2 \tau_{13}}{\partial \theta^2} \right] \dot{R}_{3\Lambda}(t + \tau_{13})$$
$$+ \left[\frac{\partial \tau_{12}}{\partial \theta} \right]^2 K_2 \ddot{R}_{2\Lambda}(t + \tau_{12}) + \left[\frac{\partial \tau_{13}}{\partial \theta} \right]^2 K_3 \ddot{R}_{3\Lambda}(t + \tau_{13}), \tag{B7}$$

$$\frac{\partial^2 I_\Lambda}{\partial \theta \partial \phi} = \frac{\partial^2 K_1}{\partial \theta \partial \phi} R_{1\Lambda}(t) + \frac{\partial^2 K_2}{\partial \theta \partial \phi} R_{2\Lambda}(t + \tau_{12}) + \frac{\partial^2 K_3}{\partial \theta \partial \phi} R_{3\Lambda}(t + \tau_{13})$$
$$+ \left[\frac{\partial K_2}{\partial \theta} \frac{\partial \tau_{12}}{\partial \phi} + \frac{\partial K_2}{\partial \phi} \frac{\partial \tau_{12}}{\partial \theta} + K_2 \frac{\partial^2 \tau_{12}}{\partial \theta \partial \phi} \right] \dot{R}_{2\Lambda}(t + \tau_{12})$$
$$+ \left[\frac{\partial K_3}{\partial \theta} \frac{\partial \tau_{13}}{\partial \phi} + \frac{\partial K_3}{\partial \phi} \frac{\partial \tau_{13}}{\partial \theta} + K_3 \frac{\partial^2 \tau_{13}}{\partial \theta \partial \phi} \right] \dot{R}_{3\Lambda}(t + \tau_{13})$$
$$+ \frac{\partial \tau_{12}}{\partial \theta} \frac{\partial \tau_{12}}{\partial \phi} K_2 \ddot{R}_{2\Lambda}(t + \tau_{12}) + \frac{\partial \tau_{13}}{\partial \theta} \frac{\partial \tau_{13}}{\partial \phi} K_3 \ddot{R}_{3\Lambda}(t + \tau_{13}), \tag{B8}$$

$$\frac{\partial^2 I_\Lambda}{\partial \phi^2} = \frac{\partial^2 K_1}{\partial \phi^2} R_{1\Lambda}(t) + \frac{\partial^2 K_2}{\partial \phi^2} R_{2\Lambda}(t + \tau_{12}) + \frac{\partial^2 K_3}{\partial \phi^2} R_{3\Lambda}(t + \tau_{13}) + \left[2\frac{\partial K_2}{\partial \phi} \frac{\partial \tau_{12}}{\partial \phi} + K_2 \frac{\partial^2 \tau_{12}}{\partial \phi^2} \right] \dot{R}_{2\Lambda}(t + \tau_{12})$$
$$+ \left[2\frac{\partial K_3}{\partial \phi} \frac{\partial \tau_{13}}{\partial \phi} + K_3 \frac{\partial^2 \tau_{13}}{\partial \phi^2} \right] \dot{R}_{3\Lambda}(t + \tau_{13}) + \left[\frac{\partial \tau_{12}}{\partial \phi} \right]^2 K_2 \ddot{R}_{2\Lambda}(t + \tau_{12}) + \left[\frac{\partial \tau_{13}}{\partial \phi} \right]^2 K_3 \ddot{R}_{3\Lambda}(t + \tau_{13}), \tag{B9}$$

where $R_{1\Lambda}(t)$, $R_{2\Lambda}(t)$, and $R_{3\Lambda}(t)$ are the noisy detector responses; $\dot{R}_{2\Lambda}(t)$, and $\dot{R}_{3\Lambda}(t)$ are the first time derivatives of these responses; $\ddot{R}_{2\Lambda}(t)$ and $\ddot{R}_{3\Lambda}(t)$ are the second time derivatives of them. The derivatives of the time delays are given by Eqs. (4.15) and (4.16). The functions K_1, K_2, and K_3 are given in Eqs. (3.8a), (3.8b), and (3.8c).

B. The Hessian for the filtered method

The Hessian $\vec{H}''_m$ for the filtered method is given in terms of the second partial derivatives of the least-squares function $L''_\Lambda(\theta, \phi)$ given in Eq. (5.20) evaluated at the minimum point (θ_m, ϕ_m) where

$$\frac{\partial L''_\Lambda(\theta, \phi)}{\partial \theta} \bigg|_{\theta_m, \phi_m} = \frac{\partial L''_\Lambda(\theta, \phi)}{\partial \phi} \bigg|_{\theta_m, \phi_m} = 0.$$

We will give the expressions corresponding to the cases (i) and (ii) in Sec. V for which the integrand in Eq. (5.20) is given by Eq. (5.19). The form of the Hessian in terms of the least-squares integral $L''_\Lambda(\theta, \phi)$ [Eq. (5.20)] is the same as the one in Eq. (B1).

We define $A(\theta, \phi, t)$ in terms of the integrand $C'(\theta, \phi, t)$ [Eq. (5.19)] and the function $G(\theta, \phi)$ defined in Sec. V in the following way:

$$A(\theta, \phi, t) = G(\theta, \phi) C'(\theta, \phi, t), \tag{B10}$$

Then the second derivatives of the least-squares integral $L''_\Lambda(\theta, \phi)$ are

$$\frac{\partial^2 L''_\Lambda(\theta, \phi)}{\partial \theta^2} \bigg|_{\theta_m, \phi_m} = \frac{2}{G^2} \left\{ \frac{1}{\Delta t} \int_{t_0}^{t_1} \left[\left[\frac{\partial A}{\partial \theta} \right]^2 + A \frac{\partial^2 A}{\partial \theta^2} \right] dt - L'_\Lambda \left[\left[\frac{\partial G}{\partial \theta} \right]^2 + G \frac{\partial^2 G}{\partial \theta^2} \right] \right\}, \tag{B11}$$

$$\frac{\partial^2 L''_\Lambda(\theta, \phi)}{\partial \theta \partial \phi} \bigg|_{\theta_m, \phi_m} = \frac{2}{G^2} \left\{ \frac{1}{\Delta t} \int_{t_0}^{t_1} \left[\frac{\partial A}{\partial \theta} \frac{\partial A}{\partial \phi} + A \frac{\partial^2 A}{\partial \theta \partial \phi} \right] dt - L''_\Lambda \left[\frac{\partial G}{\partial \theta} \frac{\partial G}{\partial \phi} + G \frac{\partial^2 G}{\partial \theta \partial \phi} \right] \right\}, \tag{B12}$$

$$\frac{\partial^2 L''_\Lambda(\theta, \phi)}{\partial \phi^2} \bigg|_{\theta_m, \phi_m} = \frac{2}{G^2} \left\{ \frac{1}{\Delta t} \int_{t_0}^{t_1} \left[\left[\frac{\partial A}{\partial \phi} \right]^2 + A \frac{\partial^2 A}{\partial \phi^2} \right] dt - L''_\Lambda \left[\left[\frac{\partial G}{\partial \phi} \right]^2 + G \frac{\partial^2 G}{\partial \phi^2} \right] \right\}, \tag{B13}$$

where the times t_0, t_1 are the limits of the integration corresponding to the minimum point and $\Delta t = t_1 - t_0$.

The derivatives of the function $A(\theta, \phi, t)$ are given below:

$$\frac{\partial A}{\partial \theta} = 2 K_1 \frac{\partial K_1}{\partial \theta} R_{1\Lambda}^{(1)}(t) + 2 K_2 \frac{\partial K_2}{\partial \theta} R_{2\Lambda}^{(2)}(t) + 2 K_3 \frac{\partial K_3}{\partial \theta} R_{3\Lambda}^{(3)}(t)$$

$$+ \left[K_1 \frac{\partial K_2}{\partial \theta} + K_2 \frac{\partial K_1}{\partial \theta} \right] [R_{2\Lambda}^{(1)}(t + \tau_{12}) + R_{1\Lambda}^{(2)}(t - \tau_{12})] + K_1 K_2 \frac{\partial \tau_{12}}{\partial \theta} [\dot{R}_{2\Lambda}^{(1)}(t + \tau_{12}) - \dot{R}_{1\Lambda}^{(2)}(t - \tau_{12})]$$

$$+ \left[K_1 \frac{\partial K_3}{\partial \theta} + K_3 \frac{\partial K_1}{\partial \theta} \right] [R_{3\Lambda}^{(1)}(t + \tau_{13}) + R_{1\Lambda}^{(3)}(t - \tau_{13})] + K_1 K_3 \frac{\partial \tau_{13}}{\partial \theta} [\dot{R}_{3\Lambda}^{(1)}(t + \tau_{13}) - \dot{R}_{1\Lambda}^{(3)}(t - \tau_{13})]$$

$$+ \left[K_2 \frac{\partial K_3}{\partial \theta} + K_3 \frac{\partial K_2}{\partial \theta} \right] [R_{3\Lambda}^{(2)}(t + \tau_{13} - \tau_{12}) + R_{2\Lambda}^{(3)}(t - \tau_{13} + \tau_{12})]$$

$$+ K_2 K_3 \frac{\partial (\tau_{13} - \tau_{12})}{\partial \theta} [\dot{R}_{3\Lambda}^{(2)}(t + \tau_{13} - \tau_{12}) - \dot{R}_{2\Lambda}^{(3)}(t - \tau_{13} + \tau_{12})], \tag{B14}$$

$$\frac{\partial A}{\partial \phi} = 2 K_1 \frac{\partial K_1}{\partial \phi} R_{1\Lambda}^{(1)}(t) + 2 K_2 \frac{\partial K_2}{\partial \phi} R_{2\Lambda}^{(2)}(t) + 2 K_3 \frac{\partial K_3}{\partial \phi} R_{3\Lambda}^{(3)}(t)$$

$$+ \left[K_1 \frac{\partial K_2}{\partial \phi} + K_2 \frac{\partial K_1}{\partial \phi} \right] [R_{2\Lambda}^{(1)}(t + \tau_{12}) + R_{1\Lambda}^{(2)}(t - \tau_{12})] + K_1 K_2 \frac{\partial \tau_{12}}{\partial \phi} [\dot{R}_{2\Lambda}^{(1)}(t + \tau_{12}) - \dot{R}_{1\Lambda}^{(2)}(t - \tau_{12})]$$

$$+ \left[K_1 \frac{\partial K_3}{\partial \phi} + K_3 \frac{\partial K_1}{\partial \phi} \right] [R_{3\Lambda}^{(1)}(t + \tau_{13}) + R_{1\Lambda}^{(3)}(t - \tau_{13})] + K_1 K_3 \frac{\partial \tau_{13}}{\partial \phi} [\dot{R}_{3\Lambda}^{(1)}(t + \tau_{13}) - \dot{R}_{1\Lambda}^{(3)}(t - \tau_{13})]$$

$$+ \left[K_2 \frac{\partial K_3}{\partial \phi} + K_3 \frac{\partial K_2}{\partial \phi} \right] [R_{3\Lambda}^{(2)}(t + \tau_{13} - \tau_{12}) + R_{2\Lambda}^{(3)}(t - \tau_{13} + \tau_{12})]$$

$$+ K_2 K_3 \frac{\partial (\tau_{13} - \tau_{12})}{\partial \phi} [\dot{R}_{3\Lambda}^{(2)}(t + \tau_{13} - \tau_{12}) - \dot{R}_{2\Lambda}^{(3)}(t - \tau_{13} + \tau_{12})], \tag{B15}$$

$$\frac{\partial^2 A}{\partial \theta^2} = \left[2 \left[\frac{\partial K_1}{\partial \theta} \right]^2 + 2 K_1 \frac{\partial^2 K_1}{\partial \theta^2} \right] R_{1\Lambda}^{(1)}(t)$$

$$+ \left[2 \left[\frac{\partial K_2}{\partial \theta} \right]^2 + 2 K_2 \frac{\partial^2 K_2}{\partial \theta^2} \right] R_{2\Lambda}^{(2)}(t) + \left[2 \left[\frac{\partial K_3}{\partial \theta} \right]^2 + 2 K_3 \frac{\partial^2 K_3}{\partial \theta^2} \right] R_{3\Lambda}^{(3)}(t)$$

$$+ \left[K_2 \frac{\partial^2 K_1}{\partial \theta^2} + 2 \frac{\partial K_1}{\partial \theta} \frac{\partial K_2}{\partial \theta} + K_1 \frac{\partial^2 K_2}{\partial \theta^2} \right] [R_{2\Lambda}^{(1)}(t + \tau_{12}) + R_{1\Lambda}^{(2)}(t - \tau_{12})]$$

$$+ 2 \left[\frac{\partial K_1}{\partial \theta} K_2 + \frac{\partial K_2}{\partial \theta} K_1 \right] \frac{\partial \tau_{12}}{\partial \theta} [\dot{R}_{2\Lambda}^{(1)}(t + \tau_{12}) - \dot{R}_{1\Lambda}^{(2)}(t - \tau_{12})]$$

$$+ K_1 K_2 \frac{\partial^2 \tau_{12}}{\partial \theta^2} [\dot{R}_{2\Lambda}^{(1)}(t + \tau_{12}) - \dot{R}_{1\Lambda}^{(2)}(t - \tau_{12})] + K_1 K_2 \left[\frac{\partial \tau_{12}}{\partial \theta} \right]^2 [\ddot{R}_{2\Lambda}^{(1)}(t + \tau_{12}) + \ddot{R}_{1\Lambda}^{(2)}(t - \tau_{12})]$$

$$+ \left[K_3 \frac{\partial^2 K_1}{\partial \theta^2} + 2 \frac{\partial K_1}{\partial \theta} \frac{\partial K_3}{\partial \theta} + K_1 \frac{\partial^2 K_3}{\partial \theta^2} \right] [R_{3\Lambda}^{(1)}(t + \tau_{13}) + R_{1\Lambda}^{(3)}(t - \tau_{13})]$$

$$+ 2 \left[\frac{\partial K_1}{\partial \theta} K_3 + \frac{\partial K_3}{\partial \theta} K_1 \right] \frac{\partial \tau_{13}}{\partial \theta} [\dot{R}_{3\Lambda}^{(1)}(t + \tau_{13}) - \dot{R}_{1\Lambda}^{(3)}(t - \tau_{13})]$$

$$+ K_1 K_3 \frac{\partial^2 \tau_{13}}{\partial \theta^2} [\dot{R}_{3\Lambda}^{(1)}(t + \tau_{13}) - \dot{R}_{1\Lambda}^{(3)}(t - \tau_{13})] + K_1 K_3 \left[\frac{\partial \tau_{13}}{\partial \theta} \right]^2 [\ddot{R}_{3\Lambda}^{(1)}(t + \tau_{13}) + \ddot{R}_{1\Lambda}^{(3)}(t - \tau_{13})]$$

$$+ \left[K_3 \frac{\partial^2 K_2}{\partial \theta^2} + 2 \frac{\partial K_2}{\partial \theta} \frac{\partial K_3}{\partial \theta} + K_2 \frac{\partial^2 K_3}{\partial \theta^2} \right] [R_{3\Lambda}^{(2)}(t + \tau_{13} - \tau_{12}) + R_{2\Lambda}^{(3)}(t - \tau_{13} + \tau_{12})]$$

$$+ 2 \left[\frac{\partial K_2}{\partial \theta} K_3 + \frac{\partial K_3}{\partial \theta} K_2 \right] \frac{\partial (\tau_{13} - \tau_{12})}{\partial \theta} [\dot{R}_{3\Lambda}^{(2)}(t + \tau_{13} - \tau_{12}) - \dot{R}_{2\Lambda}^{(3)}(t - \tau_{13} + \tau_{12})]$$

$$+ K_2 K_3 \frac{\partial^2 (\tau_{13} - \tau_{12})}{\partial \theta^2} [\dot{R}_{3\Lambda}^{(2)}(t + \tau_{13} - \tau_{12}) - \dot{R}_{2\Lambda}^{(3)}(t - \tau_{13} + \tau_{12})]$$

$$+ K_2 K_3 \left[\frac{\partial (\tau_{13} - \tau_{12})}{\partial \theta} \right]^2 [\ddot{R}_{3\Lambda}^{(2)}(t + \tau_{13} - \tau_{12}) + \ddot{R}_{2\Lambda}^{(3)}(t - \tau_{13} + \tau_{12})], \tag{B16}$$

$$\frac{\partial^2 A}{\partial \theta \, \partial \phi} = \left[2 \frac{\partial K_1}{\partial \theta} \frac{\partial K_1}{\partial \phi} + 2 K_1 \frac{\partial^2 K_1}{\partial \theta \, \partial \phi} \right] R_{1\Lambda}^{(1)}(t)$$

$$+ \left[2 \frac{\partial K_2}{\partial \theta} \frac{\partial K_2}{\partial \phi} + 2 K_2 \frac{\partial^2 K_2}{\partial \theta \, \partial \phi} \right] R_{2\Lambda}^{(2)}(t) + \left[2 \frac{\partial K_3}{\partial \theta} \frac{\partial K_3}{\partial \phi} + 2 K_3 \frac{\partial^2 K_3}{\partial \theta \, \partial \phi} \right] R_{3\Lambda}^{(3)}(t)$$

$$+ \left[K_2 \frac{\partial^2 K_1}{\partial \theta \, \partial \phi} + \frac{\partial K_1}{\partial \theta} \frac{\partial K_2}{\partial \phi} + \frac{\partial K_2}{\partial \theta} \frac{\partial K_1}{\partial \phi} + K_1 \frac{\partial^2 K_2}{\partial \theta \, \partial \phi} \right] [R_{2\Lambda}^{(1)}(t + \tau_{12}) + R_{1\Lambda}^{(2)}(t - \tau_{12})]$$

$$+ \left[\left[\frac{\partial K_1}{\partial \theta} K_2 + \frac{\partial K_2}{\partial \theta} K_1 \right] \frac{\partial \tau_{12}}{\partial \phi} + \left[\frac{\partial K_1}{\partial \phi} K_2 + \frac{\partial K_2}{\partial \phi} K_1 \right] \frac{\partial \tau_{12}}{\partial \theta} \right] [\dot{R}_{2\Lambda}^{(1)}(t + \tau_{12}) - \dot{R}_{1\Lambda}^{(2)}(t - \tau_{12})]$$

$$+ K_1 K_2 \frac{\partial^2 \tau_{12}}{\partial \theta \, \partial \phi} [\dot{R}_{2\Lambda}^{(1)}(t + \tau_{12}) - \dot{R}_{1\Lambda}^{(2)}(t - \tau_{12})] + K_1 K_2 \frac{\partial \tau_{12}}{\partial \theta} \frac{\partial \tau_{12}}{\partial \phi} [\ddot{R}_{2\Lambda}^{(1)}(t + \tau_{12}) + \ddot{R}_{1\Lambda}^{(2)}(t - \tau_{12})]$$

$$+ \left[K_3 \frac{\partial^2 K_1}{\partial \theta \, \partial \phi} + \frac{\partial K_1}{\partial \theta} \frac{\partial K_3}{\partial \phi} + \frac{\partial K_3}{\partial \theta} \frac{\partial K_1}{\partial \phi} + K_1 \frac{\partial^2 K_3}{\partial \theta \, \partial \phi} \right] [R_{3\Lambda}^{(1)}(t + \tau_{13}) + R_{1\Lambda}^{(3)}(t - \tau_{13})]$$

$$+ \left[\left[\frac{\partial K_1}{\partial \theta} K_3 + \frac{\partial K_3}{\partial \theta} K_1 \right] \frac{\partial \tau_{13}}{\partial \phi} + \left[\frac{\partial K_1}{\partial \phi} K_3 + \frac{\partial K_3}{\partial \phi} K_1 \right] \frac{\partial \tau_{13}}{\partial \theta} \right] [\dot{R}_{3\Lambda}^{(1)}(t + \tau_{13}) - \dot{R}_{1\Lambda}^{(3)}(t - \tau_{13})]$$

$$+ K_1 K_3 \frac{\partial^2 \tau_{13}}{\partial \theta \, \partial \phi} [\dot{R}_{3\Lambda}^{(1)}(t + \tau_{13}) - \dot{R}_{1\Lambda}^{(3)}(t - \tau_{13})] + K_1 K_3 \frac{\partial \tau_{13}}{\partial \theta} \frac{\partial \tau_{13}}{\partial \phi} [\ddot{R}_{3\Lambda}^{(1)}(t + \tau_{13}) + \ddot{R}_{1\Lambda}^{(3)}(t - \tau_{13})]$$

$$+ \left[K_3 \frac{\partial^2 K_2}{\partial \theta \, \partial \phi} + \frac{\partial K_2}{\partial \theta} \frac{\partial K_3}{\partial \phi} + \frac{\partial K_3}{\partial \theta} \frac{\partial K_2}{\partial \phi} + K_2 \frac{\partial^2 K_3}{\partial \theta \, \partial \phi} \right] [R_{3\Lambda}^{(2)}(t + \tau_{13} - \tau_{12}) + R_{2\Lambda}^{(3)}(t - \tau_{13} + \tau_{12})]$$

$$+ \left[\left[\frac{\partial K_2}{\partial \theta} K_3 + \frac{\partial K_3}{\partial \theta} K_2 \right] \frac{\partial (\tau_{13} - \tau_{12})}{\partial \phi} + \left[\frac{\partial K_2}{\partial \phi} K_3 + \frac{\partial K_3}{\partial \phi} K_2 \right] \frac{\partial (\tau_{13} - \tau_{12})}{\partial \theta} \right]$$

$$\times [\dot{R}_{3\Lambda}^{(2)}(t + \tau_{13} - \tau_{12}) - \dot{R}_{2\Lambda}^{(3)}(t - \tau_{13} + \tau_{12})]$$

$$+ K_2 K_3 \frac{\partial^2 (\tau_{13} - \tau_{12})}{\partial \theta \, \partial \phi} [\dot{R}_{3\Lambda}^{(2)}(t + \tau_{13} - \tau_{12}) - \dot{R}_{2\Lambda}^{(3)}(t - \tau_{13} + \tau_{12})]$$

$$+ K_2 K_3 \frac{\partial (\tau_{13} - \tau_{12})}{\partial \theta} \frac{\partial (\tau_{13} - \tau_{12})}{\partial \phi} [\ddot{R}_{3\Lambda}^{(2)}(t + \tau_{13} - \tau_{12}) + \ddot{R}_{2\Lambda}^{(3)}(t - \tau_{13} + \tau_{12})], \tag{B17}$$

$$\frac{\partial^2 A}{\partial \phi^2} = \left[2 \left[\frac{\partial K_1}{\partial \phi} \right]^2 + 2 K_1 \frac{\partial^2 K_1}{\partial \phi^2} \right] R_{1\Lambda}^{(1)}(t)$$

$$+ \left[2 \left[\frac{\partial K_2}{\partial \phi} \right]^2 + 2 K_2 \frac{\partial^2 K_2}{\partial \phi^2} \right] R_{2\Lambda}^{(2)}(t) + \left[2 \left[\frac{\partial K_3}{\partial \phi} \right]^2 + 2 K_3 \frac{\partial^2 K_3}{\partial \phi^2} \right] R_{3\Lambda}^{(3)}(t)$$

$$+ \left[K_2 \frac{\partial^2 K_1}{\partial \phi^2} + 2 \frac{\partial K_1}{\partial \phi} \frac{\partial K_2}{\partial \phi} + K_1 \frac{\partial^2 K_2}{\partial \phi^2} \right] [R_{2\Lambda}^{(1)}(t + \tau_{12}) + R_{1\Lambda}^{(2)}(t - \tau_{12})]$$

$$+ 2 \left[\frac{\partial K_1}{\partial \phi} K_2 + \frac{\partial K_2}{\partial \phi} K_1 \right] \frac{\partial \tau_{12}}{\partial \phi} [\dot{R}_{2\Lambda}^{(1)}(t + \tau_{12}) - \dot{R}_{1\Lambda}^{(2)}(t - \tau_{12})]$$

$$+ K_1 K_2 \frac{\partial^2 \tau_{12}}{\partial \phi^2} [\dot{R}_{2\Lambda}^{(1)}(t + \tau_{12}) - \dot{R}_{1\Lambda}^{(2)}(t - \tau_{12})] + K_1 K_2 \left[\frac{\partial \tau_{12}}{\partial \phi} \right]^2 [\ddot{R}_{2\Lambda}^{(1)}(t + \tau_{12}) + \ddot{R}_{1\Lambda}^{(2)}(t - \tau_{12})]$$

$$+ \left[K_3 \frac{\partial^2 K_1}{\partial \phi^2} + 2 \frac{\partial K_1}{\partial \phi} \frac{\partial K_3}{\partial \phi} + K_1 \frac{\partial^2 K_3}{\partial \phi^2} \right] [R_{3\Lambda}^{(1)}(t + \tau_{13}) + R_{1\Lambda}^{(3)}(t - \tau_{13})]$$

$$+ 2 \left[\frac{\partial K_1}{\partial \phi} K_3 + \frac{\partial K_3}{\partial \phi} K_1 \right] \frac{\partial \tau_{13}}{\partial \phi} [\dot{R}_{3\Lambda}^{(1)}(t + \tau_{13}) - \dot{R}_{1\Lambda}^{(3)}(t - \tau_{13})]$$

$$+ K_1 K_3 \frac{\partial^2 \tau_{13}}{\partial \phi^2} [\dot{R}_{3\Lambda}^{(1)}(t + \tau_{13}) - \dot{R}_{1\Lambda}^{(3)}(t - \tau_{13})] + K_1 K_3 \left[\frac{\partial \tau_{13}}{\partial \phi} \right]^2 [\ddot{R}_{3\Lambda}^{(1)}(t + \tau_{13}) + \ddot{R}_{1\Lambda}^{(3)}(t - \tau_{13})]$$

$$+ \left[K_3 \frac{\partial^2 K_2}{\partial \phi^2} + 2 \frac{\partial K_2}{\partial \phi} \frac{\partial K_3}{\partial \phi} + K_2 \frac{\partial^2 K_3}{\partial \phi^2} \right] [R_{3\Lambda}^{(2)}(t + \tau_{13} - \tau_{12}) + R_{2\Lambda}^{(3)}(t - \tau_{13} + \tau_{12})]$$

$$+ 2 \left[\frac{\partial K_2}{\partial \phi} K_3 + \frac{\partial K_3}{\partial \phi} K_2 \right] \frac{\partial (\tau_{13} - \tau_{12})}{\partial \phi} [\dot{R}_{3\Lambda}^{(2)}(t + \tau_{13} - \tau_{12}) - \dot{R}_{2\Lambda}^{(3)}(t - \tau_{13} + \tau_{12})]$$

$$+ K_2 K_3 \frac{\partial^2 (\tau_{13} - \tau_{12})}{\partial \phi^2} [\dot{R}_{3\Lambda}^{(2)}(t + \tau_{13} - \tau_{12}) - \dot{R}_{2\Lambda}^{(3)}(t - \tau_{13} + \tau_{12})]$$

$$+ K_2 K_3 \left[\frac{\partial (\tau_{13} - \tau_{12})}{\partial \phi} \right]^2 [\ddot{R}_{3\Lambda}^{(2)}(t + \tau_{13} - \tau_{12}) + \ddot{R}_{2\Lambda}^{(3)}(t - \tau_{13} + \tau_{12})], \tag{B18}$$

where $R_{n\Lambda}^{(m)}(t)$, $m,n = 1,2,3$, are the filtered noisy detector responses as defined in Sec. V, cases (i) and (ii); $\dot{R}_{n\Lambda}^{(m)}(t)$, $m,n = 1,2,3$, are the first time derivatives of these responses and $\ddot{R}_{n\Lambda}^{(m)}(t)$, $m,n = 1,2,3$, are the second time derivatives of them. The derivatives of the time delays are given by Eqs. (4.15) and (4.16). The functions $K_1, K_2,$ and K_3 are given in Eqs. (3.8a), (3.8b), and (3.8c).

APPENDIX C

In this Appendix we give the explicit forms of the coefficients of the optimal linear combination for reconstructing the waveforms $h_{opt+}(t)$ and $h_{opt\times}(t)$ of the incoming gravitational wave [Eq. (4.20)]. We also give the explicit forms of the functions $\mu_{i+}(\theta,\phi,\Delta\theta,\Delta\phi)$, $\mu_{i\times}(\theta,\phi,\Delta\theta,\Delta\phi)$, $\epsilon_{i+}(\theta,\phi,\Delta\theta,\Delta\phi)$, and $\epsilon_{i\times}(\theta,\phi,\Delta\theta,\Delta\phi)$ where $i = 1,2,3$ as given in Eqs. (6.9) and (6.10).

Let the optimal linear combination $h_{opt+}(t)$ which gives the least amount of noise in the reconstructed waveform be

$$h_{opt+}(t) = a_+(\theta,\phi) h_{1+}(t)$$
$$+ b_+(\theta,\phi) h_{2+}(t) + c_+(\theta,\phi) h_{3+}(t). \tag{C1}$$

When the noise amplitudes are reduced to zero, $h_{opt+}(t)$ should reduce to the noise-free waveform $h_+(t)$. This implies

$$a_+(\theta,\phi) + b_+(\theta,\phi) + c_+(\theta,\phi) = 1. \tag{C2}$$

We define the root-mean-squared error δh_+ in the reconstructed waveform as

$$\delta h_+ = \left[\frac{1}{\Delta t} \int_{t_0}^{t_1} [h_{opt+}(t) - h_+(t)]^2 dt \right]^{1/2}, \tag{C3}$$

where $[t_0, t_1]$ is the optimal interval of integration and $\Delta t = t_1 - t_0$. We minimize δh_+^2 with respect to $a_+(\theta,\phi)$, $b_+(\theta,\phi)$, and $c_+(\theta,\phi)$ subject to the constraint given by Eq. (C2) using the method of Lagrange multipliers. We define a new mean-squared error δh_{new+}^2 with an arbitrary parameter λ:

$$\delta h_{new+}^2 = \delta h_+^2 - \lambda [a_+ + b_+ + c_+ - 1]. \tag{C4}$$

For brevity, we refer to $a_+(\theta,\phi)$, $b_+(\theta,\phi)$, and $c_+(\theta,\phi)$ as a_+, b_+, and c_+, respectively. Using Eqs.

(4.17)–(4.19), we get

$$\delta h_{new+}^2 = \frac{1}{\Delta t} \int_{t_0}^{t_1} [(a_+ + b_+ + c_+ - 1) h_+(t)$$
$$+ A_{1+} \Lambda_1(t) + A_{2+} \Lambda_2(t + \tau_{12})$$
$$+ A_{3+} \Lambda_3(t + \tau_{13})]^2 dt$$
$$- \lambda [a_+ + b_+ + c_+ - 1], \tag{C5}$$

where $\Lambda_i(t)$ is the random process representing the noise in detector i; $h_+(t)$ is the noise-free waveform of the gravitational wave; A_{i+}, $i = 1,2,3$, are given by

$$A_{1+} = \frac{c_+ F_{2\times}}{K_3} - \frac{b_+ F_{3\times}}{K_2}, \tag{C6}$$

$$A_{2+} = \frac{a_+ F_{3\times}}{K_1} - \frac{c_+ F_{1\times}}{K_3}, \tag{C7}$$

$$A_{3+} = \frac{b_+ F_{1\times}}{K_2} - \frac{a_+ F_{2\times}}{K_1}, \tag{C8}$$

where the functions F_{i+}, $F_{i\times}$ are given in Appendix A and the functions K_i are given in Eqs. (3.8). Note that $h_{opt+}(t)$ as defined by Eq. (C1) can also be expressed in terms of the noisy detector responses $R_{i\Lambda}(t)$ $i = 1,2,3$, using the coefficients A_{i+}, $i = 1,2,3$, in the following way:

$$h_{opt+}(t) = \sum_{i=1}^{3} A_{i+} R_{i\Lambda}(t + \xi_i), \tag{C9}$$

where the time delays ξ_i are given by

$$\xi_1 = 0, \quad \xi_2 = \tau_{12}, \quad \xi_3 = \tau_{13}. \tag{C10}$$

We differentiate δh_{new+}^2 with respect to the parameters a_+, b_+, c_+, and λ and set the resulting expressions to zero. We then get

$$\frac{\partial \delta h_{new+}^2}{\partial \lambda} = a_+ + b_+ + c_+ - 1 = 0, \tag{C11}$$

$$\frac{\partial \delta h_{new+}^2}{\partial a_+} = A_{2+} \frac{F_{3\times}}{K_1} \sigma_2^2 - A_{3+} \frac{F_{2\times}}{K_1} \sigma_3^2$$
$$- \frac{\lambda}{2} + \Gamma = 0, \tag{C12}$$

$$\frac{\partial \delta h^2_{\text{new}+}}{\partial b_+} = A_{3+} \frac{F_{1\times}}{K_2} \sigma_3^2 - A_{1+} \frac{F_{3\times}}{K_2} \sigma_1^2$$

$$- \frac{\lambda}{2} + \Gamma = 0, \tag{C13}$$

$$\frac{\partial \delta h^2_{\text{new}+}}{\partial c_+} = A_{1+} \frac{F_{2\times}}{K_3} \sigma_1^2 - A_{2+} \frac{F_{1\times}}{K_3} \sigma_2^2$$

$$- \frac{\lambda}{2} + \Gamma = 0, \tag{C14}$$

$$\Gamma = \frac{1}{\Delta t} \int_{t_0}^{t_1} h_+(t) [A_{1+} \Lambda_1(t) + A_{2+} \Lambda_2(t + \tau_{12})$$

$$+ A_{3+} \Lambda_3(t + \tau_{13})] \, dt , \tag{C15}$$

where σ_i^2 is the variance of the random process $\Lambda_i(t)$. In deriving the equations above we have used the fact that the random process $\Lambda_i(t)$ is uncorrelated with the random process $\Lambda_j(t)$ unless $i = j$ and

$$\sigma_i^2 = \frac{1}{\Delta t} \int_{t_0}^{t_1} \Lambda_i^2(t) \, dt .$$

We also used Eq. (C11) to reduce Eq. (C15) to its present form. Note that the function Γ is not known since the noise-free waveform $h_+(t)$ is unavailable in the presence of the noise. We eliminate the unknown combination $\Gamma - \lambda/2$ by subtracting Eq. (C13) from Eq. (C12), and Eq. (C14) from Eq. (C13). We then get three equations involving only a_+, b_+, and c_+:

$$a_+ + b_+ + c_+ = 1, \tag{C16}$$

$$\alpha_1 a_+ + \beta_1 b_+ + \gamma_1 c_+ = 0, \tag{C17}$$

$$\alpha_2 a_+ + \beta_2 b_+ + \gamma_2 c_+ = 0, \tag{C18}$$

where

$$\alpha_1 = \frac{F_{3\times}^2}{K_1^2} \sigma_2^2 - \frac{K_3 F_{2\times} F_{3\times}}{K_1^2 K_2} \sigma_3^2, \tag{C19}$$

$$\beta_1 = - \frac{F_{3\times}^2}{K_2^2} \sigma_1^2 + \frac{K_3 F_{1\times} F_{3\times}}{K_2^2 K_1} \sigma_3^2, \tag{C20}$$

$$\gamma_1 = \frac{F_{2\times} F_{3\times}}{K_2 K_3} \sigma_1^2 - \frac{F_{1\times} F_{3\times}}{K_1 K_3} \sigma_2^2, \tag{C21}$$

$$\alpha_2 = \frac{F_{1\times} F_{3\times}}{K_1 K_3} \sigma_2^2 - \frac{F_{1\times} F_{2\times}}{K_1 K_2} \sigma_3^2, \tag{C22}$$

$$\beta_2 = \frac{F_{1\times}^2}{K_2^2} \sigma_3^2 - \frac{K_1 F_{1\times} F_{3\times}}{K_2^2 K_3} \sigma_1^2, \tag{C23}$$

$$\gamma_2 = - \frac{F_{1\times}^2}{K_3^2} \sigma_2^2 + \frac{K_1 F_{1\times} F_{2\times}}{K_3^2 K_2} \sigma_1^2. \tag{C24}$$

In deriving the equations above, we have made use of the identity

$$F_{1\times} K_1 + F_{2\times} K_2 + F_{3\times} K_3 = 0. \tag{C25}$$

We solve for the parameter c_+ using Eq. (C16), and we substitute the resulting expression in Eqs. (C17) and (C18)

to obtain

$$(\alpha_1 - \gamma_1) a_+ + (\beta_1 - \gamma_1) b_+ = - \gamma_1, \tag{C26}$$

$$(\alpha_2 - \gamma_2) a_+ + (\beta_2 - \gamma_2) b_+ = - \gamma_2. \tag{C27}$$

Equations (C26) and (C27) are linearly dependent. Equation (C27) can be obtained by multiplying Eq. (C26) by $(F_{1\times} K_1)/(F_{3\times} K_3)$. This implies that we have only two equations for the three unknowns a_+, b_+, and c_+. We leave c_+ as an arbitrary parameter without loss of generality and we solve for a_+ and b_+ in terms of c_+, the angular functions $F_{i\times}$, K_i and the variances σ_i^2, $i = 1,2,3$, using Eqs. (C16) and (C26). We then get

$$a_+ = \frac{1}{\rho} \left[K_1^2 \sigma_1^2 - \frac{K_1 K_3 F_{1\times}}{F_{3\times}} \sigma_3^2 \right] + \frac{K_1 F_{1\times}}{K_3 F_{3\times}} c_+, \tag{C28}$$

$$b_+ = \frac{1}{\rho} \left[K_2^2 \sigma_2^2 - \frac{K_2 K_3 F_{2\times}}{F_{3\times}} \sigma_3^2 \right] + \frac{K_2 F_{2\times}}{K_3 F_{3\times}} c_+, \tag{C29}$$

where $\rho = K_1^2 \sigma_1^2 + K_2^2 \sigma_2^2 + K_3^2 \sigma_3^2$.

Substituting Eqs. (C28) and (C29) into Eqs. (C6)–(C8) we obtain

$$A_{1+} = \frac{1}{\rho} (K_3 F_{2\times} \sigma_3^2 - K_2 F_{3\times} \sigma_2^2), \tag{C30}$$

$$A_{2+} = \frac{1}{\rho} (K_1 F_{3\times} \sigma_1^2 - K_3 F_{1\times} \sigma_3^2), \tag{C31}$$

$$A_{3+} = \frac{1}{\rho} (K_2 F_{1\times} \sigma_2^2 - K_1 F_{2\times} \sigma_1^2). \tag{C32}$$

We point out that the arbitrary parameter c_+ does not appear in the expressions for A_{1+}, A_{2+}, and A_{3+}. Using Eq. (C9) we see that the optimally reconstructed waveform $h_{\text{opt}+}(t)$ is unique. The total integrated noise δh_+ in the optimally reconstructed waveform $h_{\text{opt}+}(t)$ is given by

$$\delta h_+ = \left[\sum_{i=1}^{3} A_{i+}^2 \sigma_i^2 \right]^{1/2}. \tag{C33}$$

This formula gives the minimum root-mean-squared error in the reconstructed waveform $h_{\text{opt}+}(t)$ due to the noise in the detectors. In general, the error in the reconstructed waveform will be larger due to the errors in the determination of the source location [see Eqs. (6.9)–(6.11)].

Similarly, let the optimal linear combination $h_{\text{opt}\times}(t)$ which gives the least amount of noise in the reconstructed waveform be

$$h_{\text{opt}\times}(t) = a_\times(\theta,\phi) h_{1\times}(t) + b_\times(\theta,\phi) h_{2\times}(t)$$

$$+ c_\times(\theta,\phi) h_{3\times}(t). \tag{C34}$$

When the noise amplitudes are reduced to zero, $h_{\text{opt}\times}(t)$ should reduce to the noise-free waveform $h_\times(t)$. This implies

$$a_\times(\theta,\phi) + b_\times(\theta,\phi) + c_\times(\theta,\phi) = 1 . \tag{C35}$$

Using Eqs. (4.1a), (4.1b), and (4.1c) we can express $h_{\mathrm{opt}\times}(t)$ in terms of the noisy detector responses $R_{i\Lambda}(t)$, $i = 1,2,3$, in the following way:

$$h_{\mathrm{opt}\times}(t) = \sum_{i=1}^{3} A_{i\times} R_{i\Lambda}(t + \xi_i) . \tag{C36}$$

The time delays ξ_i are given in Eq. (C10); $A_{i\times}$, $i = 1,2,3$, are given by

$$A_{1\times} = \frac{b_\times F_{3+}}{K_2} - \frac{c_\times F_{2+}}{K_3} , \tag{C37}$$

$$A_{2\times} = \frac{c_\times F_{1+}}{K_3} - \frac{a_\times F_{3+}}{K_1} , \tag{C38}$$

$$A_{3\times} = \frac{a_\times F_{2+}}{K_1} - \frac{b_\times F_{1+}}{K_2} . \tag{C39}$$

For brevity, we refer to $a_\times(\theta,\phi)$, $b_\times(\theta,\phi)$, and $c_\times(\theta,\phi)$ as $a_\times$, $b_\times$, and $c_\times$, respectively. We define the root-mean-squared error $\delta h_\times$ in the reconstructed waveform as

$$\delta h_\times = \left[\frac{1}{\Delta t} \int_{t_0}^{t_1} [h_{\mathrm{opt}\times}(t) - h_\times(t)]^2 \, dt \right]^{1/2} . \tag{C40}$$

Proceeding as we have done for the $+$ polarization of the wave and using the identity

$$F_{1+} K_1 + F_{2+} K_2 + F_{3+} K_3 = 0 , \tag{C41}$$

we obtain the coefficients for the optimal reconstruction of the waveform $h_{\mathrm{opt}\times}(t)$ as introduced in Eq. (C36):

$$A_{1\times} = \frac{1}{\rho} (K_2 F_{3+} \sigma_2^2 - K_3 F_{2+} \sigma_3^2) , \tag{C42}$$

$$A_{2\times} = \frac{1}{\rho} (K_3 F_{1+} \sigma_3^2 - K_1 F_{3+} \sigma_1^2) , \tag{C43}$$

$$A_{3\times} = \frac{1}{\rho} (K_1 F_{2+} \sigma_1^2 - K_2 F_{1+} \sigma_2^2) . \tag{C44}$$

The total integrated noise $\delta h_\times$ in the optimally reconstructed waveform $h_{\mathrm{opt}\times}(t)$ is given by

$$\delta h_\times = \left[\sum_{i=1}^{3} A_{i\times}^2 \sigma_i^2 \right]^{1/2} . \tag{C45}$$

The functions $\mu_{i+}(\theta,\phi,\Delta\theta,\Delta\phi)$, $\mu_{i\times}(\theta,\phi,\Delta\theta,\Delta\phi)$, $\epsilon_{i+}(\theta,\phi,\Delta\theta,\Delta\phi)$, and $\epsilon_{i\times}(\theta,\phi,\Delta\theta,\Delta\phi)$, $i = 1,2,3$, which are introduced in Eqs. (6.9) and (6.10) are then given by

$$\mu_{i+}(\theta,\phi,\Delta\theta,\Delta\phi) = \frac{\partial A_{i+}}{\partial\theta} \Delta\theta + \frac{\partial A_{i+}}{\partial\phi} \Delta\phi , \tag{C46}$$

$$\mu_{i\times}(\theta,\phi,\Delta\theta,\Delta\phi) = \frac{\partial A_{i\times}}{\partial\theta} \Delta\theta + \frac{\partial A_{i\times}}{\partial\phi} \Delta\phi , \tag{C47}$$

$$\epsilon_{i+}(\theta,\phi,\Delta\theta,\Delta\phi) = A_{i+} \left[\frac{\partial\xi_i}{\partial\theta} \Delta\theta + \frac{\partial\xi_i}{\partial\phi} \Delta\phi \right] , \tag{C48}$$

$$\epsilon_{i\times}(\theta,\phi,\Delta\theta,\Delta\phi) = A_{i\times} \left[\frac{\partial\xi_i}{\partial\theta} \Delta\theta + \frac{\partial\xi_i}{\partial\phi} \Delta\phi \right] . \tag{C49}$$

The derivatives of the time delays τ_{12} and τ_{13} are given in Eqs. (4.15) and (4.16).

APPENDIX D

In this Appendix we outline a method for computing the probability distributions for the errors $(\Delta\theta,\Delta\phi)$ in the computed source location (θ_m,ϕ_m). For simplicity, we will analyze the unfiltered version of our method; the filtered case can be analyzed in a similar fashion.

Consider the unfiltered least-squares function $L'_\Lambda(\theta,\phi)$:

$$L'_\Lambda(\theta,\phi) = \frac{1}{\Delta t} \int_{t_0}^{t_1} \frac{\left[\sum_{i=1}^{3} K_i R_{i\Lambda}(t + \xi_i) \right]^2}{K_1^2 \sigma_1^2 + K_2^2 \sigma_2^2 + K_3^2 \sigma_3^2} \, dt , \tag{D1}$$

where ξ_i are the time delays as defined in Appendix C. One can formally expand the noisy detector responses $R_{i\Lambda}(t + \xi_i)$ as

$$R_{i\Lambda}(t + \xi_i) = R_i(t + \xi_i) + \Lambda'_i(t) , \tag{D2}$$

where $R_i(t+\xi_i)$ are the noise-free detector responses; $\Lambda'_i(t)$ is a random process equal to the random process $\Lambda_i(t + \xi_i)$. By the ergodic hypothesis, the probability distribution of the random process $\Lambda'_i(t)$ is equal to the probability distribution of the unshifted random process $\Lambda_i(t)$.

Substituting Eq. (D2) into Eq. (D1), we obtain

$$L'_\Lambda(\theta,\phi) = \frac{1}{\Delta t} \int_{t_0}^{t_1} \left[\sum_{i,j=1}^{3} K'_i K'_j R_i(t + \xi_i) R_j(t + \xi_j) + 2 \sum_{i,j=1}^{3} K'_i K'_j R_i(t + \xi_i) \Lambda'_j(t) + \sum_{i=1}^{3} K'^2_i \Lambda'^2_j(t) \right] dt , \tag{D3}$$

where $K'_i = K_i / (K_1^2 \sigma_1^2 + K_2^2 \sigma_2^2 + K_3^2 \sigma_3^2)^{1/2}$ and the cross terms involving two different random processes integrate out to zero since these processes are assumed to be uncorrelated.

As shown in Sec. VI and Appendix B, the errors $(\Delta\theta,\Delta\phi)$ are computed using the Hessian matrix of $L'_\Lambda(\theta,\phi)$ evaluated at the minimum of $L'_\Lambda(\theta,\phi)$. The elements of the Hessian matrix are second derivatives of the least-squares function with respect to the angles θ and ϕ as given in Eq. (B1) of Appendix B. Using Eq. (D3), we note that the angular dependence of $L'_\Lambda(\theta,\phi)$ is due to the angular functions K'_i and the implicit dependence of the noise-free detector responses $R_i(t + \xi_i)$ on the angles θ and ϕ.

The analytic expressions for the errors $\Delta\theta$ and $\Delta\phi$ in terms of the elements of the Hessian described above are

$$\Delta\theta = \frac{-H'_{m\theta\phi}[2 - 2L'_\Lambda(\theta_m,\phi_m)]^{1/2}}{[(H'_{m\theta\theta} - \lambda_+)^2 + H'^2_{m\theta\phi}]^{1/2}\lambda_+^{1/2}} + \frac{-H'_{m\theta\phi}[2 - 2L'_\Lambda(\theta_m,\phi_m)]^{1/2}}{[(H'_{m\theta\theta} - \lambda_-)^2 + H'^2_{m\theta\phi}]^{1/2}\lambda_-^{1/2}} , \tag{D4}$$

$$\Delta\phi = \frac{(H'_{m\theta\theta} - \lambda_+)[2 - 2L'_\Lambda(\theta_m,\phi_m)]^{1/2}}{[(H'_{m\theta\theta} - \lambda_+)^2 + H'^2_{m\theta\phi}]^{1/2}\lambda_+^{1/2}} + \frac{(H'_{m\theta\theta} - \lambda_-)[2 - 2L'_\Lambda(\theta_m,\phi_m)]^{1/2}}{[(H'_{m\theta\theta} - \lambda_-)^2 + H'^2_{m\theta\phi}]^{1/2}\lambda_-^{1/2}} , \tag{D5}$$

where

$$\lambda_\pm = \frac{\text{tr}(\vec{\vec{H}}'_m) \pm [\text{tr}(\vec{\vec{H}}'_m)^2 - 4\det(\vec{\vec{H}}'_m)]^{1/2}}{2} , \tag{D6}$$

and

$$\text{tr}(\vec{\vec{H}}'_m) = H'_{m\theta\theta} + H'_{m\phi\phi} ,$$

$$\det(\vec{\vec{H}}'_m) = H'_{m\theta\theta} H'_{m\phi\phi} - H'^2_{m\theta\phi} .$$

$H'_{m\theta\theta}$, $H'_{m\theta\phi}$ and $H'_{m\phi\phi}$ are the elements of the Hessian matrix of $L'_\Lambda(\theta,\phi)$ evaluated at its minimum as given by Eq. (B1) of Appendix B.

For the moment, let us assume that the noise-free detector responses $R_i(t + \xi_i)$ are known functions of time. From Eq. (D3), we see that the element $H'_{m\theta\phi}$ of the Hessian matrix evaluated at the minimum of the least-squares function $L'_\Lambda(\theta,\phi)$ will contain two noise terms:

$$\nu_{\theta\phi} = \frac{2}{\Delta t} \int_{t_0}^{t_1} \sum_{i,j=1}^{3} \frac{\partial^2}{\partial\theta\,\partial\phi}[K'_i K'_j R_i(t + \xi_i)] \Lambda'_j(t)\,dt , \tag{D7}$$

$$\delta_{\theta\phi} = \frac{1}{\Delta t} \int_{t_0}^{t_1} \sum_{i=1}^{3} \frac{\partial^2}{\partial\theta\,\partial\phi} K'^2_i \Lambda'^2_i(t)\,dt . \tag{D8}$$

The other elements $H'_{m\theta\theta}$ and $H'_{m\phi\phi}$ will contain identical terms with the appropriate derivatives. We will compute the probability distributions of the random variables $\nu_{\theta\phi}$ and $\delta_{\theta\phi}$.

Let $p_i(\Lambda_i)$ be the probability distribution of the random process $\Lambda_i(t)$. As mentioned above, p_i is also the probability distribution of $\Lambda'_i(t)$. The characteristic function $\chi(k)$ of a probability distribution $p(x)$ is defined by

$$\chi(k) = \int_{-\infty}^{+\infty} e^{-ikx} p(x)\,dx . \tag{D9}$$

Let $z = f(x,y)$ be a function of two random variables x and y with probability distributions $p(x)$ and $q(y)$, respectively. The characteristic function for the probability distribution of the random variable z is given by[22]

$$\chi_z(k) = \int\int e^{-ikf(x,y)} p(x) q(y)\,dx\,dy . \tag{D10}$$

If $z = ax + by$ where a, b are constants, then the characteristic function $\chi_z(k)$ is proportional to the product of the characteristic functions $\chi_x(k)$ and $\chi_y(k)$:

$$\chi_z(k) = \int\int e^{-ik(ax+by)} p(x) q(y)\,dx\,dy$$

$$= \int e^{-ikax} p(x)\,dx \int e^{-ikby} q(y)\,dy$$

$$= \chi_x(ka)\chi_y(kb) . \tag{D11}$$

If the noise in the detector responses is Gaussian, then the random variable $\nu_{\theta\phi}$ is a linear combination of random variables distributed with Gaussian distributions. This is because the integral over time can be performed as a discrete sum and at each discrete time coordinate the value of the random process can be regarded as a random variable if the integration step is larger than the relaxation time for the random process. The probability distribution of the random process $\nu_{\theta\phi}$ can then be obtained using Eqs. (D9)–(D11) with $p_i(\Lambda_i)$ substituted for $p(x)$ and $q(y)$.

The random variable $\delta_{\theta\phi}$ is a linear combination of squares of normally distributed random processes. Let $z = x^2$ where x is a normally distributed random variable with zero mean and variance σ^2. The characteristic function of the probability distribution of z is given by

$$\chi_z(k) = (1 - 2ik\sigma^2)^{-1/2} . \tag{D12}$$

Using this result and expressing the time integral as a discrete sum, the probability distribution for the random variable $\delta_{\theta\phi}$ can be computed by multiplying the characteristic functions and by performing an inverse Fourier transform on the product.

Let the analytic expressions for $\Delta\theta$ and $\Delta\phi$ in terms of the random processes $\nu_{\theta\theta}$, $\nu_{\theta\phi}$, $\nu_{\phi\phi}$, $\delta_{\theta\theta}$, $\delta_{\theta\phi}$, $\delta_{\phi\phi}$ be given by

$$\Delta\theta = G(\nu_{\theta\theta},\nu_{\theta\phi},\nu_{\phi\phi},\delta_{\theta\theta},\delta_{\theta\phi},\delta_{\phi\phi}) , \tag{D13}$$

$$\Delta\phi = H(\nu_{\theta\theta},\nu_{\theta\phi},\nu_{\phi\phi},\delta_{\theta\theta},\delta_{\theta\phi},\delta_{\phi\phi}) . \tag{D14}$$

The precise form of the functions G and H can be obtained by combining Eqs. (B1) and (D3)–(D6).

The characteristic functions $\chi_{\Delta\theta}$ and $\chi_{\Delta\phi}$ of the probability distributions of the errors $\Delta\theta$ and $\Delta\phi$ are then given by

$$\chi_{\Delta\theta}(k) = \int e^{-ikG} p_1(\nu_{\theta\theta}) p_2(\nu_{\theta\phi}) p_3(\nu_{\phi\phi})$$
$$\times p_4(\delta_{\theta\theta}) p_5(\delta_{\theta\phi}) p_6(\delta_{\phi\phi})$$
$$\times d\nu_{\theta\theta} d\nu_{\theta\phi} d\nu_{\phi\phi} d\delta_{\theta\theta} d\delta_{\theta\phi} d\delta_{\phi\phi} , \tag{D15}$$

$$\chi_{\Delta\phi}(k) = \int e^{-ikH} p_1(\nu_{\theta\theta}) p_2(\nu_{\theta\phi}) p_3(\nu_{\phi\phi})$$
$$\times p_4(\delta_{\theta\theta}) p_5(\delta_{\theta\phi}) p_6(\delta_{\phi\phi})$$
$$\times d\nu_{\theta\theta} d\nu_{\theta\phi} d\nu_{\phi\phi} d\delta_{\theta\theta} d\delta_{\theta\phi} d\delta_{\phi\phi} , \tag{D16}$$

where the functions p_i, $i = 1,2,3,4,5,6$ are the probability distributions for their arguments. The probability distributions for $\Delta\theta$ and $\Delta\phi$ are obtained by inverse Fourier transforming the expressions given in Eqs. (D15) and (D16).

In the discussion above, we assumed that we knew the noise-free detector responses $R_i(t + \xi_i)$. In reality, these functions are not known. Consider a sequence of experiments in which the source location and its waveforms are held fixed. In each experiment, the realizations of the detector noise will be different leading to slightly different computed source locations and waveforms. After the experiments are concluded, one obtains a "mean source location" and two "mean waveforms" by averaging the source locations and waveforms obtained in each experiment. These will be the closest approximations to the real source location and the real waveforms. In such a

case, we compute the best guesses for noise-free detector responses using the "mean source location" and the "mean waveforms" and we substitute these in place of the "unknown" detector responses in the equations above.

If we have only one set of three responses, we compute the probability distributions of the angular errors $\Delta\theta$ and $\Delta\phi$ in the following way: After the source location is determined using our method, we fit smooth curves to the noisy detector responses and we use these smooth curves in place of the unknown noise-free responses in the equations above to compute the desired probability distributions.

[1]D. M. Eardley, in *Gravitational Radiation,* edited by N. Deruelle and T. Piran (North-Holland, Amsterdam, 1982).

[2]K. S. Thorne, in *300 Years of Gravitation,* edited S. W. Hawking and W. Israel (Cambridge University Press, Cambridge, England, 1987).

[3]J. Weber, Phys. Rev. **117**, 306 (1960).

[4]P. F. Michelson and R. C. Taber, Phys. Rev. D **29**, 2149 (1984).

[5]R. W. P. Drever, in *Gravitational Radiation,* edited by N. Deruelle and T. Piran (North-Holland, Amsterdam, 1982).

[6]R. Weiss, in *Sources of Gravitational Radiation,* edited by L. Smarr (Cambridge University Press, Cambridge, England, 1979).

[7]R. W. P. Drever, in *Proceedings of the NATO Workshop on Gravitational Wave Data Analysis,* edited by B. F. Schutz (Kluwer, Dordrecht, 1989).

[8]R. W. P. Drever, in *The Abstracts of the Fifth Marcel Grossmann Meeting,* edited by B. Lohman, A. Peakall, and P. J. Veitch (University of Western Australia, Perth, 1988).

[9]R. Weiss and R. W. P. Drever, in *The Abstracts of the Eleventh International Conference on General Relativity and Gravitation,* edited by B. Laurent and K. Rosquist (University of Stockholm, Stockholm, 1986).

[10]J. Hough *et al.,* in *The Abstracts of the Fifth Marcel Grossmann Meeting* (Ref. 8).

[11]A. Giazotto *et al.,* in *The Abstracts of the Fifth Marcel Grossmann Meeting* (Ref. 8).

[12]R. Schilling *et al.,* in *The Abstracts of the Fifth Marcel Grossmann Meeting* (Ref. 8).

[13]B. F. Schutz and M. Tinto, Mon. Not. R. Astron. Soc. **224**, 131 (1987).

[14]S. V. Dhurandhar and M. Tinto, Mon. Not. R. Astron. Soc. **234**, 663 (1988).

[15]A. Krolak and B. F. Schutz, Gen. Relativ. Gravit. **19**, 1163 (1987).

[16]Y. Gürsel and M. Tinto, in *Proceedings of the Fifth Marcel Grossmann Meeting on General Relativity,* Perth, Australia, 1988, edited by D. Blair and M. J. Buckingham (World

Scientific, Singapore, 1989).

[17]F. B. Estabrook, Gen. Relativ. Gravit. **17**, 719 (1985).

[18]R. L. Forward, Phys. Rev. D **17**, 379 (1978).

[19]E. T. Newman and R. Penrose, J. Math. Phys. **3**, 566 (1962).

[20]M. Tinto, in *Proceedings of the NATO Workshop on Gravitational Wave Data Analysis* (Ref. 7).

[21]B. F. Schutz, *A First Course in General Relativity* (Cambridge University Press, Cambridge, England, 1985), p. 245, Exercise 14.

[22]J. Mathews and R. L. Walker, *Mathematical Methods of Physics* (Benjamin, Menlo Park, California, 1970), p. 382.

[23]L. A. Wainstain and V. D. Zubakov, *Extraction of Signals from Noise* (Dover, New York, 1970).

[24]E. O. Brigham, *The Fast Fourier Transform* (Prentice Hall, Englewood Cliffs, NJ, 1974), p. 113.

[25]B. P. Flannery, W. H. Press, S. A. Teukolsky, and W. T. Vetterling, *Numerical Recipes* (Cambridge University Press, Cambridge, England, 1986), p. 417.

[26]Flannery, Press, Teukolsky, and Vetterling, *Numerical Recipes* (Ref. 25), p. 200ff.

[27]N. Kawashima, in *The Proceedings of the Fifth Marcel Grossmann Meeting* (Ref. 16).

[28]Brigham, *The Fast Fourier Transform* (Ref. 24), p. 83ff.

[29]B. F. Schutz, *Proceedings of the NATO Workshop on Gravitational Wave Data Analysis* (Ref. 7).

[30]F. S. Acton, *Numerical Methods that (Usually) Work* (Harper and Row, New York, 1970), p. 464.

[31]Flannery, Press, Teukolsky, and Vetterling, *Numerical Recipes* (Ref. 25), p. 294ff.

[32]M. Tinto, Ph.D. thesis, University of Wales, Cardiff, Wales, 1987.

[33]K. S. Thorne (private communication).

[34]B. F. Schutz, in *Gravitational Radiation,* edited by D. Blair (Cambridge University Press, Cambridge, England, 1989).

[35]J. C. Livas, Ph.D. thesis, Massachussets Institute of Technology, Cambridge, MA, 1987.